The Pennsylvania State University

The Graduate School

Department or Architectural Engineering

PROOF-OF-CONCEPT: CMOS SENSOR BASED LIGHTING CONTROL SYSTEM INTEGRATING HIGH DYNAMIC RANGE IMAGING AND DALI

A Thesis in

Architectural Engineering

by

Abhijit Sarkar

Submitted in Partial Fulfillment
of the Requirements
for the Degree of

Master of Science

May 2005

I grant The Pennsylvania State University the nonexclusive right to use this work for the University's own purposes and to make single copies of the work available to the public on a not-for-profit basis if copies are not otherwise available.

Abhijit Sarkar

The thesis of Abhijit Sarkar was reviewed and approved* by the following:

Richard G. Mistrick
Associate Professor of Architectural Engineering
Thesis Co-Advisor

Martin Moeck
Assistant Professor of Architectural Engineering
Thesis Co-Advisor

Kyusun Choi
Assistant Professor of Computer Science

Richard A. Behr
Professor of Architectural Engineering
Head of the Department of Architectural Engineering

*Signatures are on file in the Graduate School

ABSTRACT

Modern lighting control provides a multitude of benefits, ranging from energy and cost savings, and reduction in electrical demand, to increased worker productivity and an improved lighted environment. Recent market research has shown that the present trend is towards lighting automation, as 65% of new construction or renovation in office and school buildings feature lighting automation. Daylighting control, one of the major lighting control technologies available today, can be achieved by switching or dimming, or both. Using photosensors is probably the most common practice for daylight harvesting.

A photosensor based closed loop lighting control system has its drawbacks. Since the photosensor signal greatly depends on the position of the sensor relative to the room configuration, both commissioning and calibration play a pivotal role in determining whether the system can achieve significant energy savings without raising serious occupant complaints. Even for a properly commissioned and calibrated photosensor, not all daylight conditions are appropriate. Further, the reflectance values of the surfaces (including blinds and exterior surfaces) that a photosensor sees are important. The performance of a photosensor might be adversely affected by a change in the reflectance values of different surfaces in a room. Finally, the field of view of the photosensor plays a critical role in its performance. A large field of view minimizes local impacts, but increases the potential of strong contributions from windows or the luminaires.

So there are many issues that must be addressed in order to make a photosensor based control system work. Oftentimes, contractors responsible for installing these systems do not have adequate knowledge of proper commissioning. This is one of the main reasons why photosensor based systems have seen limited application and have traditionally faced a market barrier.

The hypothesis for this research is that since we can retrieve luminance information from an image, we can use this information to determine the light level at a particular point in a room

and maintain a desired light level through automatic lighting control. In other words, a camera can be used as a photosensor. This work proposes the use of an inexpensive CMOS sensor as a light-sensing device, so that it acts as a photosensor. Additionally, a technique called High Dynamic Range (HDR) imaging, much applied in computer graphics, has been employed. If the camera gets a direct view of the daylight delivery system and/or the luminaires it controls, saturation in the image can be avoided using this technique. This novel solution, described as CamSensor in this thesis, is a proof-of-concept for the application of High Dynamic Range imaging technique in the field of lighting control.

CamSensor is in a position to exploit the ultimate flexibility that a unique lighting control technology like Digital Addressable Lighting Interface (DALI) offers. By individually controlling the luminaires and simultaneously estimating the change in the light level at different positions in the space, CamSensor can deliver a superior lighting control system. This is why DALI has been selected as the lighting control technology for this research.

TABLE OF CONTENTS

LIST OF FIGURES

LIST OF TABLES

ACKNOWLEDGEMENTS

I express my sincere gratitude to my thesis advisors Dr. Richard Mistrick and Dr. Martin Moeck for allowing me to take up this challenging research project. Dr. Moeck has long been interested in exploring the idea of using a camera as a light sensor. He has been kind enough to let me use the resources available in the new DALI lighting laboratory in our department. Dr. Mistrick has always been tremendously supportive throughout my graduate studies at Penn State. His suggestions and advice helped me a great deal in my research. I would also like to thank Dr. Kyusun Choi for being in my thesis committee and guide me with his valuable advice on hardware issues.

I owe special thanks to John Koffler of Tridonic, Atlanta, for sharing with me valuable information regarding the DALI programming and the Tridonic Busmaster, without which it wouldn't have been possible for me to use this technology effectively.

K C Yeung of CoMedia Ltd, Hong Kong (manufacturer of the Camera Module and the Evaluation Board used in this research) gave relentless feedback and advice regarding the CMOS camera module.

Greg Ward, who is well known in the field of computer graphics, gave generous feedback on HDR technique and his HDR image generation software Photosphere.

I am also grateful to Illah Nourbakhsh (Carnegie Mellon University), Paul Debevec (University of Southern California) and Celine Loscos (University College, London) for responding to my queries and providing me with important information that were valuable for this work.

My friends Youn Ju, Smita, Jan, Malay and Arin were always a source of encouragement for me. And finally my parents and my elder sister, who lent a patient ear to my

“technical” discussions that sure sounded geeky, but yet showed great forbearance and appreciation and encouraged me in my endeavor as always.

Chapter 1

INTRODUCTION

This chapter begins with a discussion on the existing technology for lighting control and its limitations. A brief description of a proposed solution for daylight responsive control is provided next, followed by the research hypothesis and advantages offered by the proposed solution.

1.1 The Importance of Lighting Control in Today's World

Previous research has shown that lighting comprises 20%-40% of total electric power consumed in commercial buildings and up to 50% in the residential buildings [1]. Modern lighting control provides a multitude of benefits, ranging from energy and cost savings, and reduction in electrical demand, to increased worker productivity and an improved lighted environment. Automatic lighting controls are capable of reducing energy consumption by up to 50% in existing buildings [2] (in the case of an electronically ballasted lighting control system in an office building in San Francisco) and by 35% in new construction [3]. Moreover, new state and federal energy codes and standards are coming into place, requiring building owners and contractors to adapt energy efficient technologies that include daylight harvesting and automatic lighting control [4] [5]. Interestingly, recent market research has shown that the present trend is towards lighting automation, as 65% of new construction or renovation in office and school buildings feature lighting automation [6]. Lighting automation enables automatic control of electric lights based on occupancy, daylight levels, personal preferences of the user regarding the

lighting environment and even peak demand. It can be part of an integrated building automation system.

1.2 Photosensor-Based Lighting Control System

There are four main lighting control technologies: switches and dimmers, occupancy sensors, daylighting controls and building automation systems. Daylighting control can be achieved by switching or dimming, or both. Using photosensors is probably the most common practice for daylight harvesting. However, the use of photosensors to control interior lighting (typically, closed loop control) is nontrivial [7] [8]. Proper design, commissioning and calibration all are critical to photosensor system performance.

1.2.1 Principles of Operation of Photosensors

A photosensor is a complete assembly that includes the optical arrangement and electronic circuitry that is coupled to an electronic component called a photocell. A photocell is typically nothing but a light responding silicon chip that converts incident radiant energy into an electrical signal [9]. Photosensors can be used indoors or outdoors. Indoor photosensors are generally closed loop, as they receive a feedback signal from the luminaires they are controlling. The outdoor photosensors are always open loop, since they do not receive any feedback signal from the electric lights they are controlling. The optical arrangement of an indoor photosensor generally includes a diffuser or lens (which may also be called an integrator) that collects light from different directions within the room, and typically an optical filter that rejects the UV and IR spectra, so as to simulate the human visual response to incident radiation. The electronic circuitry amplifies the dc voltage generated by the photocell, and after comparing it with a reference

voltage, sends an appropriate signal (termed the photosensor signal) to the control device, typically a lighting control panel. The control panel, in turn, sends a control signal (typically in the range of 0-10V) to the electronic ballasts (in the case of fluorescent luminaires). There can be other variations in photosensor-based control systems. For example, the control signal may be sent by the control circuitry, instead of the control panel. There may be other functionalities associated with the electronic circuitry as well, but the principle essentially remains the same.

1.2.2 Difficulties Associated with Closed Loop Systems

A major problem with a closed loop photosensor is its placement. If the sensor is located in such a position that it has a direct view of the daylight delivery system (the window, for example), there is a possibility that the daylight distribution may change during the course of the day, resulting in a change in the ratio of workplane illuminance and photosensor signal. This may cause the photosensor to dim down the electric light to an unacceptable level. Also, if the photosensor has a direct view of the luminaires it is controlling, a typical problem of oscillation may arise as the dimming level of the luminaire rises and lowers in quick succession, resulting in unstable operation. Since the photosensor signal greatly depends on the position of the sensor relative to the room configuration, both commissioning and calibration play a pivotal role in determining whether the system can achieve significant energy savings without raising serious occupant complaints [10]. Even for a properly commissioned and calibrated photosensor, not all daylight conditions are appropriate, as has been found in detailed modeling and computer simulations [11].

The photosensor's performance might be adversely affected by a change in the reflectance values of different surfaces in the room. For example, if someone dressed in light colored clothes stands within the view of the photosensor (which is generally mounted on the

ceiling) or white paper is spread across the work plane (desk/table), there is a chance the photosensor will overdim the lights in response to the additional light that it receives.

For this reason, the field of view of the photosensor also plays a critical role in photosensor performance [12] [13]. A large field of view minimizes local impacts, but increases the potential of strong contributions from a window and/or the luminaires. Thus, the design of the sensor involves an optimization of its parameters.

So there are a myriad of issues that must be addressed in order to make a photosensor-based control system work. Often times, contractors responsible for installing these systems do not have adequate knowledge of proper commissioning procedures[1]. This is one of the main reasons why photosensor-based systems have seen limited application and have traditionally faced a market barrier [9] [14].

A new technology called Digital Addressable Lighting Interface (DALI in short, described in detail in Chapter 4) is now available for automatic lighting control, which enables dimming of individual luminaires to different levels. This allows a DALI-based lighting control system to achieve different target illuminance values at different areas in the space, or different electric light levels from different luminaires to maintain uniform light levels. This enables a precise control of the lighted environment in a space. For this kind of control, we would need a number of photosensors (typically one for each target point) to handle multiple target points with similar or different illuminance requirements, adding to the cost and complexity of the lighting control system. Thus, in today's control industry, there is a need for an advanced daylight sensor that can reap the benefits and flexibility that a lighting control technology like DALI offers, by monitoring multiple task locations simultaneously.

---

[1] It is a systematic process that ensures that all elements of the daylighting system perform interactively and continuously according to documented design intent and the needs of the building owner [7].

1.3 Thesis Objective

This work proposes the use of an inexpensive image sensor (described in detail in Section 2.2) as a light-sensing device, so that it acts as a photosensor. Additionally, a technique called High Dynamic Range (HDR) imaging, much used in computer graphics, will be employed. Many of the problems discussed earlier can be circumvented by means of both the hardware and software associated with this solution. The solution, described as **CamSensor** in this thesis, is a proof-of-concept for the application of this technology in the field of lighting control.

The specific objectives of the work are:

1. Investigating the accuracy of CamSensor in computing the luminance values at a series of points.
2. Proposing a suitable procedure for estimating illuminance values at different points from the corresponding luminance values and determining the error associated with this approach.
3. Development of an algorithm to control individual DALI luminaires to maintain the illuminance values at multiple locations on the work plane at predetermined target levels.
4. Setting the guidelines for proper calibration and operation of CamSensor.
5. Determining the limitations of CamSensor.
6. Determining the enhancements required to the prototype so as to improve the performance of CamSensor.

1.4 Research Hypothesis

It is hypothesized that since we can retrieve radiance values at different pixels in an image, and since the radiance values are proportional to the corresponding luminance values, we can determine the luminance values at different locations on the work plane from a digital image captured with the help of an image sensor.

It is also hypothesized that a method can be formulated to convert the luminance values computed from an image to corresponding illuminance values. If that is possible, we can maintain desired illuminance levels at multiple locations through automatic lighting control where a camera works as a photosensor.

If the pixel value in an image captured with a given exposure is not proportional to the light falling on that pixel, the High Dynamic Range (HDR) imaging technique can rectify this situation and better estimate the luminance values at different locations by forming a high-contrast image from multiple-exposure images. For example, accurate information about the luminance values at an underexposed (very dark) or overexposed (very bright) location can be obtained. Thus, if a camera has a direct view of the daylight delivery system and/or the luminaires to be controlled, it will not add significant error to estimation of the illuminance levels at a target point. This will be a major advantage over the standard photosensor-based systems that are unlikely to work well in either of these two conditions.

If the relative error (i.e. the percent error) in the estimation of luminance remains constant at a particular pixel as the lighting condition changes, the change in the computed luminance at a point will still be proportional to the change in absolute luminance. It is hypothesized that an iterative refinement of the dimming levels through repeated image capturing and estimation of the present illuminance values at different locations on the workplane will help attain target light levels with reasonable accuracy.

The assumption that a high-precision image sensor with a linear response function is not mandatory for this work prompted the choice of a system that will be competitive with standard commercial photosensors in cost and performance. An inexpensive CMOS (Complimentary Metal Oxide Semiconductor) image sensor was selected over a CCD (Charge-Coupled Device) image sensor because of the reasons described in Section **2.3**. It is envisioned that CamSensor has the prospect of being a commercially viable product in the future, so cost effectiveness was a primary consideration. It is also envisioned that imaging devices based on CMOS sensors will continue to improve in quality.

It is also hypothesized that CamSensor is in a position to exploit the ultimate flexibility that a unique lighting control system like DALI offers. By individually controlling the luminaires and simultaneously estimating the change in the illuminance at different positions in a space (assuming that light is additive in nature), CamSensor can deliver superior lighting control from the perspective of DALI. This is why DALI has been selected as the lighting control technology for this work. It is important to point out that CamSensor is suitable for other lighting control systems as well, as photosensors are currently applied. However, in order to use CamSensor with other control systems, alternate control algorithms than the ones described here would need to be employed.

1.5 Capabilities of the Proposed Solution

Following is a list of the advantages that can be expected from a **full-fledged product arising out of CamSensor**. However, only the first two possibilities were investigated in this work.

1. Only one sensor can be used for different task areas with different target illuminance values (in other words, different dimming zones), provided the task

area is within the view of the camera. A graphical software interface can be used for selecting the task areas. Although the graphical software was not developed, this work considered multiple target locations on the workplane.

2. A lower resolution, less expensive CMOS sensor can be used for image capturing. In the present work, the performance of this type of sensor was investigated.
3. Direct view of the luminaires/window is allowed since it does not affect the pixel values at the target points, as long as the effect of blooming[2] is minimal. An appropriate exposure setting has to be chosen while capturing the image, so that the no target point is underexposed or saturated. Images captured with multiple exposure settings can also be considered for accurately estimating illuminance levels at different target points.
4. A change in the work plane surface reflectance can be detected. If an object is placed on the workplane at a target location, there will likely be a change in the color of the pixels at this point. If the color of the pixel at a target point is quite different from the calibration condition, the target point can be excluded or can be replaced by a nearby point that is unaffected. A smart algorithm can be used for this purpose.
5. Surveillance cameras, if installed, can be integrated with the lighting control system to capture images and send these to the master lighting controller.
6. CamSensor can also be an embedded system that does all the processing locally and sends an appropriate signal to a lighting control panel or DALI controller.
7. Alternately, an Ethernet can be used for remote processing in order to achieve higher flexibility. A wireless operation is also a possibility.

---

[2] The effect when an oversaturated pixel affects the surrounding pixels

8. With some modification in the hardware design, it may be possible to use CamSensor as an occupancy sensor as well as a photosensor. In order to detect movements of the occupants inside a space, images could be captured in regular intervals for recording any localized changes in luminance levels. In order to reduce the response time, save power and reduce heating effect, a "smart scanning" procedure can be adopted. To start with, the user will identify the entrance areas of the room (or space) in an image of the scene captured by CamSensor. When a space is unoccupied, CamSensor can selectively scan these entrance areas repeatedly to look for any change. This will allow CamSensor to detect any movement in the entrance area almost instantaneously and turn on the lights in the room. In order to determine whether there is any occupant in the room, CamSensor can compare the pixel values of the present scene with the calibration condition. This will ensure proper occupancy sensing even if the occupant is sitting or standing still. Pattern recognition techniques can be used for advanced and sophisticated applications. The sensor, however, should have a clear view of both the entrance areas and the task areas in order to be able to act simultaneously as an occupancy sensor and a photosensor.

CamSensor is not free from errors and may not be appropriate under certain conditions. Limitations of this system will be discussed at the conclusion of this document.

1.6 Organization of the Dissertation

Chapter 2 contains a description of solid state imaging sensors. Chapter 3 discusses the High Dynamic Range imaging algorithm used in CamSensor. Chapter 4 discusses the DALI technology. The test setup and equipment used in this work are described in Chapter 5. Chapter 6

discusses the experiments performed with CamSensor. The results of those experiments have been presented in the form of tables and graphs. Based on these experiments, a detailed calibration and operational procedure for CamSensor are presented in Chapter 7, followed by the final experiment and results. Chapter 8 draws conclusions from this work, including a discussion on the limitations of the system.

Appendix A contains the flowcharts and algorithms used in the software. Appendix B gives some details on the image sensor used.

Chapter 2

SOLID STATE IMAGING

Since the current work draws inspiration from previous research efforts in the field of computer graphics and photometry, a brief overview of the application of solid state imaging within these two fields is presented in this chapter.

2.1 Electronic Imaging in computer graphics and photometry

Since the invention of the Charge-Coupled Device (CCD) in 1970 at Bell Labs, electronic imaging systems based on solid-state imaging sensors have gained popularity. Compared to CCD sensors, application of Complimentary Metal Oxide Semiconductor (CMOS) technology (a low power, low heat semiconductor technology used in transistors) to imaging is relatively recent. The following section briefly describes the two technologies as they are applied to imaging systems, and the pros and cons of these two technologies.

2.2 How Solid State Sensors Work

Before the differences between different image sensors can be discussed, it is necessary to explain the principle of operation of these sensors. This section gives a brief overview of the physics involved in the operation of image sensors.

When quanta of light (photons) impinge on and penetrate a semiconductor substrate, they transfer a part of their energy to the substrate which causes the generation of charge carriers (electron-hole pairs). The electrons and holes can be separated by using a reverse-biased

photodiode or a MOS capacitor, also called the image cell or pixel (comes from Picture Elements). Electrons are accumulated by the reversed-biased and electrically isolated junction capacitances of the image cells. The number of electrons collected is proportional to the light intensity. The charges are then transported in packets to the output pin of the sensor either by means of a MOS (Metal Oxide Semiconductor) switch with a sensing line or by a shift register. A source follower amplifier converts the charge packets into a series of voltages [15].

For capturing color images, different color filters, namely red, green and blue, are used on individual image cells, so only a single wavelength of light reaches a pixel. Thus, one pixel records only one color. Out of a group of four adjacent pixels, two store green color, and one each stores red and blue. An image processing and color interpolation technique is then applied to reproduce the original color, sometimes leaving color artifacts in the final image. This kind of sensor is called a Mosaic Image Sensor. Very recently, a Direct Image Sensor has been developed that directly captures colors in three different layers in a single exposure, taking advantage of the fact that different wavelengths of light penetrate silicon to different depths. This results in sharper pictures with better color, free from color artifacts [16].

Several of the individual image cells or pixels combine to form a sensor. Solid state imaging can be line sensing (linear imagers) or area sensing (array imagers). In linear imagers, the pixels are arranged in a single row. In the latter case, the image cells are arranged in a matrix format.

2.2.1 Charge-Coupled Device (CCD) Imagers

The Charge-Coupled Device or CCD is basically a series of closely spaced MOS (Metal Oxide Semiconductor) capacitors. CCD imagers are further subdivided into three categories based on the transfer mechanism of the electrons: frame transfer devices, interline transfer

devices and frame-interline-transfer devices. While their working principles are essentially the same, the relative placement of the charge collecting photosites and the CCD shift registers (temporary storage cells) are different in these devices. Consequently the mechanism of transferring the charge from the former to the latter is also a bit different [15] [18].

For example, in the case of an Area Array Interline CCD (Figure 2-1), the charges are first accumulated in the photodiodes, and then the charge packets are shifted from the photodiodes into the adjacent vertical CCD shift registers via the transfer gates. The CCD and the transfer gates are insensitive towards light. After this, charge accumulation in the pixels resumes while the vertical CCD arrays transfer their charges to a horizontal output register. Subsequently, the charges from the horizontal output register are converted into electrical voltage or current signals by the output amplifier. The process of transferring charges from the shift register to the output register and subsequent horizontal readout continues until the whole sensor is empty [15] [17].

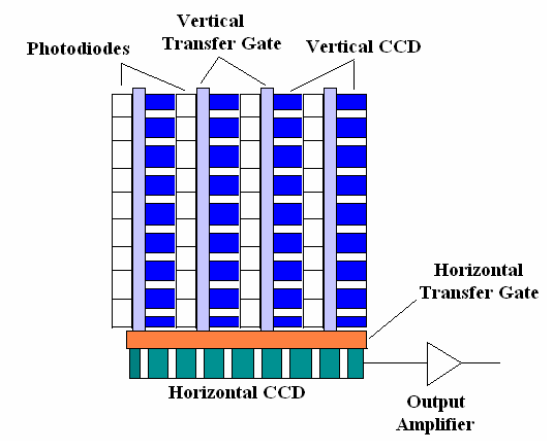

Figure 2-1: Area Array Interline CCD Structure

2.2.2 Complimentary Metal Oxide Semiconductor (CMOS) Imagers

In the case of a CMOS sensor (Figure 2-2), a charge can be transferred on a pixel-by-pixel basis; it does not have to be sequential. A CMOS sensor is basically a two-dimensional addressable array of pixels. A particular pixel can be selected by means of row and column address logic in the form of a shift register or decoder. Analog Signal Processors connected to the pixel array perform different functions like charge accumulation, gain, sample and hold, fixed pattern noise reduction etc. All signal processing and associated circuitry are integrated into a single chip [21].

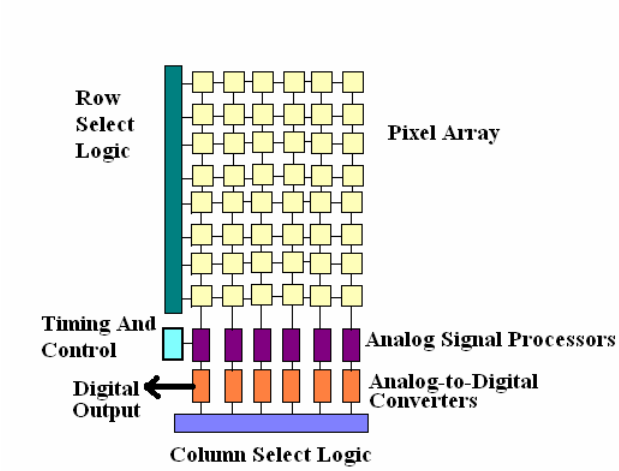

Figure 2-2: CMOS Structure

In earlier CMOS sensors, a pixel consisted of a photodiode and an access transistor. A selection transistor was used for row-column addressing. For these passive pixels, the pixel size was small and the fill factor (the ratio of light sensitive area to the total photosite area [18]) was large, however the fixed-pattern noise (a non-uniform pattern seen in the output of the image sensor under no illumination [18]) was high. In 1991, an active pixel sensor (APS) was described,

which is a sensor with an active amplifier integrated within each pixel. This reduced the fill factor, but significantly improved the signal-to-noise ratio and the dynamic range [19] [20]. The dynamic range is an extremely important parameter, and is defined as the ratio of the maximum output signal, or saturation level, of an image sensor to the noise level of the imager under no illumination [18]. It is an index of the ability of the sensor to respond to change in the intensity of the light over a wide range.

The performance of CMOS APS is comparable with CCD technology and offers many advantages [21].

2.3 Pros and Cons of CCD and CMOS Image Sensors

CCD's have long been the de facto standard in digital imaging because of their high quality and low noise. However this technology has some disadvantages.

- The entire content of the CCD must be read out and time must be allowed for sequential reading, even to simply view a small part of the whole image. This reduces the speed of the imaging system.
- Since CCD process technologies necessitate the use of supporting circuitry that cannot be integrated onto the silicon, it increases the cost and complexity of manufacturing the CCD sensors, as well as the system's power consumption.
- Traditionally, the CCD has faced the problems of blooming (charge leaking from one pixel into the surrounding ones), fading (loss of charge in the process of transferring), and smearing (image quality being adversely affected due to the light arriving during the readout process). However, most of these problems have been solved in recent years [19].

The advantages of CMOS sensors are numerous [17] [19] [22]:

- Digital logic, clock drivers, A/D conversion, etc. can be integrated into the same chip as the CMOS pixel array, making CMOS sensors compact, low-voltage and low-power.
- These imagers can be manufactured using the infrastructure used in the semiconductor industry, which does not need to be customized – so the manufacturing cost is significantly less.
- Random access to the pixels enables electronic windowing, zooming and panning.

However, there are reasons why CMOS sensors have so far achieved a relatively low market penetration:

- CMOS sensors have relatively large fixed-pattern noise. As already described, individual pixels have amplifiers. Variation in the gain and offset of the amplifiers give rise to static pattern noise [19]. However, there are ways to reduce it [22].
- There are other sources of noise - for example, temporal noise, which includes reset noise of the image cell, channel noise of the in-pixel voltage follower, noise due to dark current and noise added along the readout signal path [23]. Different noise sources, as well as the concepts to reduce them, have been discussed in [23]. It will be important to point out here that for any image sensor, the fundamental source of noise is the quantum noise of the incoming photon flux (due to the fact that the sensor cannot trap all photons impinging on the sensor), but solid state sensors are insensitive to low light level as well [24].
- Low fill factor of CMOS sensors, due to the requirement of accommodating other circuitry beside each of the sensor cells, leads to less sensitivity compared to their CCD counterparts. To remedy this problem, support circuitry is covered

with an opaque metal layer and a microscopic lens is placed over the entire area covering the photosensitive cell and support circuitry so that light is redirected to the image cell [22].

The foregoing sections give an indication that major successes have been achieved in the research and development of CMOS sensors as imaging devices. In the coming years, this trend is expected to continue, and in many applications including digital cameras, CMOS sensors are expected to replace their CCD counterparts [17].

2.4 Use of Solid State Imaging in Computer Graphics

An outdoor scene containing sunlight and shadow can have a luminance range of 10000 to 1. The human eye can accommodate a similar luminance range in a single view [28]. These scenes with high light level contrast are called High Dynamic Range (HDR) scenes[3]. However, a standard 24-bit image capturing device typically provides 8 bits of brightness data at each pixel. As a result, an image of a high contrast scene ends up being too dark in some areas and too bright, or saturated, in others. The quest to seek solutions to this classical problem of computer graphics (which is closely related to photography) has led to the development of the research area of High Dynamic Range imaging. It can be subdivided further into the following categories: HDR image generation, HDR image representation (encoding) and HDR image display. This thesis mostly deals with HDR image generation. However for the sake of completeness, a brief description is provided for the other two categories as well.

---

[3] Dynamic range is basically the range of subject brightness values over which a change in subject brightness will create a change in image brightness.

2.4.1 HDR Image Generation

There are mainly two ways to generate High Dynamic Range images, physically-based rendering and multiple-exposure image capture. The first is a process where rendering software computes the color values that correspond to the spectral radiance at each point of the rendered image. The Radiance lighting simulation software is one of the most authentic works on physically-based rendering [25].

The most obvious approach to multiple-exposure image capture is to sequentially capture multiple images of the same scene with different exposures. By combining differently exposed pictures of the same scene, we can obtain a single picture of extended dynamic range. A detailed description of this procedure is discussed in Chapter 3.

A multiple-exposure image can also be generated by other procedures like spatially varying pixel exposures.

2.4.2 HDR Image Representation

Conventionally, the digital image formats have been dictated by the limitations of display devices. Although the internal operation of computer graphics applications depends on the floating point representation of the color, most of the time they are converted to 24-bit integer values while writing the results to a file. This results in a loss of accuracy and dynamic range. One solution to this problem is to use a floating point pixel format. An efficient way to do that is to use an 8-bit mantissa for each primary followed by an 8-bit exponent common to the RGB primaries [28]. This 32-bit RGBE representation provides over 77 orders of magnitude in dynamic range. On the negative side, it can produce quantization artifacts and it is unable to represent some highly saturated colors. A new pixel encoding approach has been proposed in [28]

that uses a log representation of luminance and a CIE (u', v') representation of color. Termed as LogLuv, this 32-bit encoding covers the full range of perceptible luminance of 38 orders of magnitude and has been incorporated into the TIFF standard.

The encodings discussed above are suitable for the transfer, manipulation and storage of HDR color images.

2.4.3 HDR Image Display

What we get from a rendering algorithm is basically an image that contains the spectral radiance values. In order to convert this spectral image to a display image (that can be sent to a CRT or LCD), the spectral radiance values are first converted to tristimulus values, for example CIE XYZ (using CIE observer functions). Then each tristimulus value is mapped to the target display's color space. This process is called tone mapping [26].

The other alternative for High Dynamic Range image display is rendering based on an image appearance model that attempts to predict the perceptual response towards spatially complex stimuli [29].

2.5 Use of Solid State Imaging in Photometry

Over a decade ago, the luminance mapping technique relying on CCD technology was identified as an effective method of luminance measurement [31]. It has been a standard method used in Astronomical imaging. Even the computer graphics community regarded an image as a collection of photometric measurements, and a camera as an array of light meters [30]. So the basic philosophy of research concerning solid state imaging remains the same in both lighting and computer graphics, although the final destination is different.

The CapCalc system described in [31] is comprised of a solid-state video camera with a photopic correction filter for acquiring luminance and spatial information from a scene. It was connected to a computer with an image acquisition board for storing and analyzing the data. The possibility of using a luminance mapping technique for lighting quality assessment, in particular glare evaluation, has also been investigated [33].

Standard luminance meters use a silicon photodiode or a photo-multiplying tube (PMT) as the light sensor. However recent advances in imaging devices based on CMOS and CCD technologies enable the use of these devices for luminance measurement. These imaging photometers have a high dynamic range – there are 16-bit systems that cover a luminance range of 65000:1 [34]. Obviously, these systems are expensive and are meant for high-end applications.

Very recently, a software simulation tool named Virtual Lighting Laboratory has been developed that utilizes physically-based imaging to create an environment where advanced lighting analysis and experimentation can be performed [39] [40].

The only published research work on the application of solid state imaging in lighting control was a logical extension of CapCalc, described as ImCon in [32]. The prototype described in this work included a calibrated CCD camera with a resolution of 165 X 192 pixels, an image acquisition board, a personal computer and peripheral lighting control gear. The concept was to compute the surface brightness at various locations in the room and use that information to adjust different luminaires, in order to maintain desired luminance levels. The paper also proposed to detect events that required a specific luminance profile and adjust the electric lights accordingly. The operation of ImCon involved segmentation of the image to detect different key surfaces, specification of the desired radiance values and identifying the key tasks in the space by means of simple heuristics. However, the capabilities of ImCon were rather limited and full performance analysis was not available during the initial implementation. Further research work on ImCon was not reported.

Chapter 3

HIGH DYNAMIC RANGE IMAGING AND RADIANCE COMPUTATION

This chapter describes the mathematical aspects of High Dynamic Range imaging and the process of deriving a camera response function. The issues discussed here have been dealt with in [30] and [35]. The algorithm has been discussed in detail in [35].

3.1 The Nonlinear Nature of the Image Response Function

The pixel values obtained from digital (or analog) images are not true measurements of the brightness or luminance in the scene. The pixel value and the quantity of light falling on the corresponding sensor element are not even linearly related. During the process of image capturing, several nonlinear mappings are involved. This is true for CCD as well as CMOS sensors. Although CCD sensor elements respond to the incident photons in a linear fashion, most digital cameras apply a nonlinear mapping to the CCD response in order to simulate the nonlinear response characteristic of photographic film, which is to ensure better quality of the images while printing on standard media (display device or paper) or when sending the image to a display device with limited dynamic range. CMOS sensors are inherently nonlinear in nature. A major source of nonlinearity is the gamut clamping, or the saturation limit of the imaging device, where any pixel with a brightness value beyond a certain limit is mapped to the same maximum value.

3.2 Factors Affecting Image Sensor Response

There are three principal factors affecting the image sensor response: i) the exposure setting with which an image is captured, ii) the spectral sensitivity of the image sensor and iii) the intensity of the light source illuminating the scene. The first factor has been dealt with in great detail in this work. However, the effect of the other two factors on the image sensor response has not been investigated. This section gives a brief explanation of why these factors are important for this application.

An image sensor responds differently to different wavelengths of light. If it is a color image sensor, then the red, green and blue channel will have different spectral sensitivity. Thus, the image sensor response will differ for light sources with different Spectral Power Distribution (SPD). This means that the radiance values[4] obtained from an image will be dependent on the SPD of the sources operating during the image capturing process. This is undesirable for CamSensor operation. A spectral calibration of the sensor will help determine how the computed radiance values should be corrected for a particular combination of sources in order to make the camera response independent of the type of lamps used in the luminaires [37]. This factor has been taken into account in the calibration phase, though a bit differently, as will be explained later.

Charge-Coupled Devices (CCD) and Active Pixel Sensor (APS) technology (for example, Complimentary Metal Oxide Semiconductor or CMOS) based image sensors generally have a linear intensity-response function. However, if the dynamic range[5] of the sensor is larger

---

[4] In fact these are the relative radiance values proportional to the absolute luminance, but for the sake of simplicity, we will exclude the term relative in the remainder of the document.

[5] Dynamic range is the range of subject brightness values over which a change in subject brightness will create a change in image brightness.

than the camera, there might be a nonlinear mapping between the raw sensor output and the camera response [36].

The foregoing discussion can be expressed mathematically by the Eq. 1 [36]:

$$R_i = \Phi(e \int_{\lambda_l}^{\lambda_h} S_i(\lambda)\, I(\lambda)\, d\lambda + n_i) \qquad (1)$$

Where,

R_i is camera response for a pixel of the i^{th} sensor type (red, green or blue), $S_i(\lambda)$ is the spectral sensitivity of the i^{th} sensor type, $I(\lambda)$ is the incident power density per unit time at wavelength λ, e is the exposure duration, and n_i is a variable signifying the dark noise and other factors causing response variability for the i^{th} sensor type.

3.3 Extending Dynamic Range by Exposure Bracketing

Scenes with a high contrast between two areas cannot be captured efficiently with standard imaging devices. In these cases, some areas will be too dark and some areas will be saturated. One way to bypass this limited dynamic range problem is to take multiple pictures with different exposures and combine them to form a single image. However, because of the nonlinearity in the response function of the imaging device, they cannot be combined in a simple additive way.

3.4 Determination of the Camera Response Function

According to the reciprocity rule, the exposure (X) at a certain sensor element site is the product of the irradiance[6] E and exposure time (Δt). Now, the digital value (Z) at a pixel is a function of the exposure X at that pixel as shown in Eq. 2. The function f is unknown.

$$Z = f(X) \tag{2}$$

In order to compute the digital value Z, the RGB values at a pixel first have to be converted to the CIE XYZ colorimetric system by the following matrix:

$$\begin{bmatrix} X \\ Y \\ Z \end{bmatrix} = \begin{bmatrix} 0.5142 & 0.3239 & 0.1620 \\ 0.2651 & 0.6701 & 0.0648 \\ 0.021 & 0.1228 & 0.8530 \end{bmatrix} \begin{bmatrix} R \\ G \\ B \end{bmatrix}$$

If the image corresponds to a luminous scene, we can obtain luminance (L) by multiplying Y by a constant. For a photographic image, for example, this constant depends upon the exposure time, f-stop and film speed [28]. However, in this work, the computed CIE Y value has been used as the pixel value Z[7]. So for properly exposed pixels, Z should be proportional to the luminance for a particular exposure setting. It should also be noted that the sensor response to the incident light depends on the spectral response of the sensing element at that pixel location, which is not necessarily the photopic response. So, in this chapter, the term irradiance is used instead of illuminance, and radiance is used instead of luminance.

---

[6] Radiometric quantity corresponding to photometric quantity illuminance (light level at a point).

[7] The equation used to compute Y is: Y = 0.31R + 0.59G + 0.11B, as per the image sensor product specification.

In this work, a series of 8 photographs have been considered with digital exposure settings of 2, 4, 8, 16, 32, 64, 128 and 255, taken from the same vantage point in quick succession so that the irradiance, E_i, remains constant at a particular pixel.

Let Z_{ij} be the pixel value for pixel i in the image j. E_i is the irradiance at pixel i and Δt_j is the exposure time for the image j. from Eq. **2**,

$$Z_{ij} = f(X_{ij}) = f(E_i * \Delta t_j) \tag{3}$$

Considering f as invertible and taking the natural logarithm of both sides,

$$\ln[f^{-1}(Z_{ij})] = \ln(E_i) + \ln(\Delta t_j)$$

Simplifying,

$$g(Z_{ij}) = \ln(E_i) + \ln(\Delta t_j) \tag{4}$$

Both the function g and E_i are unknown, while Z_{ij} and Δt_j are known. This equation can be solved by considering an over-determined system of equations (number of equations greater than the number of unknowns).

So the following objective function must be minimized (least square solution determined):

$$\Phi = \sum_{i=1}^{N} \sum_{j=1}^{P} [\, g(Z_{ij}) - \ln(E_i) - \ln(\Delta t_j)]^2 + \lambda \sum_{z=1}^{254} [g(z-1) - 2g(z) + g(z+1)]^2 \tag{5}$$

Where,

N = number of pixels considered

P = number of images (8, in this case)

λ = weighting factor for the smoothness term (the second term in Eq. **5**)

Z = pixel value assumed to vary from 0 (white) to 255 (black)

g = the image response function – which essentially is a series of points corresponding to the pixel values (from 0 to 255)

A weighting function is introduced so as to give preference to the pixel values in the middle range, rather than near the minimum and maximum, where the response function has a steeper slope.

The weighting function is as follows:

$$\begin{aligned} w(z) &= z - Z_{min} \qquad \text{if } z <= 0.5 * (Z_{min} + Z_{max}) \\ &= Z_{max} - z \qquad \text{if } z > 0.5 * (Z_{min} + Z_{max}) \end{aligned} \tag{6}$$

So, the final equation is:

$$\Phi = \sum_{i=1}^{N} \sum_{j=1}^{P} [\, w(Z_{ij}) \{ g(Z_{ij}) - \ln(E_i) - \ln(\Delta t_j) \}]^2 + \lambda \sum_{z=1}^{254} [\, w(z)\{g(z-1) - 2g(z) + g(z+1)\}]^2 \tag{7}$$

In order to minimize the above objective function, the following partial differential equations should hold:

$\partial\Phi / \partial g = 0$ [denoting $g(Z_{ij})$ by g]

$\partial\Phi / \partial E = 0$ [denoting $\ln(E_i)$ by E]

$\partial\Phi / \partial g_1 = 0$ [denoting $\{g(z-1) - 2g(z) + g(z+1)\}$ by g_1]

So we get,

$$\sum_{i=1}^{N} \sum_{j=1}^{P} [\, w(Z_{ij}) \{ g(Z_{ij}) - \ln(E_i) \}] = \sum_{i=1}^{N} \sum_{j=1}^{P} [\, w(Z_{ij}) \ln(\Delta t_j)] \tag{8}$$

$$\sum_{i=1}^{N} \sum_{j=1}^{P} [- w(Z_{ij}) \{g(Z_{ij}) - \ln(E_i)\}] = \sum_{i=1}^{N} \sum_{j=1}^{P} [w(Z_{ij}) \ln(\Delta t_j)] \tag{9}$$

$$\lambda \sum_{z=1}^{254} [\, w(z)\{g(z-1) - 2g(z) + g(z+1)\}\,] = 0 \qquad (10)$$

Additionally, the value at the middle of the response curve is set to 0.

$$g(Z_{mid}) = 0 \text{ where } Z_{mid} = 0.5 * (Z_{min} + Z_{max}) \qquad (11)$$

Eq. **8**, Eq. **9**, Eq. **10** and Eq. **11** are used to form the matrices.

The final equation of the system is

$$\mathbf{A.\ x = B} \qquad (12)$$

Where,

A (N * P + 255, N + 256) is the system matrix

x (N + 256, 1) is the solution matrix containing the 256 g values and N number of irradiance values [$\ln(E_i)$].

B (N * P + 255, 1) is the matrix containing the N * P values of [$w(Z_{ij})\ln(\Delta t_j)$].

A. x signifies the matrix multiplication of **A** and **x**.

Eq. **12** is solved for x to obtain the camera response function.

Radiance at the i^{th} pixel in the image with j^{th} exposure can be computed by solving Eq. **13** for $\ln(E_i)$.

$$\ln(E_i) = \sum_{j=1}^{P} [\, w(Z_{ij}) \{\, g(Z_{ij}) - \ln(\Delta t_j) \,\}\,] \,/\, \sum_{j=1}^{P} [\, w(Z_{ij})] \qquad (13)$$

Chapter 4

Digital Addressable Lighting Interface (DALI)

Conventional lighting control systems include analog (0-10V) interfaces and proprietary digital control technologies. Analog control systems are hard-wired, cannot control individual luminaires to different levels, are expensive to implement, and cannot be reconfigured easily. Further, fluorescent ballasts from different manufacturers respond in different ways. Proprietary control systems offer greater flexibility, but installation can be cumbersome and expensive.

DALI, an acronym of Digital Addressable Lighting Interface, is an industry standard open protocol for digital communication between the individual components of a lighting system. DALI incorporates simplified communication methods providing optimum functionality, and therefore is simpler and more cost-effective than many other complex Building Management Systems (BMS). DALI itself cannot replace a Building Management System (also described as a Building Automation System), but it is possible to integrate DALI as a subsystem into a more powerful and sophisticated BMS. However, it can also function as a stand alone lighting control system.

4.1 History of DALI

In the mid ‘90s, high energy costs encouraged researchers in Europe to develop a better solution to control fluorescent lighting than the conventional 0-10V analog dimming system. One of the main issues was to deal with different and incompatible communication protocol and equipment. A rapid adoption of the new standard required seamless integration of ballasts,

sensors, controllers, switches and control systems. Leading control equipment manufacturers like Philips, Osram, Tridonic, Helvar, Huco and Vossloh-Schwabe developed the DALI standard. A working group, called the DALI Activity Group or DALI AG [53] was formed to develop a draft of the new standard, which was designated as Annex E of the European electronic ballast standard IEC 60929 [47]. This was the first proposed DALI standard, and was released on January 10, 2000.

4.2 The DALI Standard

DALI is an open system architecture that allows exchangeability of dimming ballasts from different manufacturers. In fact, the interfacing can be extended to other devices like sensors in the lighting system. Each of these devices is intelligent in the sense that each device can communicate with other devices and can hold information like its own address, operating parameters etc. All these components communicate with each other in a local system that is simple and free from interference. So, it is a flexible and decentralized lighting system that provides a full solution, that is, fixture, lamp, ballast, control and wiring. Each DALI system can consist of a maximum of 64 ballasts connected via a twisted-pair cable to a DALI controller. The controller in turn can be connected with other controllers to form a larger system.

DALI is suitable for mid-size rooms. The maximum distance between two DALI components is 300 meters (984 feet). Physical low level voltage is 0V (-4.5V to 4.5V) [digital value = 0] and high level voltage is 16V (9.5V to 22.5V) [digital value = 1]. Maximum allowable voltage drop is 2 V and maximum allowable drive current is 250 mA. Each device connected to the interface can draw up to 2 mA.

The data communication rate is pretty low, 1.2 Kbps, i.e. 1200 bits per second. Thus, additional measures need to be taken when interfacing a DALI system with a faster communication system.

Wiring is simplified in this standard – each device has only a power input and a digital control input. The control input is polarity independent. Scenes and groups in a DALI system can be assigned and modified without rewiring. A maximum of 16 groups and 16 scenes can be defined.

The software is one of the key components in the DALI system. The devices can communicate with each other through messages. The first part of a DALI message contains the address of the device it is meant for, and the second part is the command. The commands can be directed to all devices on the system (broadcast mode), to a group of devices, or to a particular device. The DALI controller can send arc power control commands, configuration commands or query commands. The ballast and other devices can answer the query commands and send status messages back to the controller. The DALI standard defines a logarithmic dimming curve allowing the light level to vary from 0.1% to 100%. This allows the human eye to observe the light change in a linear fashion.

DALI ballasts are capable of storing the operating parameters in their memory. These include sixteen different light levels for sixteen scenes, maximum and minimum light levels to attain, current light level, system failure and power-on levels, fade time and fade rate. As already mentioned, the status of each ballast and lamp can be accessed by the DALI controller.

4.3 Advantages of DALI

Following are some advantages offered by DALI [48]:

1. Individual devices or a group of devices can be controlled separately. It is a unique feature of this technology that it allows control of individual luminaires in a space. This brings a tremendous amount of flexibility in lighting control.
2. With DALI, dimming is no longer restricted to architectural lighting, daylight harvesting and conference rooms, lighting control can be implemented anywhere in the facility to achieve significant energy savings [**49**].
3. Precise energy monitoring and reporting can be a great advantage for a DALI based system, leading to LEED (Leadership in Energy and Environmental Design) credit for green buildings.
4. With DALI being an open industry protocol, functional security and device compatibility is quite high. It is guaranteed that the products from different control manufacturers will be interoperable.
5. Control line wiring is simple and straightforward, with no polarity, no group formation and no termination resistor. This makes the installation simpler than an analog system.
6. Faults in the devices can be detected through the control device status messages.
7. Individual devices are intelligent in the sense that each can store its individual address and other operating parameters.
8. Different types of devices can be identified and distinguished. Examples of these types are standard units, units for emergency lighting, units for low voltage halogen lamps etc.
9. A control device can be automatically detected by a DALI system and can be assigned an address automatically.
10. Group and scene formation is simple and is handled by the DALI software – no hardware modification is necessary for reconfiguring the system.

11. Fade time and fade rate can be adjusted while dimming a luminaire.
12. Data communication is free of interference.
13. Switching of external relays is not necessary, which reduces system maintenance cost.

4.4 Disadvantages of DALI

1. No more than 64 devices/control units can be connected to a single DALI controller.
2. Exceeding the maximum current/voltage limit causes reduced signal integrity. Considering the power consumption of each component is critical to successful system planning.
3. A DALI system requires DALI enabled dimming ballasts for each of the luminaires. Dimming ballasts are considerably more expensive than standard ballasts. This greatly increases the initial cost and also the maintenance cost. It should be noted that in many situations, individual dimming of luminaires is not a requirement. Thus, this technology is not suited for all applications.
4. There are proprietary digital lighting control systems developed by leading lighting control manufacturers that offer many of the functions and flexibility that DALI has, yet their initial costs are lower than that of DALI.
5. Installation/commissioning time is also a matter of consideration for a DALI based system.
6. Until now, there has been a limited availability of DALI compatible controls in the European and American markets.

Although DALI has been described by many experts as revolutionary, this technology has seen a rather slow adoption to the global market. The market segment where DALI seems to have a bright future is the commercial sector. In the coming days, lighting automation and personal control over the lighted environment will be of greater importance than ever before, and DALI is well equipped to exploit that market demand.

4.5 The DALI Lighting Laboratory at Penn State

The new lighting laboratory in the department of Architectural Engineering at Penn State is the first educational research facility in the country equipped with DALI technology. It has been developed in a 26' X 45' room with removable ceiling tiles. Lamps, ballasts and luminaires have been donated by different manufacturers like Tridonic, Erco, Zumtobel and Peerless. The laboratory has eight 20A lighting circuits and four Tridonic DALI Busmaster and COM ports capable of handling 4 X 64 DALI devices. At least ten different types of DALI luminaires have been installed in the laboratory [Figure 4-1 and Figure 4-2]. The luminaires, including wallwashers, spotlights, direct and direct indirect luminaires, downlights etc, help achieve many different lighting conditions.

Figure 4-1: DALI Luminaires with the Whip-flex Cords Mounted on the Ceiling

Tridonic's WinDimNet® software allows full control of each of these luminaires through the Internet from anywhere in the world. A Webcam is also installed in the laboratory to allow the user to view the lighting effect while controlling the luminaires over the Internet. A portion of this laboratory was used in this research.

Figure 4-2: Different DALI Luminaires installed on the ceiling

As discussed in Section **5.1.3**, a software application was written specifically for CamSensor - WinDimNet® was not used.

A more detailed description of the lighting laboratory is provided in [**50**], [**51**] and [**52**].

Chapter 5

TEST SETUP AND EQUIPMENT USED

5.1 Description of CamSensor

CamSensor consists of both hardware and software components as listed below:

1. Camera Module for capturing images that are used to obtain illuminance information
2. The Master Control is the computer that centrally oversees the entire system
3. CamSensor software
4. DALI Busmaster that controls the DALI system
5. DALI luminaires that are controlled by CamSensor software
6. The task area where one or more target light levels are to be maintained

Figure 5-1 shows the block diagram of the system.

The following subsections describe the different components of CamSensor.

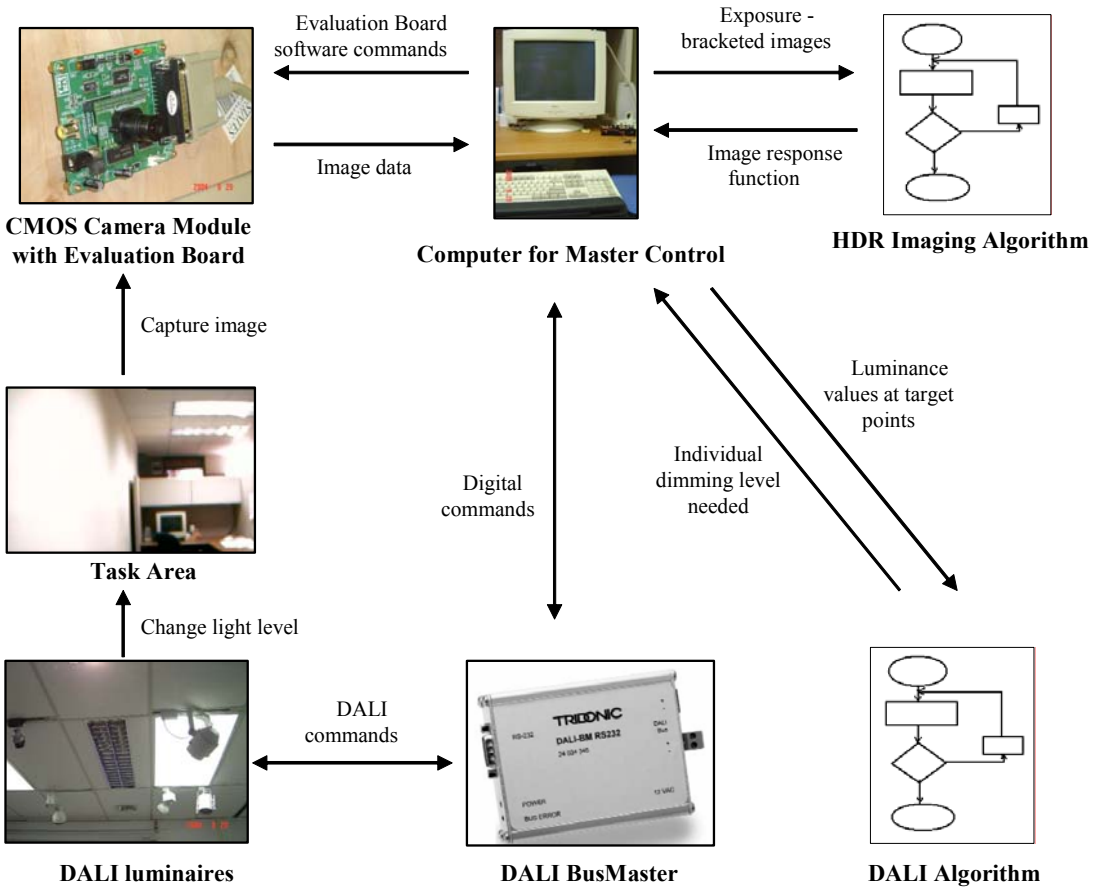

Figure 5-1: Block Diagram of CamSensor

5.1.1 The Camera Module

Figure 5-2 shows the CEV38 evaluation board with C3188A camera module. It is a 1/3" color camera module using a CMOS image sensor OV7620 manufactured by Omnivision.

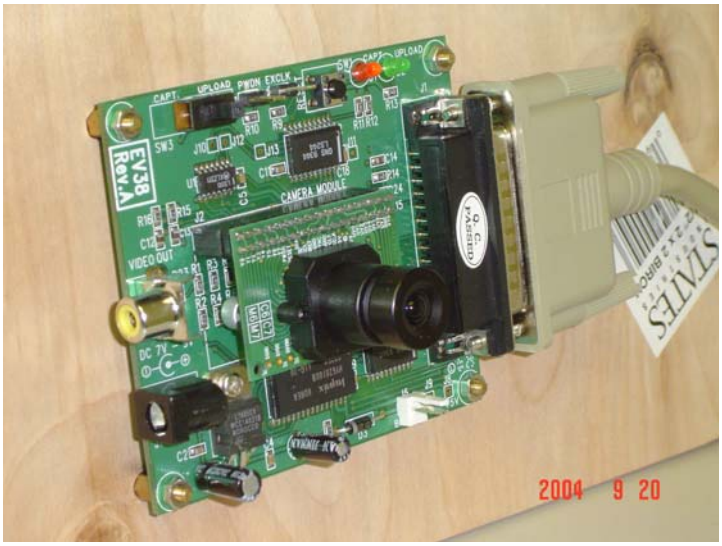

Figure 5-2: C8166A Camera Module

All camera functions, such as exposure, gamma, gain, white balance, color matrix, windowing etc, are programmable through an I^2C interface [41]. The image sensor has an array size of 664 X 492 pixels and 500:1 electronic exposure. It has 8 bit/16 bit data output formats, namely, YCrCb 4:2:2, GRB 4:2:2 and RGB raw data format. The available image size is 314 X 208 pixels.

The key specifications for OV7620, the single-chip CMOS image sensor, are discussed in Appendix 2. The C3188A camera module based on this image sensor and the CEV38 Evaluation Board for the camera module are third-party products developed by CoMedia Ltd., Hong Kong and supplied by different vendors in the US. Figure 5-3 shows a block diagram of the EV 38 [42]. The evaluation board can be connected to the computer through a parallel port cable. It also comes with evaluation software that can be used to capture and upload images (from the board to the computer) through the evaluation board. Unfortunately, the evaluation software is available only in the Windows 95/98 platform.

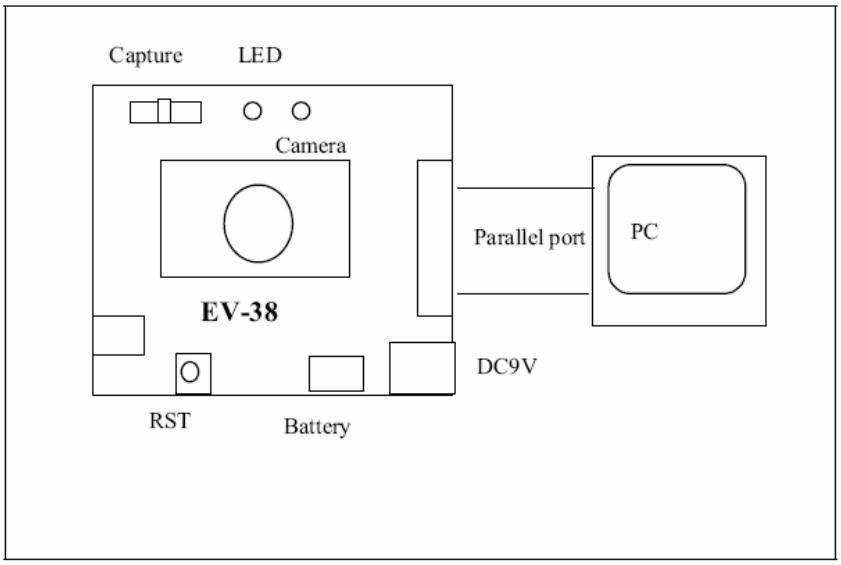

Figure 5-3: EV38 Block Diagram

Figure 5-4 shows a screen shot of the EV38 evaluation software. The Auto mode has to be disabled to change the exposure setting. The *Capture/Upload* button on the evaluation board is pushed to the *Capture* position to capture an image. Then, it is pushed back to the Upload position, and the Upload button in the evaluation software is pressed to fetch the image data from the evaluation board to the computer. It can then be saved as a bitmap image.

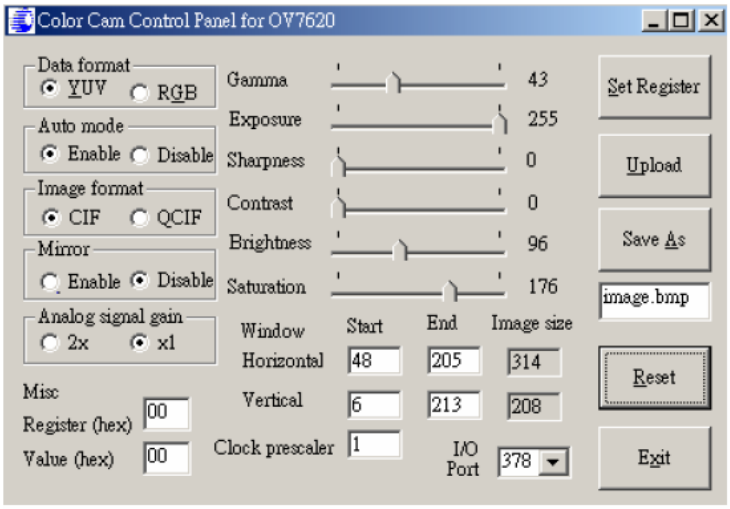

Figure 5-4: EV38 Evaluation Software

At lower exposure settings, e.g., 2, 4 or 8, the sensor has an occasional banding issue, with wide horizontal bands appearing on the image taken with lower exposure settings. At times this effect is more aggravated. Computer Vision researchers elsewhere have encountered the same problem [46]. This effect is more likely to be seen at low exposure settings under low light levels [44]. Figure 5-5 shows this banding effect for an exposure setting of 16 seen at an early stage of the work.

Because of this banding issue (and also because of the low resolution of the images), standard High Dynamic Range (HDR) imaging software like Photosphere could not be used to generate a High Dynamic Range image from a series of images captured by the Camera Module [45].

However in the later stage of this research, the banding problem was not noticeable, even at low exposure values.

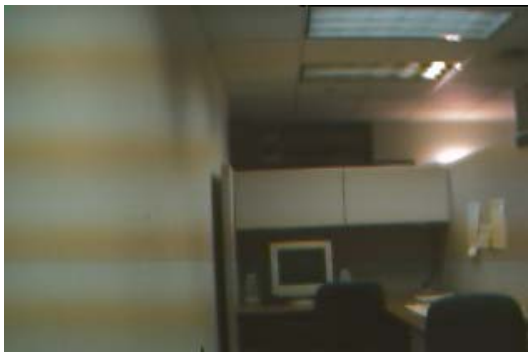

Figure 5-5: Banding Issue

5.1.2 The Master Control

The computer is the master control that is central to the entire system. It is connected to the CMOS camera module through a parallel cable and to the DALI Busmaster through a serial cable. Since the evaluation software works only on a Windows 95/98 platform, and the available systems do not use these operating systems, a separate computer was necessary to interface with the camera module. Another computer operating on Windows XP was used to control the DALI luminaires. But, for the sake of simplicity, it can be assumed there is only one computer used for master control by CamSensor. Only the image capturing process in the present CamSensor system is manual. However in a full-fledged system, the image capturing will be controlled by CamSensor software.

5.1.3 CamSensor Software

The software for CamSensor, residing in the master control, can be divided into two main parts – one that deals with the HDR imaging and the other that handles the DALI algorithm. HDR imaging routines are executed during both the calibration and the operation phases, whereas the DALI routines are called only during the regular operation of CamSensor. Details of the steps involved in these two phases are discussed in Chapter 7.

5.1.4 DALI Busmaster

The DALI [Figure 5-6] Busmaster is the bridge between the luminaires that use the DALI communication protocol and the computer that uses a standard RS232 serial communication protocol. The Busmaster controls the way messages are exchanged between the master control (i.e., the computer) and the slaves (i.e. the luminaires). The Busmaster, in turn, is linked to a junction box which is not shown in the figure. The luminaires are connected to the junction box through DALI cables and T-connectors.

Figure 5-6: DALI Busmaster (Courtesy: TridonicAtCo)

5.1.5 DALI Luminaires

Six DALI luminaires were used in the test setup. Figure 5-7 shows the part of the classroom-cum-lighting laboratory with all the DALI luminaires. Six recessed DALI luminaires were used as dimmable electric lights. L-1 and L-2 were direct VDT fixtures (2 lamps, T8, 32W), while L-3, L-4, L-5 and L-6 were recessed louvered direct fixtures (2 lamps, T5, 54W).

Four recessed 2 X 4 troffers (4 lamps, T5, 32W) were used in the final experiment to simulate daylight, as daylight availability in the space was very limited. These were dimmable DALI luminaires, but throughout the experiment, they were operating at full output. They have been marked as DL in Figure 5-7.

Additionally, some luminaires were used to maintain a constant light level during some experiments (described as nondimmable luminaires in the rest of the document). This was required so as to improve the signal-to-noise ratio of the camera. In the last experiment described in Chapter 6 and in the final experiment described in Chapter 7, four CFL downlights (CFL 42W)

each dimmed to 30% were used as nondimmable luminaires. In all other cases, two recessed 2 X 4 troffers (4 lamps T8 32W) were used, unless otherwise mentioned.

Figure 5-7: Six DALI Luminaires with Numbering

5.1.6 The Task Area

Figure 5-8 shows the target points with numbers to identify them. These labels have been followed throughout this document.

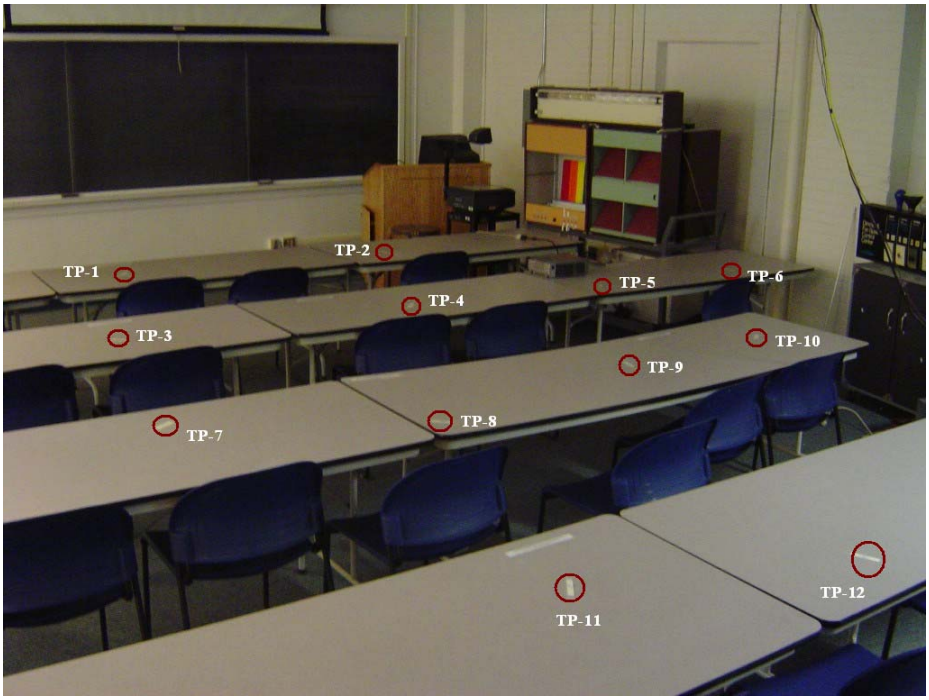

Figure 5-8: Twelve Target Points with Labels

Figure 5-9 shows the floor plan of the lighting laboratory showing the locations of the DALI luminaires and test points used in this work. L-1 through L-6 are dimmable DALI luminaires and the luminaires marked as DL are for simulating daylight.

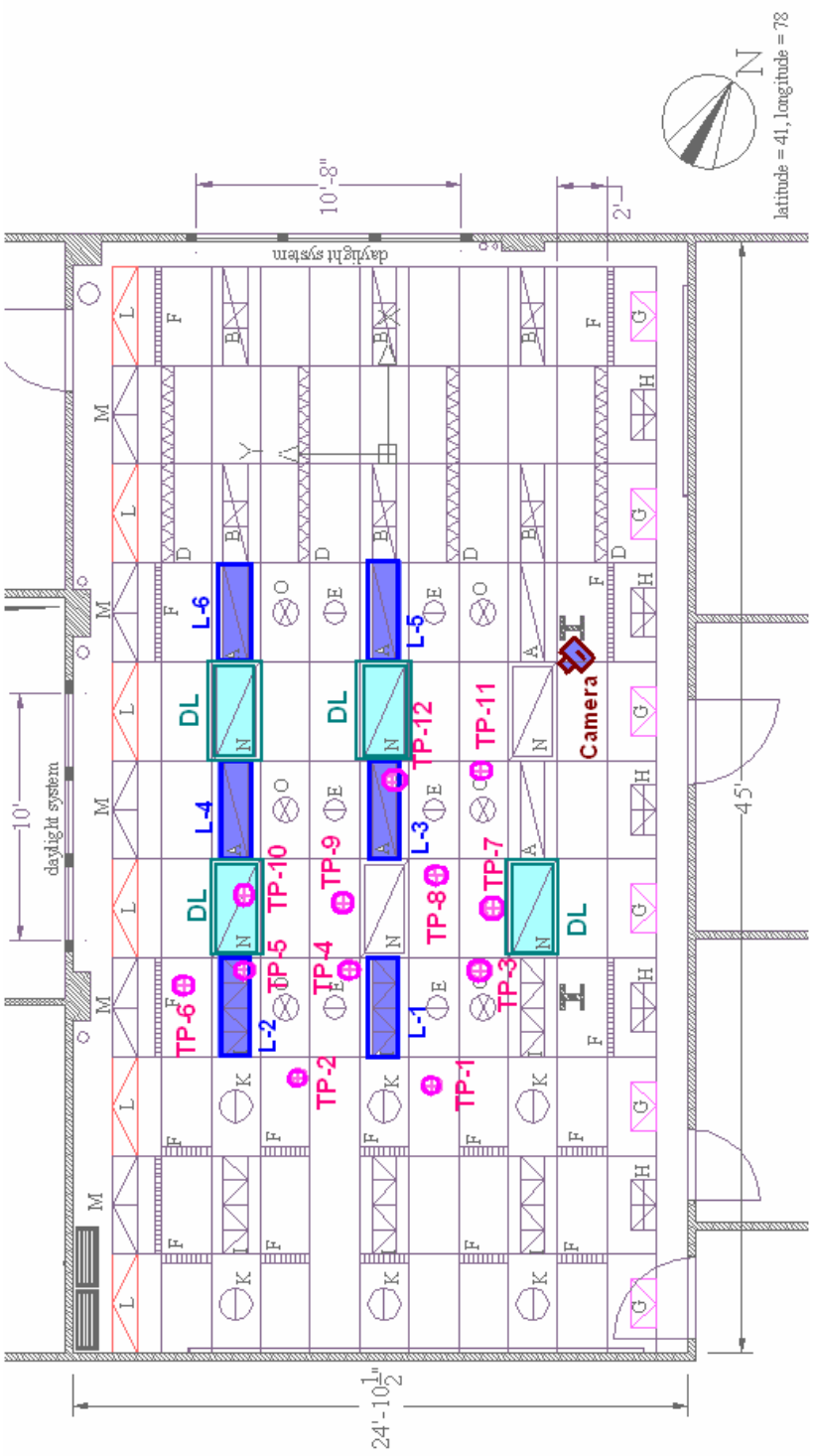

Figure 5-9: Ceiling Plan of the Lighting Laboratory Showing the Locations of the Luminaires and the Test Points (Original Drawing by Courtesy of Dr. Martin Moeck)

Chapter 6

EXPERIMENTS AND RESULTS

This chapter describes different experiments performed on CamSensor that evaluate the performance of the system. There are several aspects in the calibration and operation of CamSensor that were investigated. These include: i) estimation of luminance from the scene image, ii) estimation of illuminance from luminance and iii) dimming the electric lights based on the estimated illuminance at different test points. Considering these issues individually helped determine the various sources of error and the amount of error contributed by these sources. Knowledge gained from these experiments is utilized in the next chapter, where the method of calibration and operation is detailed, followed by the final experiment based on this method.

A total of ten experiments were performed. Experiments 1 through 4 validate the principal research hypotheses, and involve no imaging. Experiments 5 through 7 determine the errors associated with the imaging system. Experiments 8, 9 and 10 identify the most appropriate procedure to calibrate and operate CamSensor. Following is the list of the experiments that will be discussed in subsequent sections:

1. The first experiment was conducted to determine the relationship between the arc power levels of DALI ballasts and the corresponding light output from DALI luminaires. It will be shown that the relationship is nonlinear and needs to be taken into account in the CamSensor algorithm.
2. The second experiment considered the effect of different electric lighting conditions on the ratio of illuminance and luminance measured on a Lambertian surface. The

experiment showed that unless there was a specular reflection, the deviation in the ratio was not significant.

3. The effect of different daylight conditions on the ratio of illuminance and luminance on different surfaces was investigated in this experiment.
4. The fourth experiment was to determine the effect of different light levels on the ratio of illuminance and luminance measured on different surfaces. Another goal was to determine whether the ratio of luminance with a diffuse surface and luminance on the desk (without a diffuse surface) at full output of a luminaire can be used to determine illuminance at any other dimming level due to the same luminaire, assuming the luminance on the desk is known at that level.
5. The effects of spatial location of the pixel and the exposure settings of the camera on the estimation of surface luminance from radiance (computed from the scene image) were considered in the fifth experiment.
6. The next experiment was related to the camera response function derived by the High Dynamic Range imaging technique. The goal was to consider the effect of changing the smoothness parameter in the algorithm. Different values of this parameter were used to compute the image response function, which was then used to compute radiance. It was found that a change in this parameter did not greatly affect the results.
7. The seventh experiment was conducted to determine the error in estimating luminance from radiance at different test points.
8. This experiment determined whether illuminance due to multiple luminaires dimmed to different levels could be estimated, assuming the luminance values with and without the diffuse surface at full output were known for each of the luminaires.
9. In the ninth experiment, the Lambertian characteristics of different surfaces were investigated. This helped determine that bleached baking flour pressed evenly on a

piece of paper was the most appropriate Lambertian surface for the calibration of CamSensor.

10. The last experiment was a final verification of the anticipated method of operation of CamSensor. In this experiment, the illuminance values were estimated from the available information and the error associated with this method was determined. Imaging was not involved in this experiment in order to isolate the error due to the approximations associated with the method. The final experiment, described in Chapter 7, uses the same procedure as followed in this test.

In the subsequent discussions, the term "dimming level" has been used quite frequently. This term refers to the arc power input of the lamps inside DALI luminaires, and is the same as the luminaire ballast output. Note that the dimming level is not synonymous with the light level for a DALI luminaire. For example, 60% dimming level means a DALI luminaire is operating at 60% of full ballast power output. Theoretically, the minimum dimming level for a DALI ballast can be 0.1%. However, DALI ballasts have a "physical minimum level" which is the minimum arc power level and is determined by the ballast electronics. The value of this minimum level is stored in the ballast memory.

In many of the experiments described below, a constant light level provided by the nondimmable luminaires has been maintained during the experiment. This was done for the following reasons:

1. Using a constant light level increases the signal-to-noise ratio for the image sensor. For example, a difference of 2 units in the reading from an actual value of 10 units gives 20% measurement error, but if the actual level is 30 units, the measurement error

comes down to 6%. The percent error due to noise increases as the light level is lowered[8].

2. Two recessed lensed troffers were used as nondimmable luminaires mainly to show that the error in estimating illuminance from luminance was more in case of troffers. This was due to the specular reflections, as the troffers were more at a mirror angle with respect to the measurement position. This would not be a problem if different combination of luminaires, contributing from different directions in different amount, were not used. This issue is further discussed in Section **6.9**. Most of the times, incandescent spotlights, or as in the final experiment, fluorescent downlights were used, whose contributions were guaranteed to be non-specular when viewed from the camera vantage point. That way, this source did not introduce additional error due to specular reflections.

3. Using incandescent spotlights as nondimmable luminaires showed that bright spots of light on the wall would work with CamSensor even if they are not present during the calibration of the system. Conventional photosensors will not perform well under this kind of lighting condition. Incandescent spots are sources of infrared, just like daylight, so they basically simulated direct sunlight hitting the wall. Although the spotlights were at a much lower intensity, they were sufficient to cause local saturation in the scene image, but the test points did not suffer from the saturation problem.

---

[8] This is true for most of the electronic devices. In fact S/N ratio is an important parameter for many devices.

6.1 Relationship between the Arc Power Level of a DALI Luminaire and the Illuminance at Different Test Points As Measured

The aim of this test was to determine whether the illuminance at a test point changed proportionally as the dimming level of a luminaire was changed. For example, if a luminaire arc power input were changed from 100% to 50%, this test was to verify that the illuminance at the test point changed by 50% as well.

Each of the six DALI luminaires was individually dimmed from 100% to 10% in steps of 10% and the illuminance at each dimming level was recorded at a test point closest to the luminaire under test. Although the percent light output at a given dimming level of a luminaire was essentially the same at different test points, the test point closest to the luminaire had the greatest contribution, which was helpful in taking proper measurement. Illuminance levels were measured with an illuminance meter. Figure 5-7 and Figure 5-8 in the previous chapter show the locations of the test points and the luminaires respectively.

Table 6-1 lists the percent illuminance levels for different luminaires at different percent dimming levels. These values are obtained by dividing the light output at different dimming levels of each luminaire by the light output at full power for the same luminaire. Figure 6-1 shows the plots of the same data.

Table 6-1: % Ballast Output vs. % Light Output (in lux) for Different Luminaires

% Level	L-1	L-2	L-3	L-4	L-5	L-6
100	100	100	100	100	100	100
90	91.07	90.64	93.66	91.59	93.34	93.88
80	82.82	82.64	88.18	85.29	87.63	86.59
70	73.17	73.53	82.36	80.26	80.74	79.76
60	65.46	65.57	76.48	74.71	74.67	73.41
50	55.57	55.85	68.9	67.3	67.18	66.59
40	45.5	45.55	61.1	59.15	58.74	59.06
30	33.59	33.68	49.68	47.88	47.68	48
20	22.48	22.6	36.6	35.29	35.2	35.53
10	10.8	10.65	19.45	18.68	18.55	19.06

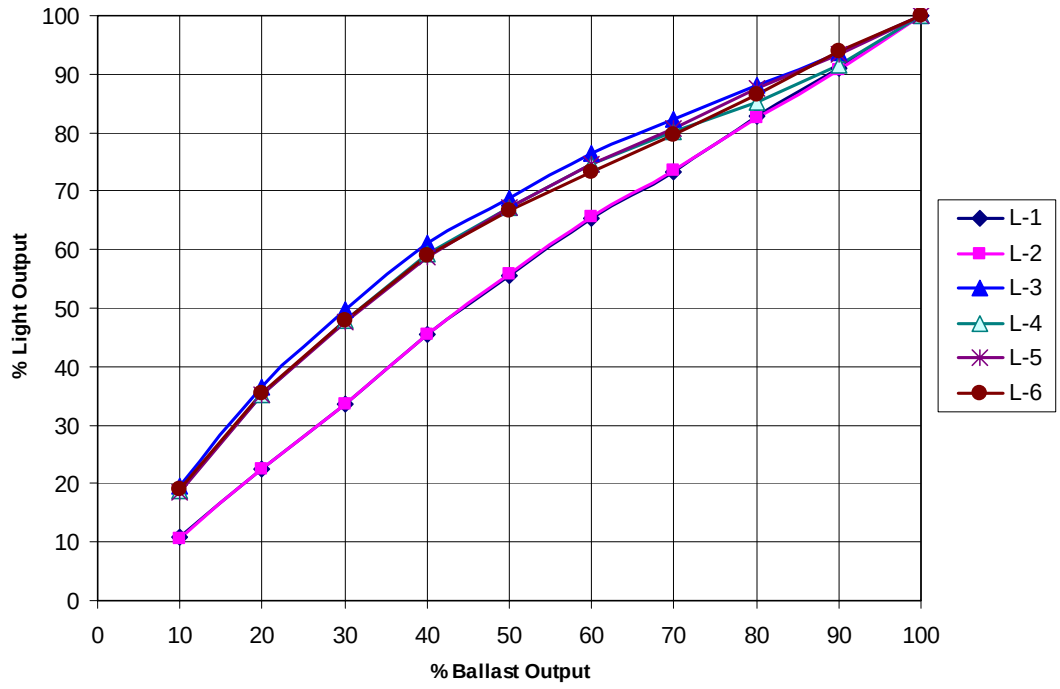

Figure 6-1: Relationship Between the % Light Level and % Ballast Output At Different Test Points

As is evident from the graph, the relationship between the illuminance levels at the test points and the dimming level (or arc power level) of the DALI luminaire follow a nonlinear pattern. This can be assumed to be due to the fact that DALI ballasts follow a logarithmic dimming pattern as discussed in Chapter 5. It should be noted that the lower graph is more linear in nature and represents luminaires L-1 and L-2, which have 2 lamps, T8, 32W. Each of the luminaires L-3 through L-6 has 2 lamps, T5, 54W and shows similar dimming pattern. So, the relationship between the % ballast output and the % light output is dependent on the type of ballast. All T8 ballasts follow similar pattern, and so do all T5 ballasts.

Table **6-2** shows the average values of percent light outputs at different dimming levels for T8 and T5 ballasts. These values have to be considered while dimming the DALI luminaires so as to achieve the desired light levels.

Let us consider an example. If the required light level due to L-3 (with T5 lamps) is determined by the CamSensor algorithm to be 70% of the full light output, then the required dimming percentage must be between 60% and 50% and must be calculated through interpolation. For a dimming level of 60%, the light output is 74.82% and for a dimming level of 50%, the light output is 67.49%. So, $(60 - x) / (60 - 50) = (74.82 - 70) / (74.82 - 67.49)$, from which we get $x = 53.42$. Thus we must dim the ballast to 53% (rounded off to an integer) of full power in order to obtain 70% of full light output.

Table 6-2: Percent Light Level vs. Percent Ballast Output for Different Ballasts

% Level	T8-32W	T5-54W
100	100	100
90	90.86	93.12
80	82.73	86.92
70	73.35	80.78
60	65.52	74.82
50	55.71	67.49
40	45.53	59.51
30	33.64	48.31
20	22.54	35.66
10	10.73	18.94

In order to account for the nonlinearity of the DALI dimming curve in the real-life situation, images of the workplane(s) will be captured at different dimming levels one luminaire at a time. Then the radiance levels will be evaluated at the test points from each of these images and corresponding luminance and illuminance values will be estimated. From this information, the relationship between the percent light level and the percent ballast output can be determined and can later be used to compute the required dimming levels. The total number of images needed to be captured in this process is equal to the number of luminaires times the number of dimming levels (say 10). This must be a part of the calibration process and the dimming curve data must be saved for future reference.

6.2 Effect of Different Electric Lighting Conditions on the Ratio of Illuminance and Luminance as Measured For a Lambertian Surface

This test was conducted to determine whether the ratio of illuminance and luminance on an assumed Lambertian surface remain constant for different lighting conditions. This information is very important for this work since the computed radiance value at a point, which is proportional to the luminance, must be converted to illuminance. Thus, knowledge of the impact

of different lighting conditions on the E/L ratio is vital. It is not possible to directly convert luminance to illuminance as measured on a non-Lambertian (that is specular) surface. So to start with, a Lambertian surface must be considered. White bond papers and grey papers with rough texture were used for this purpose and the results were very similar. Results with the white paper are summarized here.

Different test points and different luminaires were considered. They were chosen in such a way that the chances of specular reflections at the test points were higher due to the relative positions of these points, the luminaires and the measurement position. Two measurement directions were chosen for luminance, one was the same as the camera location (View-1) and the other was directly opposite this location across the room (View-2). The two measurement locations were 180° apart with respect to the test point TP-8. Figure **6-2** shows both measurement positions in plan view. An Illuminance meter and a luminance meter were used for the measurement. The white paper was placed right on the marked test points.

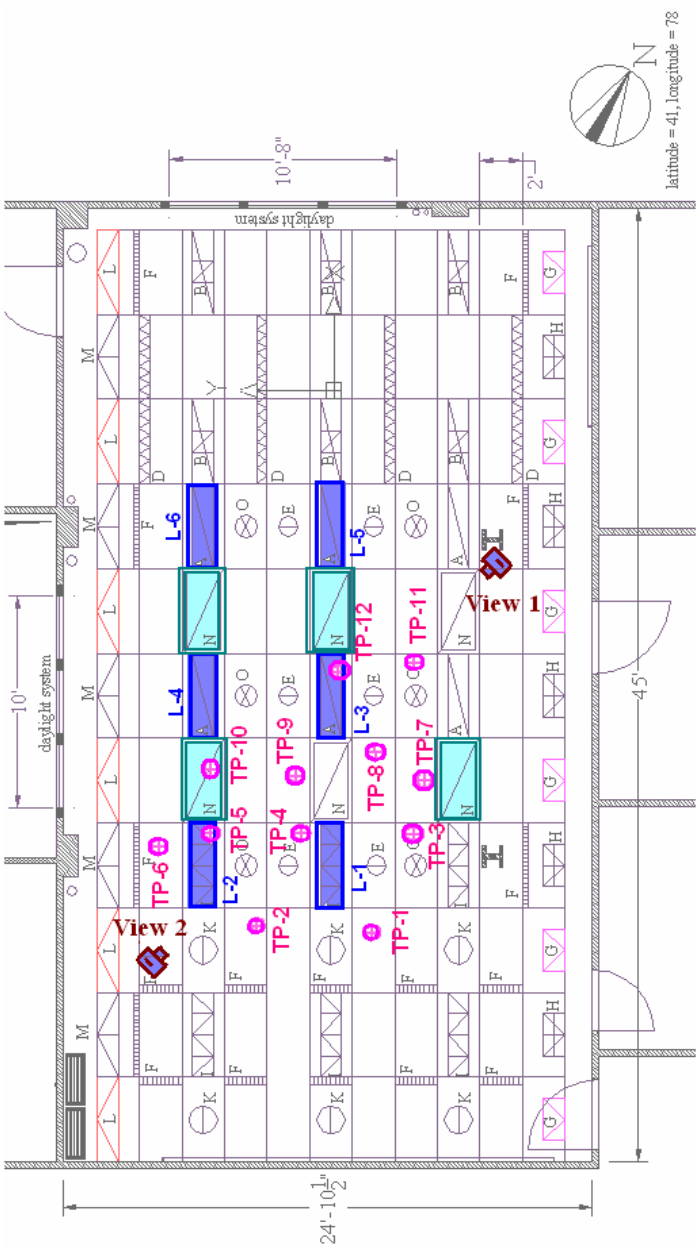

Figure 6-2: View-1 and View-2

Since, for a Lambertian surface, E * ρ = π * L, where E, ρ and L are the illuminance, reflectance of the surface and the luminance (which is the same in all directions) respectively, the E/L ratio should be equal to π/ρ. The reflectance, ρ, of the white paper was found to be close to 78%. So the E/L ratio for the white paper used in the experiment should always be approximately

4.03. However, even the white bond paper is not a perfect Lambertian surface, so an error will be introduced. The error will be more when the incident light makes a mirror angle at the test point with respect to the measurement point. In the tables provided below, this error (deviation of the E/L ratio from 4.03) is listed. It is to be noted that the nondimmable lights (ND), which are incandescent spotlights, are always on. As in other cases, the purpose was to reduce the amount of luminance measurement error relative to the actual value. No light source other than the DALI luminaires and the spotlights are present.

Table 6-3 lists the E/L ratios for TP-8 as seen from View-1 for different lighting conditions. The average ratio and the absolute deviation from the mean [$\Sigma(X\text{-}X_{av})$ / n] are also listed. Each of six luminaires is turned on individually to 100%. All + ND signifies when all the luminaires are fully on, along with the nondimmable lights.

Table 6-3: E/L Ratios for TP-8 View-1 (E in lux and L in cd/m^2)

Condition	E	L at TP-8_View-1	Ratio	% Error
ND	19.4	4.85	4	-0.74
All + ND	588	145	4.06	0.74
L-1+ND	180.9	46	3.93	-2.48
L-2+ND	73	22	3.32	-17.62
L-3+ND	278	63.1	4.41	9.43
L-4+ND	91	23.8	3.82	-5.21
L-5+ND	32.7	7.83	4.18	3.72
L-6+ND	28	6.94	4.03	0
		average =	3.969	
		abs deviation from mean =	0.209	

Note that light coming from L-2 reflects almost at a mirror angle at TP-8 when seen from View-1. Contributions from L-5 and L-6 cause diffuse reflections in the direction of the measurements, so the error is less. Table 6-4 shows how the error drastically reduces when the luminance is measured from View-2. This is obvious since a specular reflection cannot occur simultaneously at two opposite directions as long as the light is incident from one single direction.

Table 6-4: E/L Ratios for TP-8 View-2 (E in lux and L in cd/m^2)

Condition	E	L at TP-8_View-2	Ratio	% Error
ND	19.4	4.79	4.05	0.5
All + ND	588	140	4.2	4.22
L-1+ND	180.9	42	4.31	6.95
L-2+ND	73	18.9	3.86	-4.22
L-3+ND	278	66.3	4.19	3.97
L-4+ND	91	23	3.96	-1.74
L-5+ND	32.7	8.3	3.94	-2.23
L-6+ND	28	7	4	-0.74
		average =	4.064	
		abs deviation from mean =	0.127	

For some conditions, View-1 gives better results than View-2. Table 6-5 and Table 6-6 list the E/L ratios at TP-9 due to L-2 and L-5. While light from L-2 causes specular reflection at TP-9 for View-1, the same situation arises for L-5 and View-2. Interestingly, the errors seem quite symmetrical.

Table 6-5: E/L Ratios for TP-9 View-1 (E in lux and L in cd/m^2)

Condition	E	L at TP-9_View-1	Ratio	% Error
L-2+ND	198.5	42.9	4.63	14.89
L-5+ND	25.7	6.13	4.19	3.97
		average =	4.41	
		abs deviation from mean =	0.22	

Table 6-6: E/L Ratios for TP-9 View-2 (E in lux and L in cd/m^2)

Condition	E	L at TP-9_View-2	Ratio	% Error
L-2+ND	198.5	51.3	3.87	-3.97
L-5+ND	25.7	7.43	3.46	-14.14
		average =	3.665	
		abs deviation from mean =	0.205	

From this test, it can be concluded that the specular reflection at a test point causes the E/L ratio to change to some extent. This is likely to occur when light falls on a test point only from a mirror angle for the camera positions. In the worst possible scenario, if the nondimmable light (or daylight, in a real-life condition) causes specular reflections at one or more test points, all conditions will include that source and so all E/L ratios will deviate from the expected value. **Thus, specular reflections from daylight at any test point must be avoided by placing the CamSensor at a strategic location**.

If two CamSensor units can be placed at diagonally opposite positions across the room, and radiance values are computed with white paper on the test points (radiance proportional to both illuminance and luminance), the lower of the two computed values can be used to reduce errors. This method can be used without the white paper (radiance proportional to luminance) as well. Reflectance of a non-Lambertian surface depends on the directions of incident and reflected light. If no light source causes a specular reflection in a particular view position, the reflectance of a non-Lambertian surface can be assumed to be the same as the average reflectance of the surface. As will be discussed later, the calibration data include radiance values with and without a Lambertian surface placed on the test points.

Note that the relative positions of a test point and the electric lights do not change. So the reflectance of the desk for the combination of a given test point and a given luminaire always remains the same, whether or not the luminaire causes specular reflection at that point. But since the direction of the daylight can change over the course of the day, the E/L ratio on the desk can be significantly different from the average value in cases where specular reflections of daylight occur.

6.3 Effect of Different Daylight Conditions on the Ratio of Illuminance and Luminance for Different Surfaces

In the previous experiment, the effect of different electric light conditions on the E/L ratio was investigated. But as the daylight condition changes throughout the day, its effect on this ratio might be more crucial since the daylight contribution can be more significant than the electric light contribution in daylit spaces. In this test, illuminance and luminance values were measured with meters on three different surfaces throughout the day. The surfaces considered were: the desk, white bond paper and bleached flour spread smoothly across a piece of paper [Figure 6-3]. The three surfaces were adjacent to each other, although the illuminance values were separately measured for each of the surfaces. The desk was somewhat specular when viewed from a direction opposite the window, whereas the bond paper and powdered flour were fairly diffuse. A classroom with a fair amount of daylight was used for the test. A sunny day with a clear sky was chosen so as to observe the effect of a change of daylight on the E/L ratio throughout the day.

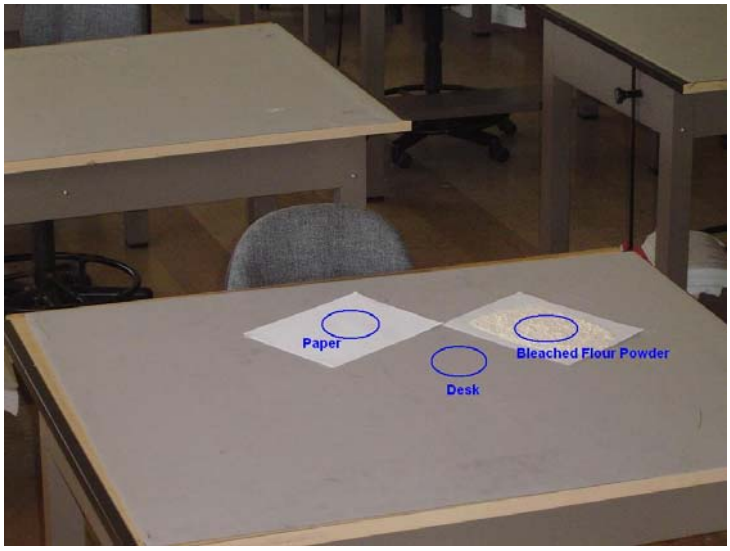

Figure 6-3: Three Surfaces Considered in the Current Test

Luminance measurement was done from three different positions, thereby getting three sets of illuminance/luminance ratios for each round of measurement. Figure 6-4 shows a schematic of the room where the experiment was performed. Views of the desk from three measurement locations are also shown in Figure 6-5, Figure 6-6 and Figure 6-7.

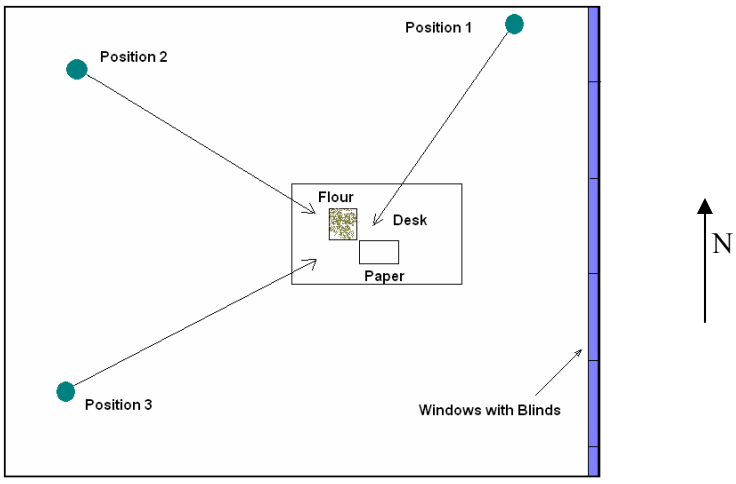

Figure 6-4: Schematic of the Measurement Positions and the Desk

Figure 6-5: View of the Desk from Position 1

Figure 6-6: View of the Desk from Position 2

Figure 6-7: View of the Desk from Position 3

Position 1 and 3 are almost diagonally opposite each other. Figure 6-8, Figure 6-9 and Figure 6-10 further show the relative positions of the surfaces and the meter for all three positions. The meter was about 1.68 meters (5.5 feet) above the desk.

Figure 6-8: Measuring Luminance from Position 1

Figure 6-9: Measuring Luminance from Position 2

Figure 6-10: Measuring Luminance from Position 3

Three different daylight conditions were chosen, namely, one with closed blinds, one with 0° (horizontal) blinds and one with no blinds. The experiment started at 11:10 AM on December 27 2004 and was conducted until 4:50 PM, with illuminance and luminance readings taken at one hour intervals (except for the last two measurements, which were performed at half hour intervals, as the daylight level was reducing fast).

Figure 6-11, Figure 6-12, Figure 6-13, Figure 6-14, Figure 6-15, Figure 6-16 and Figure 6-17 show the lighting conditions throughout the day. A closed blind condition was not considered for the 4 PM and 4:30 PM tests as the resultant illuminance was low. For the same reason, a horizontal blind condition was not considered for the 4:30 PM test. Horizontal blind and no blind conditions were not considered for the 2 PM test as well, since direct sunlight hit the desk during this period, which was not a good condition for the test.

Figure **6-11**: Daylight condition at 11 AM: closed blinds, horizontal blinds and no blinds

Figure **6-12**: Daylight condition at 12 noon: closed blinds, horizontal blinds and no blinds

Figure **6-13**: Daylight condition at 1 PM: horizontal blinds and no blinds (closed blinds condition is very similar to that at 12 noon)

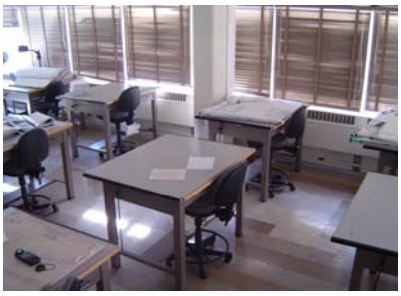

Figure **6-14**: Daylight condition at 2 PM: closed blinds and no blinds

Figure **6-15**: Daylight condition at 3 PM: closed blinds, horizontal blinds and no blinds

Figure **6-16**: Daylight condition at 4 PM: horizontal blinds and no blinds

Figure 6-17: Daylight condition at 4:30 PM: no blinds

Table 6-7 lists the values of illuminance (E) and luminance (L) at different times of the day for all three surfaces. The time of each test is noted in the table. For example, the 11 AM test was actually conducted from 11:10 AM to 11:30 AM. The luminance readings were recorded as quickly as possible, ensuring that the variation in the illuminance on the desk before and after the luminance measurement was not significant.

Table 6-7: Measured Illuminance (lx) and Luminance values (cd/m^2)

Time	Metric	Position	Blind Closed			0 degree Blind			No Blind		
			Desk	Paper	Flour Powder	Desk	Paper	Flour Powder	Desk	Paper	Flour Powder
11:10 AM - 11:30 AM	E	-	103.4	107.1	99.8	342	369	332	989	1143	938
	L	1	14	25.5	20.9	41.6	90.5	76.5	131	283	220
		2	14.7	27	19.9	74.6	102	61.6	192	314	183
		3	15.6	27.8	20.2	133	107	58.9	351	337	186
12:10 PM - 12:30 PM	E	-	86.1	89.1	84.7	558	588	555	1358	1427	1257
	L	1	12.9	21.6	17.2	67.5	144	120	169	353	280
		2	12.4	22	16.3	105	160	97.4	233	383	236
		3	23	32.8	17	240	179	99.7	434	410	237
1:10 PM - 1:30 PM	E	-	65.8	67.3	65.8	711	752	683	1416	1528	1364
	L	1	11.1	16.8	13.5	89.1	188	158	183	379	299
		2	9.94	17	13.1	132	205	127	246	413	254
		3	9.82	16.9	13.7	274	233	128	455	449	256
2:10 PM - 2:33 PM	E	-	78.2	80.4	77.3						
	L	1	14.7	19.4	16.4						
		2	12	19.8	15.6						
		3	11.7	19.7	16.3						
3:10 PM - 3:30 PM	E	-	52.6	53.8	49.9	673	651	726	401	408	405
	L	1	9.15	12.5	10.4	72.6	140	138	51.5	109	94.7
		2	8.4	12.5	9.65	162	153	107	143	126	60.6
		3	7.72	11.9	9.49	188	152	99.3	174	122	60.2
4:00 PM - 4:15 PM	E	-				127.2	129.4	130.7	189.3	43.3	169.2
	L	1				13	31.1	29.3	18.6	43.3	37.5
		2				73.4	42	19.5	96.8	66.5	27.2
		3				69.6	39.4	19.1	82.4	59.4	28.2
4:40 PM - 4:50 PM	E	-							61.6	63.5	55.5
	L	1							5.59	13.1	11.3
		2							27.4	17.2	7.15
		3							16.9	13.9	6.64

Table 6-8 shows the E/L ratios for each of the conditions. From that, Table 6-9 has been derived so as to list the E/L ratios for a particular surface under different lighting and blind conditions.

Table 6-8: Illuminance/Luminance Ratios Under Different Conditions

Time	Position	Blind Closed			0 degree Blind			No Blind		
		Desk	Paper	Flour Powder	Desk	Paper	Flour Powder	Desk	Paper	Flour Powder
11:10 AM - 11:30 AM	1	7.386	4.2	4.775	8.221	4.077	4.34	7.55	4.039	4.264
	2	7.034	3.967	5.015	4.584	3.618	5.39	5.151	3.64	5.126
	3	6.628	3.853	4.941	2.571	3.449	5.637	2.818	3.392	5.043
12:10 PM - 12:30 PM	1	6.674	4.125	4.924	8.267	4.083	4.625	8.036	4.042	4.489
	2	6.944	4.05	5.196	5.314	3.675	5.698	5.828	3.726	5.326
	3	3.743	2.716	4.982	2.325	3.285	5.567	3.129	3.48	5.304
1:10 PM - 1:30 PM	1	5.928	4.006	4.874	7.98	4	4.323	7.738	4.032	4.562
	2	6.62	3.959	5.023	5.386	3.668	5.378	5.756	3.7	5.37
	3	6.701	3.982	4.803	2.595	3.227	5.336	3.112	3.403	5.328
2:10 PM - 2:33 PM	1	5.32	4.144	4.713						
	2	6.517	4.061	4.955						
	3	6.684	4.081	4.742						
3:10 PM - 3:30 PM	1	5.749	4.304	4.798	9.27	4.65	5.261	7.786	3.743	4.277
	2	6.262	4.304	5.171	4.154	4.255	6.785	2.804	3.238	6.683
	3	6.813	4.521	5.258	3.58	4.283	7.311	2.305	3.344	6.728
4:00 PM - 4:15 PM	1				9.785	4.161	4.461	10.18	1	4.512
	2				1.733	3.081	6.703	1.956	0.651	6.221
	3				1.828	3.284	6.843	2.297	0.729	6
4:40 PM - 4:50 PM	1							11.02	4.847	4.912
	2							2.248	3.692	7.762
	3							3.645	4.568	8.358

Figure 6-18, Figure 6-19 and Figure 6-20 are the graphical representation of the same data.

Table 6-9: Illuminance/Luminance Ratios for Different Surfaces

Condition	Desk-Posn1	Desk-Posn2	Desk-Posn3	Paper-Posn1	Paper-Posn2	Paper-Posn3	Flour-Posn1	Flour-Posn2	Flour-Posn3
11 AM_CL-BL	7.386	7.034	6.628	4.2	3.967	3.853	4.775	5.015	4.941
12 Noon_CL-BL	6.674	6.944	3.743	4.125	4.05	2.716	4.924	5.196	4.982
1 PM_CL-BL	5.928	6.62	6.701	4.006	3.959	3.982	4.874	5.023	4.803
2 PM_CL-BL	5.32	6.517	6.684	4.144	4.061	4.081	4.713	4.955	4.742
3 PM_CL-BL	5.749	6.262	6.813	4.304	4.304	4.521	4.798	5.171	5.258
11 AM_0D-BL	8.221	4.584	2.571	4.077	3.618	3.449	4.34	5.39	5.637
12 Noon_0D-BL	8.267	5.314	2.325	4.083	3.675	3.285	4.625	5.698	5.567
1 PM_0D-BL	7.98	5.386	2.595	4	3.668	3.227	4.323	5.378	5.336
3 PM_0D-BL	9.27	4.154	3.58	4.65	4.255	4.283	5.261	6.785	7.311
4 PM_0D-BL	9.785	1.733	1.828	4.161	3.081	3.284	4.461	6.703	6.843
11 AM_W/O-BL	7.55	5.151	2.818	4.039	3.64	3.392	4.264	5.126	5.043
12 Noon_W/O-BL	8.036	5.828	3.129	4.042	3.726	3.48	4.489	5.326	5.304
1 PM_W/O-BL	7.738	5.756	3.112	4.032	3.7	3.403	4.562	5.37	5.328
3 PM_W/O-BL	7.786	2.804	2.305	3.743	3.238	3.344	4.277	6.683	6.728
4 PM_W/O-BL	10.177	1.956	2.297	1	0.651	0.729	4.512	6.221	6
4:30 PM_W/O-BL	11.02	2.248	3.645	4.847	3.692	4.568	4.912	7.762	8.358

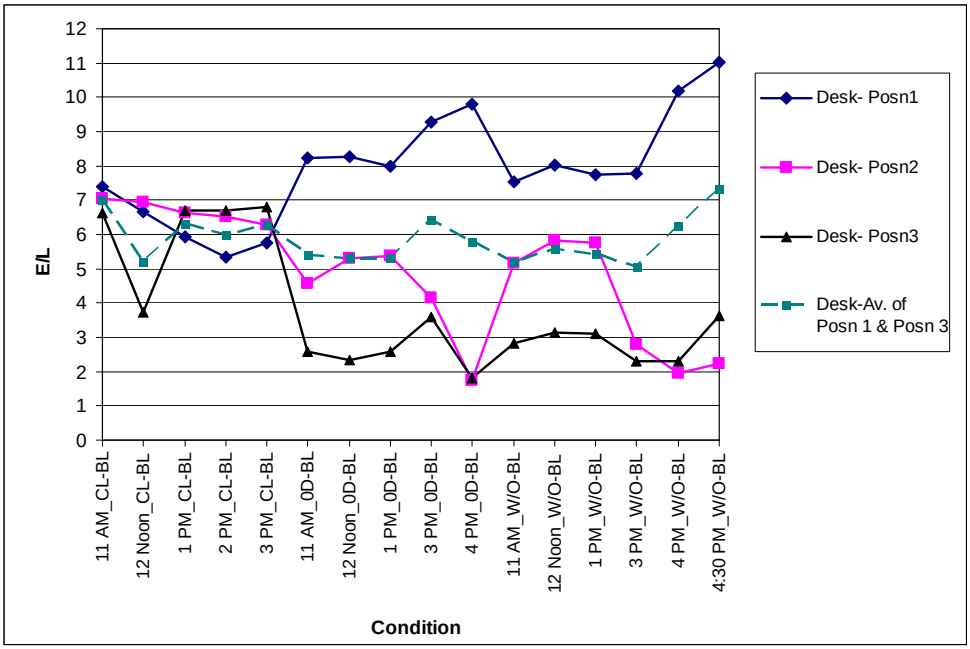

Figure 6-18: E/L Ratio for the Desk Under Different Conditions

As is evident from Figure **6-18**, illuminance and luminance do not maintain a constant relationship under different lighting conditions. Throughout the day, the ratio varies quite significantly. The only way to limit the deviation is to consider the average of the ratios for position 1 and position 3 (graph shown in the dotted line). As discussed before, position 1 and position 3 are almost diagonally opposite, with position 1 looking away from window.

The bond paper, however, does a pretty good job at maintaining a constant E/L ratio, particularly at position 1. At 3 PM, the ratio rises, on account of direct sunlight, when the rise in

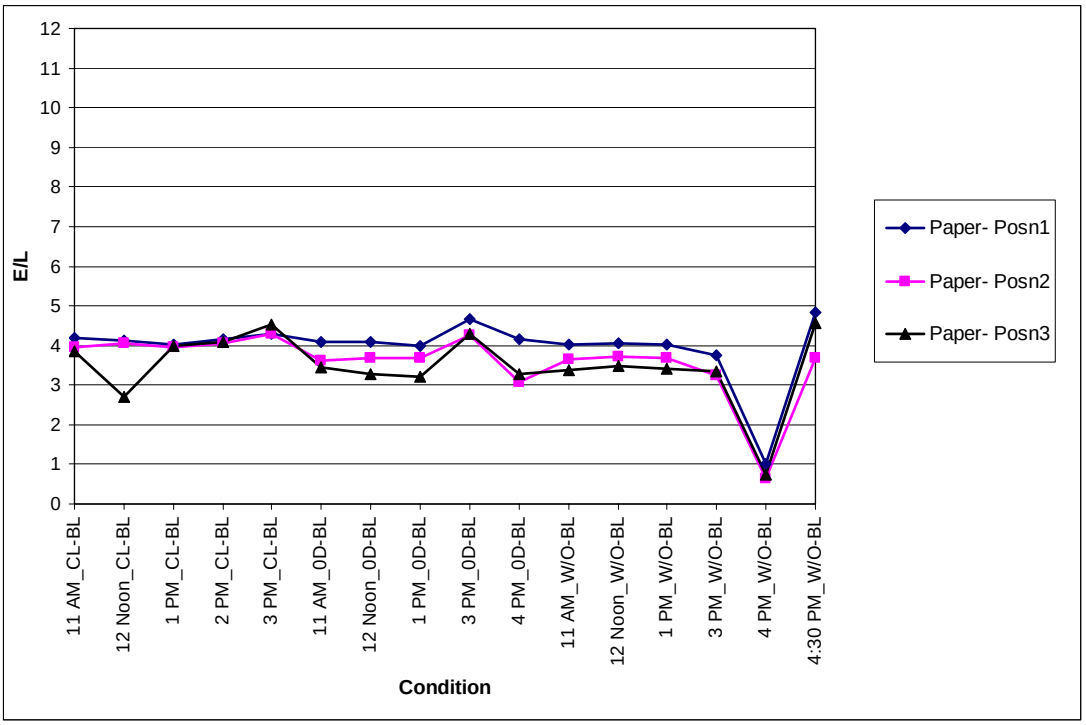

Figure **6-19**: E/L Ratio for the Paper Under Different Conditions

illuminance value is more than the rise in luminance. However, at the 4 PM without blinds condition, the luminance value drastically increases, bring down the E/L ratio. This apparent anomaly in this region may also be due to measurement limitations as the daylight condition was rapidly changing and between the time the illuminance was measured and the luminance was

measured, the daylight condition might have changed. However, position 3 in general shows more deviation as this position sees more specular reflections than the other two positions do.

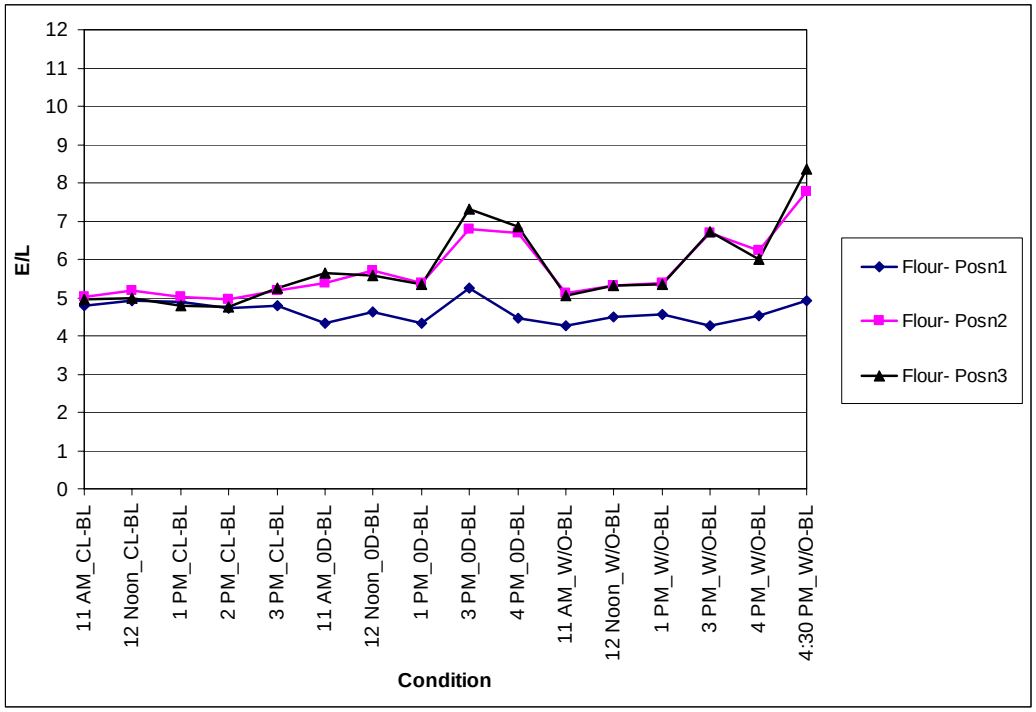

Figure **6-20**: E/L Ratio for the Flour Powder Under Different Conditions

Beached baking flour shows a little different trend in maintaining the E/L ratio, particularly under the conditions where direct sunlight falls on the desk. Although the time lapse between the illuminance and luminance measurement introduces an error, it can be inferred that the E/L ratio does not vary as drastically under direct sunlight as it does in the case of paper. This evidently is because of the more diffuse nature of the powder compared to the paper. Position 1 recorded a fairly constant ratio of illuminance and luminance throughout the day.

In spite of some probable measurement errors, the following can be concluded from this experiment:

- The desk surface used in the test, which is similar to typical desk surfaces in terms of reflectance and specularity, does not work well in maintaining a constant E/L ratio and cannot be used directly by CamSensor to estimate illuminance from radiance for daylight.
- Position 1 works the best for measurement of luminance.
- Bleached baking flour or diffuse bond paper can be used as a Lambertian surface (results of the test on the Lambertian characteristic of different surfaces have been included later in the chapter).

6.4 Determination of the Error in Estimating Illuminance from the Ratio of Desk Luminance Values with and without a Diffuse Surface at Different Dimming Levels

This test was conducted to investigate the effect of dimming of different luminaires on the ratio of illuminance and luminance at a test point. It was also the goal to determine whether the ratio of luminance with and without a diffuse surface at full output of a luminaire can be used to determine illuminance at any other dimming level, if the luminance on a desk is known at that light level. Test Point 7 was chosen for this test, since this point was more prone to specular reflections, and the error was likely to be higher at this point than at any other point. As before, incandescent spotlights were used in the peripheral space as the nondimmable lights (ND) in order to reduce the measurement error, particularly luminance. In all cases described in this section, the contribution of nondimmable lights was subtracted out. All luminaires were considered individually and also when all were on simultaneously. An Illuminance meter and a luminance meter were used for the measurement. White bond paper with 78% reflectance was used in this test as the diffuse surface.

Table **6-10**: Illuminance and Luminance Values at TP-8 Under Different Luminaires at 100% (E in lux and L in cd/m^2)

Condition	E_1	L_{DIFF1} (with paper)	E_1 / L_{DIFF1}	L_{DESK1} (without paper)	C1= L_{DIFF1}/ L_{DESK1}
All	568.6	140.15	4.057	56.44	2.483
L-1	161.5	41.15	3.925	16.74	2.458
L-2	53.6	17.15	3.125	6.94	2.471
L-3	258.6	58.25	4.439	23.14	2.517
L-4	71.6	18.95	3.778	7.04	2.692
L-5	13.3	2.98	4.463	1.06	2.811
L-6	8.6	2.09	4.115	0.66	3.167

Table **6-10** shows the illuminance (E_1), the luminance with paper (L_{DIFF1}) and the luminance without paper (L_{DESK1}) as individual luminaires were turned on to 100%. C_1 is the ratio of these two luminance values, which is used to approximate the illuminance as discussed next.

Table **6-11** shows illuminance (E_2) and the luminance on the desk (L_{DESK2}) as individual luminaires were dimmed down to 50% of full power (ballast output). The first row is for the condition when all were dimmed down to 50%. It also computes illuminance (E_3) by multiplying L_{DESK2} with C_1 and another constant C. Here C is equal to π/ρ (= 4.03), where ρ is the reflectance of the white paper (approximately 78%).

Table **6-11**: Illuminance (Measured and Computed) and Luminance Values at TP-8 Under Different Luminaires at 50% (E in lux and L in cd/m^2)

Condition	E_2 (Measured)	L_{DESK2} (without paper)	$E_3 = L_{DESK2} * C_1 * C$ (Computed)	E_2 / E_3	% Error
All	295.6	28.44	284.585	1.039	3.73
L-1	73.1	7.74	76.67	0.953	-4.88
L-2	23.6	3.11	30.97	0.762	-31.23
L-3	156.9	13.34	135.314	1.16	13.76
L-4	41.2	3.97	43.07	0.957	-4.54
L-5	8	0.65	7.363	1.087	7.96
L-6	5.2	0.4	5.105	1.019	1.83

The percent errors in estimating illuminance for different lighting conditions are also listed. The maximum error (31%) occurs for L-2, as this luminaire forms almost a mirror angle with respect to the camera position at TP-8.

Now different dimming conditions of the same luminaire will be considered and the errors will be estimated.

Table 6-12 shows the measured and computed illuminance values and the luminance values with and without paper for different dimming levels of L-4. As before, nondimmable incandescent spotlights were present for all conditions, but their contribution was removed from all measurements before computation.

Table 6-12: Illuminance and Luminance Values at TP-8 Under L-4 at Different Dimming Levels (E in lux and L in cd/m^2)

% Dimming	E_1	L_{DIFF1} (with paper)	E_1/L_{DIFF1}	L_{DESK1} (without paper)	$C_1=L_{DIFF1}/L_{DESK1}$
100	91.3	22.1	4.131	9.88	2.237

% Dimming	E_2(Measured)	L_{DESK2} (without paper)	$E_3= L_{DESK2}* C_1* C$ (Computed)	E_2/ E_3	% Error
80	77	8.53	76.899	1.001	0.13
60	67.3	7.6	68.515	0.982	-1.81
50	59.4	6.93	62.475	0.951	-5.18
40	56.1	6.5	58.598	0.957	-4.45
20	40.2	5.01	45.166	0.89	-12.35

It has to be noted that at the low dimming level, even a small amount of difference between the actual and the estimated illuminance appears as a high percent error.

Table 6-13 is for the condition where all luminaires are on. Table 6-14 gives the results for TP-9 with only L-2 on.

Table 6-13: Illuminance and Luminance Values at TP-8 Under All Luminaires at Different Dimming Levels (E in lux and L in cd/m^2)

% Dimming	E_1	L_{DIFF1} (with paper)	E_1/L_{DIFF1}	L_{DESK1} (without paper)	$C_1=L_{DIFF1}/L_{DESK1}$
100	504	121	4.165	49.7	2.435

% Dimming	E_2 (Measured)	L_{DESK2} (without paper)	$E_3= L_{DESK2}* C_1* C$ (Computed)	E_2/ E_3	% Error
80	430	42.9	420.98	1.021	2.1
60	360	35.8	351.307	1.025	2.41
40	272	27.4	268.878	1.012	1.15
20	159.4	16.3	159.953	0.997	-0.35

Table 6-14: Illuminance and Luminance Values at TP-9 Under L-2 at Different Dimming Levels (E in lux and L in cd/m^2)

% Dimming	E_1	L_{DIFF1} (with paper)	E_1/L_{DIFF1}	L_{DESK1} (without paper)	C1= L_{DIFF1}/L_{DESK1}
100	176.6	48.6	3.634	20.9	2.325

% Dimming	E_2 (Measured)	L_{DESK2} (without paper)	$E_3=L_{DESK2}*C_1* C$ (Computed)	E_2/E_3	% Error
80	149.3	17.5	163.971	0.911	-9.83
60	120.9	14.3	133.987	0.902	-10.82
40	89.3	10.5	98.382	0.908	-10.17
20	52.2	6.18	57.905	0.901	-10.93

The errors for L-2 are relatively high because it forms almost a mirror angle with respect to the camera position at TP-9.

So the method of estimating illuminance from measured luminance with and without paper should work with acceptable accuracy as long as the incident light is not at a mirror angle. If the constant C (which is π/ρ) is not known because of the unknown reflectance of the paper, the

estimated relative illuminance would still be proportional to the actual illuminance value. But for the purpose of calibrating CamSensor, estimating absolute illuminance from luminance is essential. It is necessary to have either an illuminance reading, or a luminance reading of a diffuse surface, to determine the correlation between the luminance and the illuminance on the desk.

6.5 Effect of Spatial Location of the Pixel and the Exposure Settings on the Relationship between Measured L and Computed Radiance

It was important to determine whether the ratio between the measured luminance and the computed radiance at a particular pixel depends on the spatial location of the pixel in the image. It is possible for the proportionality factor to be different at different positions on the sensor array – in particular, it may depend on the pixel's angle from the lens' optical axis. This effect is known as vignetting. At smaller apertures, this problem is typically less prominent. So in high dynamic range imaging, the exposure is varied by changing only the shutter speed and keeping the aperture constant.

Figure 6-21 shows the setup to test CamSensor for its vignetting effect. Four strings were attached on a white board horizontally, vertically and diagonally, as shown in the figure. At five different points along each of the strings, radiance values were computed and compared with the measured luminance values. The luminance meter was held at the same location as the camera, approximately five feet away from the board. Different exposure settings were used to capture images for radiance computation.

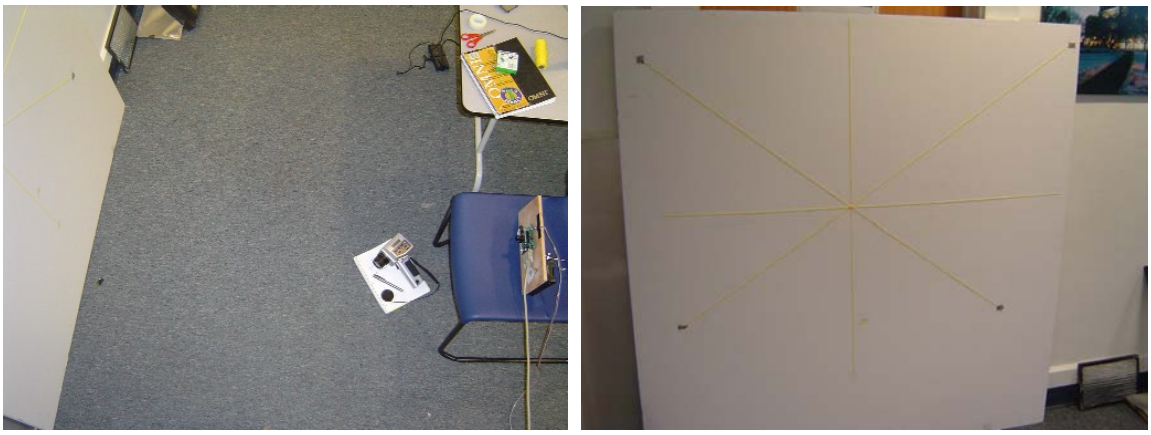

Figure 6-21: White Board with Strings to Test Vignetting

Table 6-15: Coordinates of the Pixels Considered in Test-4

Point	X	Y
1	18	26
2	58	86
3	97	144
4	148	220
5	187	281
6	5	294
7	44	234
8	99	153
9	144	86
10	188	25
11	3	151
12	40	152
13	98	153
14	177	155
15	205	156
16	105	21
17	105	92
18	102	137
19	101	245
20	98	307

Table 6-15 lists the coordinates of the twenty points along the straight lines, divided in groups of five as follows:

Group-1 (points 1-5): for pixels on the diagonal line from top left to bottom right

Group-2 (points 6-10): for pixels on the diagonal line from top right to bottom left

Group-3 (points 11-15): for pixels on the vertical line from top to bottom

Group-4 (points 16-20): for pixels on the horizontal line from left to right

Note that X signifies the pixel row and Y signifies the pixel column.

Figure **6-22** shows the locations of all the points. The measured luminance values at these points are shown in parenthesis.

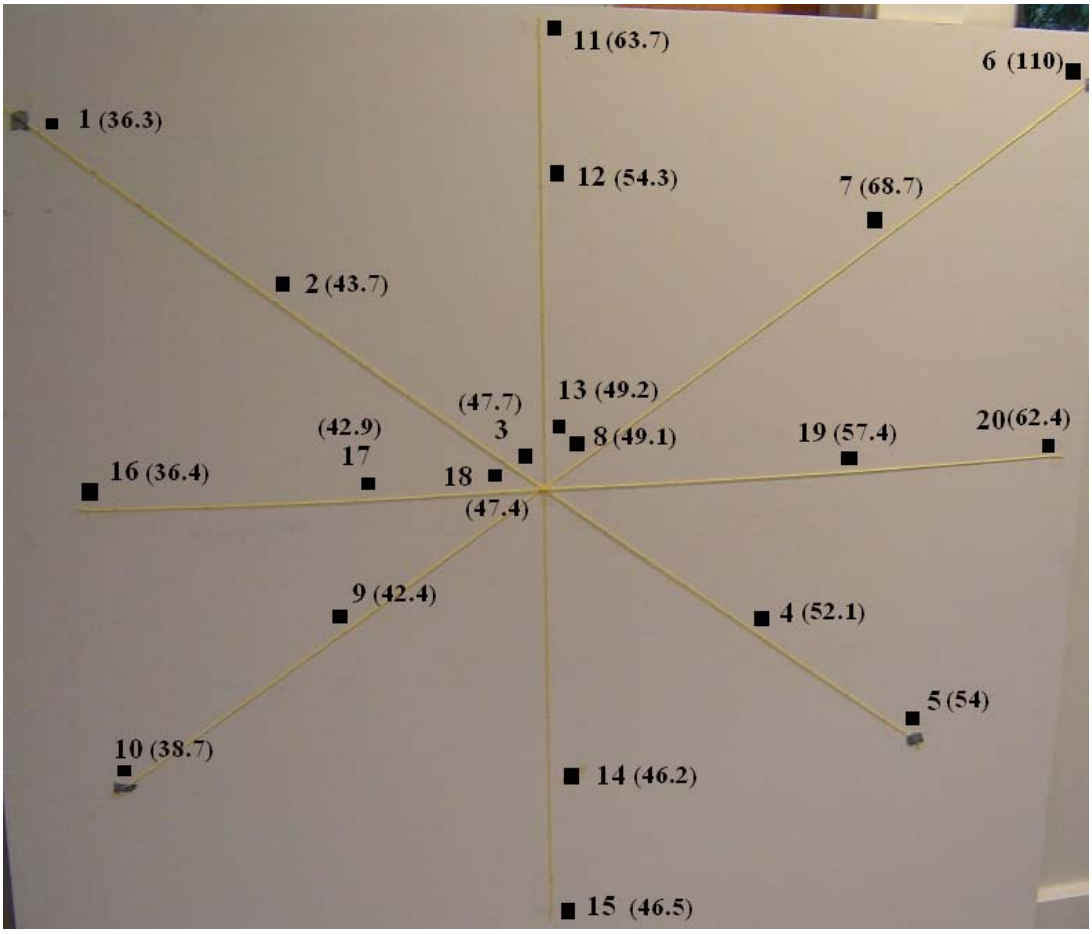

Figure **6-22**: Measurement Points and Corresponding Luminance Values (cd/m^2)

Table 6-16 and Table 6-17 show how the ratio of luminance and radiance varies for different exposure values at different points. As can be seen from the tables, the ratio varies significantly from one point to the other. This is more noticeable for the lower exposure values. At the exposure setting of 8, the values at most points get clamped. At the exposure setting of 16, the ratio of measured luminance and computed radiance varies considerably from one point to the other. Evidently, for this set of data, there is more error in estimating the luminance values at lower exposure settings, because the average luminance level on the board is somewhat low. An exposure setting of 64 or 128 provides a better result.

Table 6-16: Comparison of Luminance and Computed Radiance for different Exposure Values

Point	Measured L (cd/m^2)	Computed R (exp=8)	Ratio (exp=8)	Computed R (exp=16)	Ratio (exp=16)	Computed R (exp=32)	Ratio (exp=32)
1	36.3	9.93	3.656	4.97	7.304	4.12	8.811
2	43.7	9.93	4.401	4.97	8.793	22.14	1.974
3	47.7	9.93	4.804	8.01	5.955	35.71	1.336
4	52.1	9.93	5.247	12.45	4.185	41	1.271
5	54	9.93	5.438	8.46	6.383	36.53	1.478
6	110	25.52	4.31	56.57	1.944	80.56	1.365
7	68.7	10.01	6.863	29.04	2.366	57.6	1.193
8	49.1	9.93	4.945	9.44	5.201	37.54	1.308
9	42.4	9.93	4.27	4.97	8.531	22.88	1.853
10	38.7	9.93	3.897	4.97	7.787	8.38	4.618
11	63.7	9.93	6.415	14.42	4.417	44	1.448
12	54.3	9.93	5.468	11.61	4.677	40.67	1.335
13	49.2	9.93	4.955	9.49	5.184	37.18	1.323
14	46.2	9.93	4.653	6.9	6.696	33.36	1.385
15	46.5	9.93	4.683	5.75	8.087	30.85	1.507
16	36.4	9.93	3.666	4.97	7.324	8.19	4.444
17	42.9	9.93	4.32	4.97	8.632	24.89	1.724
18	47.4	9.93	4.773	7.55	6.278	34.71	1.366
19	57.4	9.93	5.78	18.14	3.164	48.18	1.191
20	62.4	9.93	6.284	17.45	3.576	46.72	1.336

Table 6-17: Comparison of Luminance and Computed Radiance for different Exposure Values (contd.)

Point	Measured L (cd/m^2)	Computed R (exp=64)	Ratio (exp=64)	Computed R (exp=128)	Ratio (exp=128)
1	36.3	18.92	1.919	24.38	1.489
2	43.7	35.81	1.22	34.96	1.25
3	47.7	47.34	1.008	55.11	0.866
4	52.1	51.38	1.014	56.33	0.925
5	54	47.74	1.131	54.3	0.994
6	110	84.48	1.302	85.04	1.294
7	68.7	61.05	1.125	65.87	1.043
8	49.1	48.65	1.009	56.24	0.873
9	42.4	36.42	1.164	37.71	1.124
10	38.7	24.05	1.609	28.27	1.369
11	63.7	53.63	1.188	56.71	1.123
12	54.3	50.92	1.066	60.96	0.891
13	49.2	48.25	1.02	53.8	0.914
14	46.2	44.74	1.033	47.16	0.98
15	46.5	43.34	1.073	46.8	0.994
16	36.4	23.26	1.565	27.96	1.302
17	42.9	38.23	1.122	39.2	1.094
18	47.4	46.24	1.025	54.85	0.864
19	57.4	56.91	1.009	66.41	0.864
20	62.4	56	1.114	66.42	0.939

Table 6-18 is obtained by dividing the ratios of each group for a particular exposure by the middle number in that group. For example, all ratios in group 1-5 for exposure setting 8 have been divided by 2.35, the ratio at point 3. The middle number in each group represents a pixel which is closer to the center of the image sensor. As can be seen, the ratio generally increases as we go outward towards the periphery of the image. For lower exposure, this is not always the case, but as pointed out, lower exposure settings are inappropriate for this test.

Table 6-18: Change of Luminance/Radiance Ratio with Distance from the Center

Point	Computed R (exp=8)	Computed R (exp=16)	Computed R (exp=32)	Computed R (exp=64)	Computed R (exp=128)
1	0.76	1.23	6.6	1.9	1.72
2	0.92	1.48	1.48	1.21	1.44
3	1	1	1	1	1
4	1.09	0.7	0.95	1.01	1.07
5	1.13	1.07	1.11	1.12	1.15
6	0.87	0.37	1.04	1.29	1.48
7	1.39	0.45	0.91	1.12	1.2
8	1	1	1	1	1
9	0.86	1.64	1.42	1.15	1.29
10	0.79	1.5	3.53	1.59	1.57
11	1.29	0.85	1.09	1.17	1.23
12	1.1	0.9	1.01	1.05	0.97
13	1	1	1	1	1
14	0.94	1.29	1.05	1.01	1.07
15	0.95	1.56	1.14	1.05	1.09
16	0.77	1.17	3.26	1.53	1.51
17	0.9	1.37	1.26	1.09	1.27
18	1	1	1	1	1
19	1.21	0.5	0.87	0.98	1
20	1.32	0.57	0.98	1.09	1.09

Figure 6-23 is a graphical depiction of Table 6-16 and Table 6-17. As stated before, a constant calibration factor of 10 has been used in the computation.

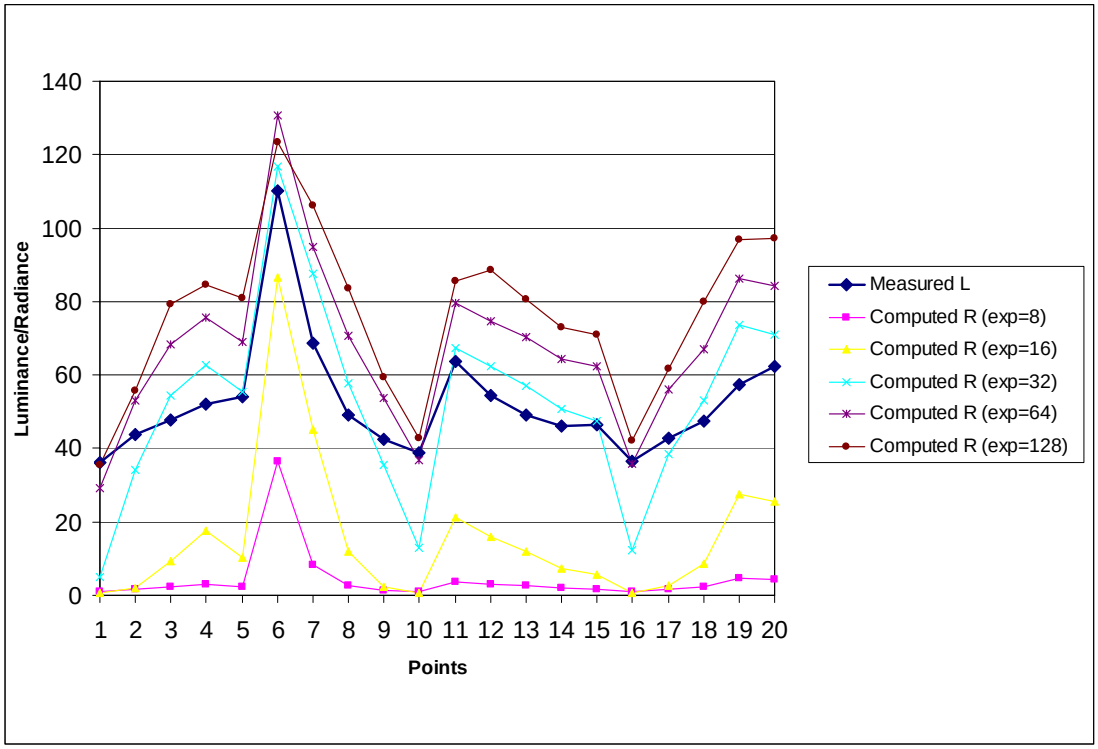

Figure **6-23**: Change of Luminance/Radiance Ratio with Distance from the Center

This test could not accurately determine the exact amount of the error introduced by vignetting because of the error associated with the luminance measurement. This error was mainly due to the fact that the sensors in the meter and the camera did not see exactly the same area and also the location of the sensors in these two devices was not exactly the same. However it can be concluded from this experiment that the effect of vignetting is present in this image sensor.

Also, using the right exposure setting is very important for proper estimation of the luminance levels in the scene. A thumb rule for choosing the right exposure setting can be the highest setting that does not cause image saturation in the workplane area. In other words, it is advisable to choose the longest exposure that allows sufficient integration time, yet does not cause saturation near the test points in the image.

The effect of vignetting can be corrected using the following formula [**38**]:

$$E = L\, \pi/4\, (d/f)^2 \cos^4(\alpha)$$

Where,

L = the radiance at a point on an object (scene radiance) [9]

E = the irradiance at the corresponding pixel location in the image (image irradiance)

d = diameter of the image lens

f = distance of the image plane from the lens

α = the angle a ray from a patch on the surface of the object makes with the optical axis of the lens

In a full-fledged system, this formula can be employed to compensate for the vignetting effect. For the prototype, many of the parameters used in the equation were not available, and so the vignetting effect could not be taken into account in the computation. This introduces some error in estimating the luminance and illuminance at test points located in the periphery of the scene.

[9] Irradiance and radiance are radiometric quantities corresponding to illuminance and luminance, which are in the domain of visual spectrum

6.6 Effect of Changing Lambda on the Derivation of Response Function

As described in the High Dynamic Range algorithm in Section **3.4**, the constant λ is the smoothness term. The purpose of this test was to determine the effect of changing λ on the derivation of the overall image response function. The image response function was derived with different λ and then the radiance values were computed at the same set of points on the white board as described in the previous test. Finally the computed values were compared with the measured luminance values to determine the value of λ for which the computed values give the most accurate estimation of the measured luminance values. The exposure setting was kept constant at 64. Table **6-19** summarizes the findings.

Table **6-19**: Effect of λ on Computed Radiance Values (x 10) at an Exposure Setting of 64

Point	Measured	Computed Radiance (exp=64)							
		λ=10	Ratio	λ=70	Ratio	λ=100	Ratio	λ=500	Ratio
1	36.3	14.85	2.444	14.87	2.441	14.92	2.433	13.35	2.719
2	43.7	35.14	1.244	35.45	1.233	35.52	1.23	35.39	1.235
3	47.7	49.16	0.97	48.49	0.984	48.38	0.986	48.79	0.978
4	52.1	52.65	0.99	52.83	0.986	52.83	0.986	53.69	0.97
5	54	49.44	1.092	48.91	1.104	48.82	1.106	49.26	1.096
6	110	91.6	1.201	88.88	1.238	88.48	1.243	91.97	1.196
7	68.7	62.82	1.094	64.65	1.063	65.16	1.054	67.64	1.016
8	49.1	49.99	0.982	49.88	0.984	49.82	0.986	50.37	0.975
9	42.4	35.88	1.182	36.12	1.174	36.18	1.172	36.08	1.175
10	38.7	22.49	1.721	22.18	1.745	22.21	1.742	20.92	1.85
11	63.7	56.59	1.126	55.23	1.153	55.34	1.151	56.52	1.127
12	54.3	52.08	1.043	52.32	1.038	52.33	1.038	53.13	1.022
13	49.2	49.73	0.989	49.45	0.995	49.39	0.996	49.89	0.986
14	46.2	46.88	0.985	45.63	1.012	45.51	1.015	45.7	1.011
15	46.5	45.18	1.029	44.01	1.057	43.9	1.059	44.04	1.056
16	36.4	21.34	1.706	21.14	1.722	21.18	1.719	19.81	1.837
17	42.9	38.01	1.129	38.12	1.125	38.15	1.125	38.11	1.126
18	47.4	48.33	0.981	47.28	1.003	47.17	1.005	47.46	0.999
19	57.4	57.82	0.993	58.92	0.974	59.28	0.968	61.08	0.94
20	62.4	58.04	1.075	57.87	1.078	58.15	1.073	59.77	1.044

Measured luminance values are first listed in the table. Then the computed radiance values for three different λ (at the same exposure value) are listed. The ratios of measured luminance and computed radiance values are listed alongside. Finally the radiance values for a different exposure value are shown. Note that the constant λ is used in determining the image response function. So, to compute the radiance values with a particular λ, we first need to determine the image response function and then compute the radiance values using that function. It also must be noted that the all original radiance values have been multiplied by 10 in order to arrive at the numbers shown in Table **6-19**.

Evidently, changing λ does not affect the radiance values to a great extent. Figure **6-24** plots the ratio of radiance and luminance at different points for different λ and exposure values. As can be seen, the graphs for different λ almost coincide with each other.

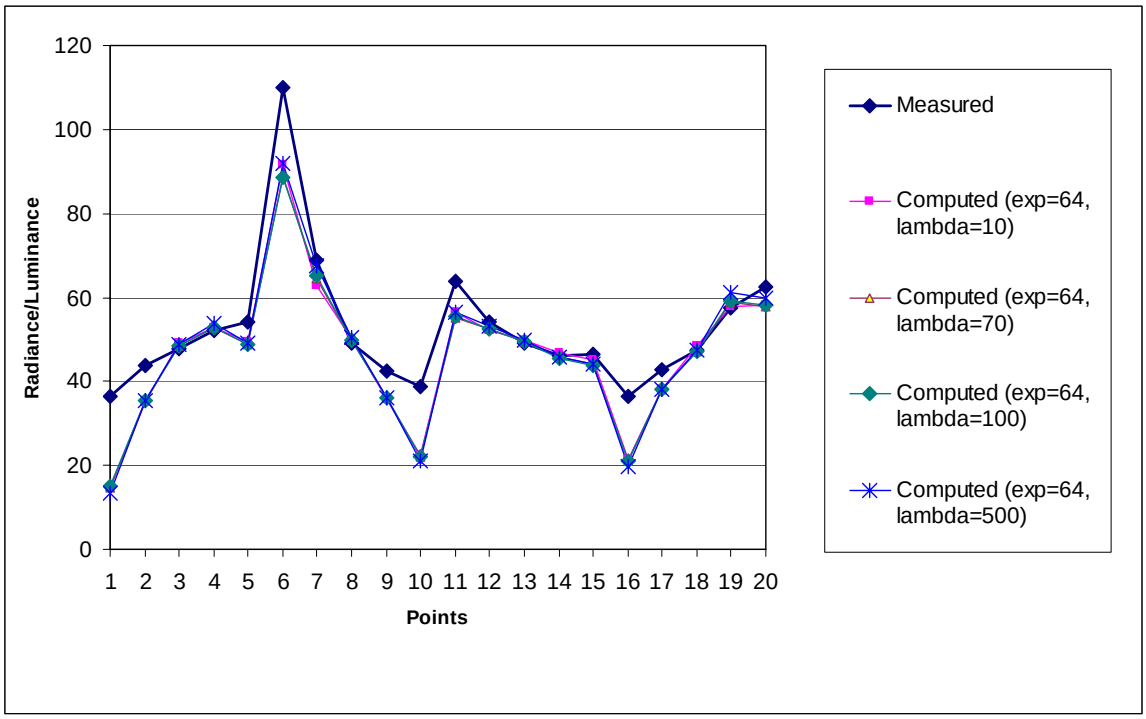

Figure **6-24**: Measured Luminance vs. Computed Radiance

To conclude, the effect of changing λ on the computed radiance values is not significant. A value of 70 will be used in all subsequent tests described in this document, as has been used in all preceding tests.

6.7 Determination of the Error in Estimating Luminance from Radiance

The purpose of this test was to determine the approximate error in estimating luminance from radiance values, or in other words, how proportional the two quantities are. Twelve test points were considered, as shown in Figure 6-25. All test points were covered with bleached flour spread smoothly across pieces of paper. Diffuse surfaces were used because luminance is more or less the same when measured from different directions. So, even if there was a slight difference in the position of the luminance meter and the camera, the error would not be significant. Even if the luminance meter and CamSensor did not see the same area, variation of luminance levels across the diffuse surface should be minimal.

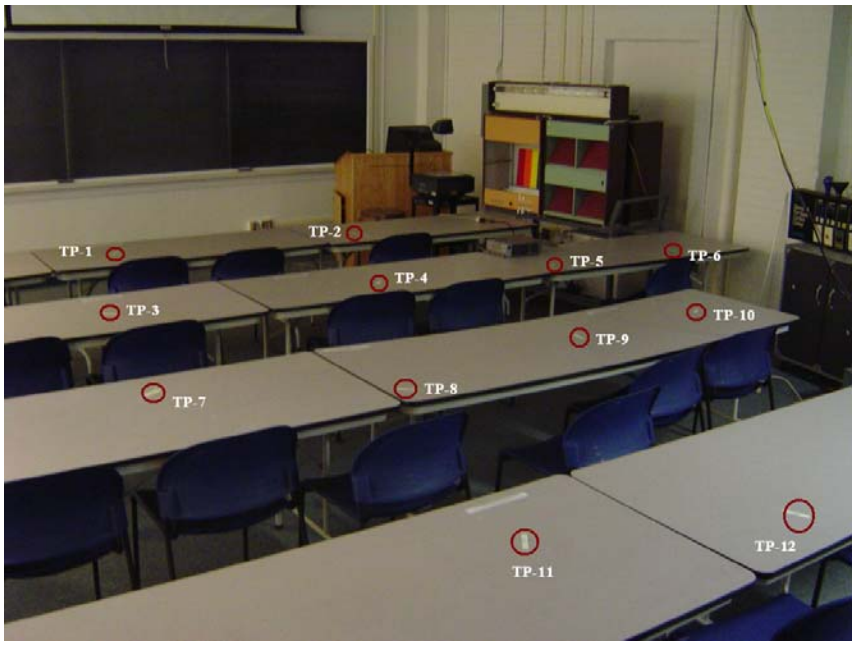

Figure 6-25: Scene for Computing Radiance

Luminance values on these test points were measured from the same camera vantage point. Then, radiance values were computed from images captured with different exposure settings. Since the radiance is proportional to luminance, an average proportionality factor for each exposure was used to convert the radiance values for a particular exposure to corresponding luminance values. The errors were determined by comparing the computed luminance values with the measured ones. For the exposure settings of 32, 64 and 128, L-1 through L-6 were dimmed to 20% of full power. There was no other light source used for these settings. However, for exposure settings of 4, 8 and 16, a higher light level was required, so additional luminaires were used, as shown in Figure 6-26. L-1 through L-6 were at full output, four 1 lamp, 42W compact fluorescent downlights were dimmed to 30% (denoted as ND in the figure) and four recessed 2 X 4 troffers (4 lamps, T5, 32W) were at full output (denoted as DL in the figure).

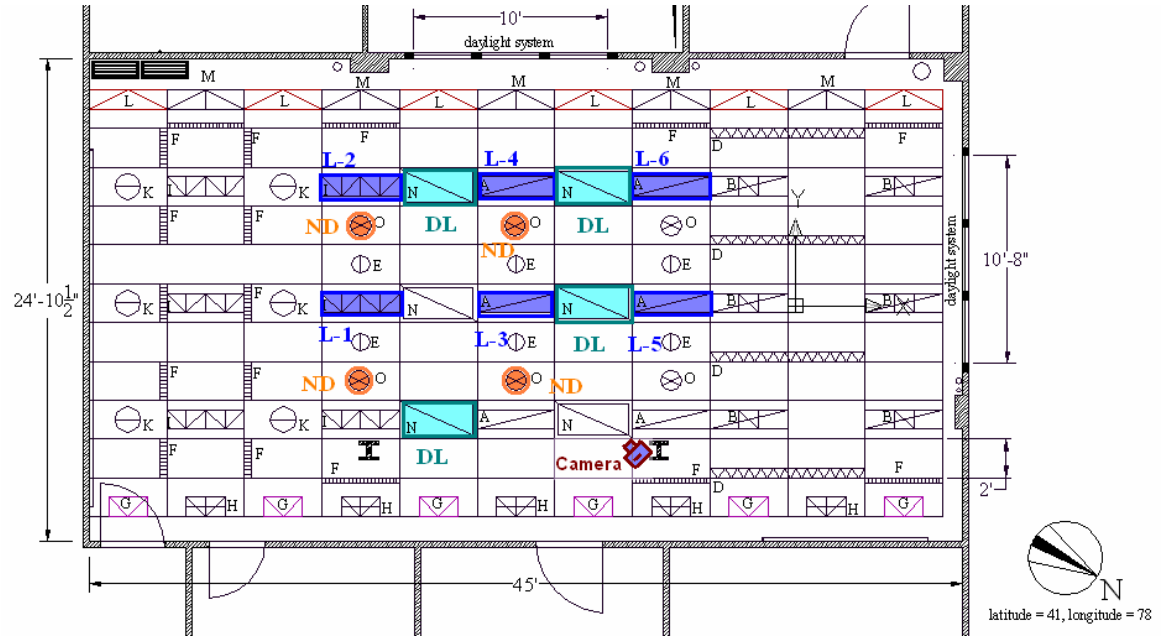

Figure 6-26: Luminaires Used in the Experiment

Table 6-20 gives the coordinates of the twelve test points used in this test. The locations are also shown in Figure 6-25. Note that the computed radiance at each test point is actually the average of the radiance values computed at each pixel and eight surrounding pixels.

Table 6-20: Pixel Coordinates of the Test Points in the Image

Point	X	Y
1	37	71
2	37	166
3	63	69
4	58	169
5	60	241
6	62	286
7	98	87
8	103	173
9	94	236
10	89	285
11	193	170
12	182	283

Table 6-21 and Table 6-22 show measured luminance values at different test points and also the computed radiance values at exposure settings of 32, 16, 8 and 4. The ratios of measured luminance and computed radiance values are shown for each exposure and the average of these ratios are also listed.

Table 6-21: Measured Luminance and Computed Radiance at the Exposure Settings of 32, 64 and 128

		Computed R					
Test Point	**Measured L**	**exp=32**	**Ratio L/R**	**exp=64**	**Ratio L/R**	**exp=128**	**Ratio L/R**
TP1	9.2	0.86	10.698	0.89	10.337	0.93	9.892
TP2	14.7	1.69	8.698	1.8	8.167	1.72	8.547
TP3	18.2	1.94	9.381	2.02	9.01	1.93	9.43
TP4	29.1	3.65	7.973	3.53	8.244	3.27	8.899
TP5	27.3	3.38	8.077	3.27	8.349	3.03	9.01
TP6	20.5	2.31	8.874	2.37	8.65	2.24	9.152
TP7	23.5	2.74	8.577	2.74	8.577	2.56	9.18
TP8	34.8	4.68	7.436	4.45	7.82	4.25	8.188
TP9	43.4	5.71	7.601	5.35	8.112	4.75	9.137
TP10	37.6	4.55	8.264	4.35	8.644	4.11	9.148
TP11	33	4.33	7.621	4.16	7.933	3.89	8.483
TP12	49.3	5.9	8.356	5.56	8.867	4.86	10.144
Av Ratio			8.463		8.559		9.101

Table 6-22: Measured Luminance and Computed Radiance at the Exposure Settings of 4, 8 and 16

		Computed R					
Test Point	**Measured L**	**exp=4**	**Ratio L/R**	**exp=8**	**Ratio L/R**	**exp=16**	**Ratio L/R**
TP1	88	8.5	10.353	8.46	10.402	8.78	10.023
TP2	118	14	8.429	13.81	8.545	13.43	8.786
TP3	220	26.46	8.314	24.28	9.061	22.44	9.804
TP4	268	35.54	7.541	32.1	8.349	29.21	9.175
TP5	255	33.12	7.699	29.96	8.511	27.03	9.434
TP6	186	22.77	8.169	21.45	8.671	19.89	9.351
TP7	304	39.08	7.779	35.1	8.661	32.38	9.389
TP8	342	49.23	6.947	44.03	7.767	38.37	8.913
TP9	385	52.72	7.303	47.21	8.155	38.71	9.946
TP10	347	45.01	7.709	40.24	8.623	36.08	9.618
TP11	246	34.16	7.201	30.84	7.977	28.39	8.665
TP12	292	38.13	7.658	34.26	8.523	31.59	9.243
Av Ratio			7.925		8.604		9.362

Computed radiance values at different exposure settings shown in Table 6-21 and Table 6-22 are multiplied by the average ratio (the last column) to obtain the corrected radiance values of Table 6-23 and Table 6-24. Percent errors in estimating the luminance values at different test points are also listed. % error = (measured – computed)/measured *100.

Table 6-23: Percent Error in Estimating Luminance from Radiance at the Exposure Settings of 32, 64 and 128

		Corrected R					
Test Point	**Measured L**	**exp=32**	**% Error**	**exp=64**	**% Error**	**exp=128**	**% Error**
TP1	9.2	7.3	20.7	7.6	17.4	8.5	7.6
TP2	14.7	14.3	2.7	15.4	-4.8	15.7	-6.8
TP3	18.2	16.4	9.9	17.3	4.9	17.6	3.3
TP4	29.1	30.9	-6.2	30.2	-3.8	29.8	-2.4
TP5	27.3	28.6	-4.8	28	-2.6	27.6	-1.1
TP6	20.5	19.5	4.9	20.3	1	20.4	0.5
TP7	23.5	23.2	1.3	23.5	0	23.3	0.9
TP8	34.8	39.6	-13.8	38.1	-9.5	38.7	-11.2
TP9	43.4	48.3	-11.3	45.8	-5.5	43.2	0.5
TP10	37.6	38.5	-2.4	37.2	1.1	37.4	0.5
TP11	33	36.6	-10.9	35.6	-7.9	35.4	-7.3
TP12	49.3	49.9	-1.2	47.6	3.4	44.2	10.3
Max % Error			20.7		17.4		11.2

Table 6-24: Percent Error in Estimating Luminance from Radiance at the Exposure Settings of 4, 8 and 16

		Corrected R					
	Measured L	**exp=4**	**% Error**	**exp=8**	**% Error**	**exp=16**	**% Error**
TP1	88	67.4	23.4	72.8	17.3	82.2	6.6
TP2	118	111	5.9	118.8	-0.7	125.7	-6.5
TP3	220	209.7	4.7	208.9	5	210.1	4.5
TP4	268	281.7	-5.1	276.2	-3.1	273.5	-2.1
TP5	255	262.5	-2.9	257.8	-1.1	253.1	0.7
TP6	186	180.5	3	184.6	0.8	186.2	-0.1
TP7	304	309.7	-1.9	302	0.7	303.1	0.3
TP8	342	390.1	-14.1	378.8	-10.8	359.2	-5
TP9	385	417.8	-8.5	406.2	-5.5	362.4	5.9
TP10	347	356.7	-2.8	346.2	0.2	337.8	2.7
TP11	246	270.7	-10	265.3	-7.8	265.8	-8
TP12	292	302.2	-3.5	294.8	-1	295.7	-1.3
Max % Error			23.4		17.3		8

As seen in Table 6-23 and Table 6-24, the maximum percent error always occurs at TP-1. At other test points the errors are comparatively less. It can be concluded that if a proper exposure is chosen, the error in estimating luminance can be limited within 11% for most of the test points. As already pointed out, it is preferable to choose the longest exposure that allows sufficient integration time, yet does not cause saturation at the test points.

6.8 Determination of the Relationship between Dimming Levels and Computed Luminance

The purpose of this test was to verify that as the dimming level of a luminaire is changed, the estimated luminance at any test point due to that luminaire changes by the same ratio. This correspondence between the dimming level and the estimated luminance must be valid under all conditions.

Only one luminaire, L-1, was used in this experiment. The dimming level of the luminaire was changed from 100% (full power) to 10% in steps of 10% and the luminance values were computed at each of the twelve test points whose coordinates are shown in Table 6-25. Figure 6-27 shows the image of the scene.

Table 6-25: Pixel Coordinates of the Twelve Test Points

	X	Y
TP-1	37	71
TP-2	37	166
TP-3	63	69
TP-4	58	169
TP-5	60	241
TP-6	62	289
TP-7	98	87
TP-8	103	173
TP-9	94	236
TP-10	89	285
TP-11	193	170
TP-12	182	283

Figure 6-27: Image of the Scene Captured by CamSensor (L-1 at 100% Output)

Table 6-26: Computed Luminance Values for Two Exposure Settings for Different Dimming Levels of L-1

% Ballast o/p	Exposure	TP-1	TP-2	TP-3	TP-4	TP-5	TP-6
100	32	61.87	71.67	124.06	139.08	86.48	15.9
100	16	58.02	69.06	122.66	132.82	84.34	14.41
90	32	56.26	64.8	112.97	122.89	79.26	13.92
90	16	53.39	61.61	112.19	121.84	78.46	13.91
80	32	50.89	59.38	104.58	112.78	72.33	12.68
80	16	48.07	56.08	102.74	112.54	71.33	12.7
70	32	45.38	53.55	93.65	102.52	65.13	10.91
70	16	42.57	50	92.69	101.27	63.12	11.69
60	32	40.96	47.96	84.28	92.04	58.32	9.99
60	16	35.8	44.19	82.98	90.8	55.98	10.85
50	32	33.99	41.06	72.71	79.07	50.21	8.22
50	16	31.9	37.94	69.94	77.11	47.34	9.62
40	32	28.68	34.29	60.9	65.69	41.15	7.18
40	16	24.9	30.02	59.26	64.16	39.86	8.7
30	32	21.15	25.39	45.61	49.59	31	5.53
30	16	16.3	20.44	41.6	47.03	26.51	6.77
20	64	16.38	19.1	33.98	36.64	23.52	4.74
20	32	12.76	15.31	30.61	33.22	19.3	3.77
10	64	7.33	8.47	16.66	17.87	10.94	2.52
10	32	6.56	7.65	13.81	15.42	8.9	2.93

Table 6-27: Computed Luminance Values for Two Exposure Settings for Different Dimming Levels of L-1 (contd.)

% Ballast o/p	Exposure	TP-7	TP-8	TP-9	TP-10	TP-11	TP-12
100	32	95.68	88.02	102.32	70.47	22.68	14.41
100	16	93.39	85.7	100.83	67.69	18.63	13.35
90	32	86.86	80.46	92.88	65.32	19.76	12.87
90	16	85.05	77.95	91.47	61.09	16.64	12.39
80	32	78.86	72.91	85.11	59.36	18.08	10.85
80	16	76.38	69.28	83.4	56.69	16.95	10.88
70	32	72.03	65.78	76.68	53.57	16.1	9.93
70	16	68.54	63.84	74.96	50.67	14.47	9.82
60	32	64.74	59.86	68.91	47.61	14.3	9.05
60	16	61.9	55.98	66.54	44.42	13.1	7.5
50	32	55.55	50.72	59.25	40.57	11	7.04
50	16	52.04	49.38	57.32	38.04	11.63	8.34
40	32	46.21	42.84	48.92	33.77	9.93	6.36
40	16	42.69	38.89	47.35	30.53	9.83	7.52
30	32	34.09	31.83	36.93	25.15	7.7	5.38
30	16	28.67	26.72	32.83	21.1	7.61	5.98
20	64	26.45	23.65	27.79	19.28	5.97	4.08
20	32	22.5	20.39	24.09	15.76	5.2	3.93
10	64	12.17	11.04	13.28	8.72	3.18	2.28
10	32	10.74	9.15	11.42	8.11	3.45	2.95

Table 6-26 and Table 6-27 show luminance values computed from images captured with two different exposure settings for each dimming level. The average luminance values are listed in Table 6-28 and Table 6-29. Percent light outputs at different dimming levels are also listed.

Table 6-28: Average Luminance Values for Different Dimming Levels of L-1

% Ballast o/p	% Light o/p	TP-1	TP-2	TP-3	TP-4	TP-5	TP-6
100	100	59.945	70.365	123.36	135.95	85.41	15.155
90	90.86	54.825	63.205	112.58	122.365	78.86	13.915
80	82.73	49.48	57.73	103.66	112.66	71.83	12.69
70	73.35	43.975	51.775	93.17	101.895	64.125	11.3
60	65.52	38.38	46.075	83.63	91.42	57.15	10.42
50	55.71	32.945	39.5	71.325	78.09	48.775	8.92
40	45.53	26.79	32.155	60.08	64.925	40.505	7.94
30	33.64	18.725	22.915	43.605	48.31	28.755	6.15
20	22.54	14.57	17.205	32.295	34.93	21.41	4.255
10	10.73	6.945	8.06	15.235	16.645	9.92	2.725

Table 6-29: Average Luminance Values for Different Dimming Levels of L-1 (contd.)

% Ballast o/p	% Light o/p	TP-7	TP-8	TP-9	TP-10	TP-11	TP-12
100	100	94.535	86.86	101.575	69.08	20.655	13.88
90	90.86	85.955	79.205	92.175	63.205	18.2	12.63
80	82.73	77.62	71.095	84.255	58.025	17.515	10.865
70	73.35	70.285	64.81	75.82	52.12	15.285	9.875
60	65.52	63.32	57.92	67.725	46.015	13.7	8.275
50	55.71	53.795	50.05	58.285	39.305	11.315	7.69
40	45.53	44.45	40.865	48.135	32.15	9.88	6.94
30	33.64	31.38	29.275	34.88	23.125	7.655	5.68
20	22.54	24.475	22.02	25.94	17.52	5.585	4.005
10	10.73	11.455	10.095	12.35	8.415	3.315	2.615

Table 6-30 and Table 6-31 list the luminance values at different target points as the percent of corresponding luminance values at full output.

Table 6-30: Percent Luminance Output vs. Percent Light Output at Different Test points

% Light o/p	TP-1	TP-2	TP-3	TP-4	TP-5	TP-6
100	100	100	100	100	100	100
90.86	91.46	89.82	91.26	90.01	92.33	91.82
82.73	82.54	82.04	84.03	82.87	84.1	83.73
73.35	73.36	73.58	75.53	74.95	75.08	74.56
65.52	64.03	65.48	67.79	67.25	66.91	68.76
55.71	54.96	56.14	57.82	57.44	57.11	58.86
45.53	44.69	45.7	48.7	47.76	47.42	52.39
33.64	31.24	32.57	35.35	35.54	33.67	40.58
22.54	24.31	24.45	26.18	25.69	25.07	28.08
10.73	11.59	11.45	12.35	12.24	11.61	17.98

Table 6-31: Percent Luminance Output vs. Percent Light Output at Different Test points (contd.)

% Light o/p	TP-7	TP-8	TP-9	TP-10	TP-11	TP-12
100	100	100	100	100	100	100
90.86	90.92	91.19	90.75	91.5	88.11	90.99
82.73	82.11	81.85	82.95	84	84.8	78.28
73.35	74.35	74.61	74.64	75.45	74	71.15
65.52	66.98	66.68	66.67	66.61	66.33	59.62
55.71	56.9	57.62	57.38	56.9	54.78	55.4
45.53	47.02	47.05	47.39	46.54	47.83	50
33.64	33.19	33.7	34.34	33.48	37.06	40.92
22.54	25.89	25.35	25.54	25.36	27.04	28.85
10.73	12.12	11.62	12.16	12.18	16.05	18.84

Figure 6-28 is a graphical representation of the above tables. As can be seen from the tables and the graph, at light levels below 30%, the percent luminance values do not track the percent light levels as well. As pointed out earlier, at lower light levels, the error in estimating the luminance values increases. For the same reason, percent luminance values deviate more for TP-6, since the luminance values themselves are rather low at this point.

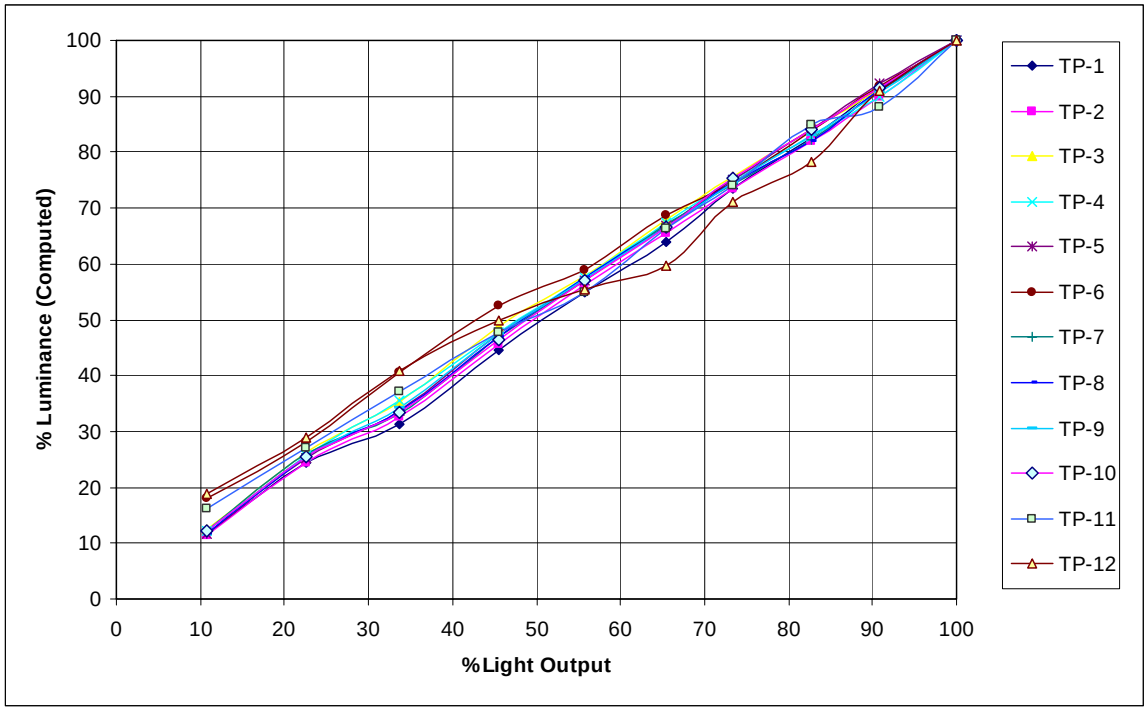

Figure 6-28: Percent Luminance Output vs. Percent Light Output at Different Test points

Thus, it can be concluded from this experiment that the luminance output is consistent with the light output at different dimming levels.

6.9 Test of Lambertian Characteristics of Different Surfaces

In most of the previous experiments, only one or two luminaires were considered. The error in these experiments partially depended on whether the camera saw specular reflections due to one or both of these luminaires. If there is specular reflection in the direction of the luminance measurement, the luminance and the illuminance will not have the same relationship as in other directions. In real life situations, multiple luminaires will contribute to a given test point from multiple directions, so it is important to have a Lambertian or close to Lambertian surface in

order to work with multiple light sources and yet be able to convert luminance to illuminance at a given test point. This section describes a test that determines the Lambertian characteristics of four different materials, namely, a letter size (21.6 cm X 27.9 cm or 8.5” X 11”) diffuse white bond paper used in earlier experiments, bleached baking flour pressed evenly onto a piece of paper (roughly 15.2 cm X 20.3 cm or 6” X 8”), a gray card (10.8 cm X 7 cm or 4.25” X 2.75”) with 30% reflectance (N6 Munsell gray), and a Barium Sulphate sample (6.4 cm X 6.4 cm or 2.5” X 2.5”).

A single 100W tungsten halogen spotlight was used as the only light source to illuminate the sample at a vertical angle of around 40° from normal. The luminance values were measured at horizontal angles of 0°, 90°, 180° and 270°. The meter was held roughly at the mirror angle. Illuminance on the material was measured with an illuminance meter. Before measuring the luminance values for each material, the illuminance reading was taken since there was a possibility that the samples were not all placed at the exact location. The luminance and illuminance values were measured at the center of the test material.

Table 6-32 shows the measured illuminance and luminance values. E/L ratios were determined for all four directions, and the average of the four is shown for each of the materials. The percent errors with respect to the average ratio show how the E/L ratio deviates from the average value at different horizontal angles. Reflectance, denoted as ρ, can be computed from the

Table 6-32: Reflectance of Different Materials Computed at Different Angles

Surface	E (lx)	Hor Angle wrt Luminaire	L (cd/m^2)	E/L	Average E/L	% Error wrt Av Ratio	π * L / E	Av Reflectance
Flour	2082	0	495	4.206	3.979	-5.705	0.747	0.747
		90	479	4.347		-9.249	0.723	
		180	635	3.279		17.592	0.958	
		270	510	4.082		-2.589	0.77	
White Paper	2087	0	513	4.068	3.617	-12.469	0.772	0.787
		90	530	3.938		-8.875	0.798	
		180	837	2.493		31.075	1.26	
		270	526	3.968		-9.704	0.792	
Barium Sulphate	2142	0	580	3.693	3.697	0.108	0.851	0.836
		90	561	3.818		-3.273	0.823	
		180	611	3.506		5.166	0.896	
		270	568	3.771		-2.002	0.833	
Gray Paper	2240	0	230	9.739	9.649	-0.933	0.323	0.294
		90	199	11.256		-16.655	0.279	
		180	353	6.346		34.232	0.495	
		270	199	11.256		-16.655	0.279	

equation ρ = π * L / E, provided we are considering a Lambertian surface. Here, the average reflectance was the average of the (π * L / E) values at 0°, 90° and 270°. At 180°, the specular or mirror reflection provided a much higher value and was not considered in the computation of average reflectance. This, in essence, separates the diffuse and specular reflections from the material under consideration. In fact, for a surface that is not Lambertian, it is more precise to speak in terms of a Bi-Directional Reflectance Distribution Function (BRDF), which is a more specific evaluation of the reflectance. It is a measure of light reflected in different directions when it comes in contact with a certain material. In terms of radiometric units, BRDF is defined as the ratio of the radiance in the outgoing direction and radiance flux density (irradiance) for an

incident direction [54]. In terms of photometric units, it is the ratio of luminance in a given direction from the surface to the illuminance measured on the surface. For an ideal diffuse reflector, the BRDF is independent of both incoming and outgoing directions, and is represented by a constant (ρ). The reflectance of the diffuse material is $\rho_d = \pi * \rho$. In our case, the multiplication factor is the reciprocal of BRDF.

Table 6-33 shows the average multiplication factors (MF) to be used for different materials. These factors are used to convert luminance to illuminance values. These factors were obtained by dividing π by the average reflectance values obtained previously. The table also lists the percent errors for each of the materials due to the use of only one MF in four different directions. This error comes from the fact that no material is perfectly Lambertian. However, the Barium Sulphate sample is fairly Lambertian and thus the error arising from using an average MF is small. Since Barium Sulphate chips were not available for all the test points and flour worked as a better diffuse surface than the paper at the mirror angles, bleached flour pressed on a diffuse white paper was used as the Lambertian surface in the final test.

Table 6-33: Multiplication Factors for Different Materials

Surface	Hor Angle wrt Luminaire	Ave MF to be Used	% Error wrt Av MF
Flour	0	4.206	0
	90		-3.352
	180		22.04
	270		2.948
White Paper	0	3.992	-1.904
	90		1.353
	180		37.55
	270		0.601
Barium Sulphate	0	3.758	1.73
	90		-1.597
	180		6.706
	270		-0.346
Gray Paper	0	10.686	8.862
	90		-5.334
	180		40.614
	270		-5.334

The method used to determine the MF has reasonable accuracy for the purpose of the calibration of CamSensor. The average MF for the diffuse white paper determined in the earlier experiment (using different luminaires and different test points) was 4.03, instead of 3.993 (less than 1% deviation). Also, this method gives an average reflectance of 29.4% for the gray paper, while the actual value is 30% (an error of 2%).

6.10 Predicting Illuminance from the Knowledge of Target Illuminance Values

In Section 6.4, a method for estimating the illuminance was described. First, the ratio of luminance values measured with and without diffuse surfaces (denoted by L_{DIFF} and L_{DESK} respectively) was computed at each test point with the luminaires at full output. Then the luminance values on the desk were measured at all test points for other dimming levels, when the

diffuse surfaces were not present. These luminance values, when multiplied by the ratio computed earlier, gave the projected values of luminance with diffuse surfaces under the current dimming levels. The projected luminance values were used to estimate illuminance at the test points using the formula: $E / L = \pi / \rho$. This way illuminance could be computed from the luminance on the desk, even though the desk was not Lambertian.

The current section further explores the issue of estimating the illuminance from luminance and comes up with an algorithm that will be used in the final experiment. In the experiment described in this section, illuminance at the test points at full output of the luminaires is estimated from the corresponding luminance measured with diffuse surfaces placed on the test points. Then, for a set of target illuminance values desired at the test points, required dimming levels of the luminaires are determined. Finally, the luminaires are dimmed to these levels and deviation of the light levels at different test points from the corresponding target levels is measured. The process is repeated three times to simulate the performance of the system during continuous operation.

Once again, the camera was not involved in this test so as to get an error estimate solely due to the approximation and assumption involved in this method. Illuminance and luminance meters were used for all measurements.

Two test points, TP-8 and TP-10 and two luminaires, L-2 and L-3 were considered in this test. Illuminance contributions at two test points were measured by turning on each of the luminaires individually, as well as by turning on both at the same time. The illuminance due to a combination of additional luminaires acting as added constant light sources (described as DL in the tables) was also measured. Luminance values in each of these lighting conditions were measured from the same position as the camera, both with and without the Lambertian surfaces (bleached baking flour) placed on the test points. If the luminance on a diffuse surface placed at any test point is L_{DIFF}, the projected illuminance on that given point will be, $E = L_{DIFF} * \pi / \rho$,

where ρ is the reflectance of bleached flour. From the experiment described in Section **6.9**, E (projected) = L_{DIFF} * 4.206. It is important to note here that under normal operating conditions, diffuse (Lambertian) surfaces are unlikely to be present on the desk, and illuminance cannot be derived directly from the desk luminance. Thus luminance on a diffuse surface (L_{DIFF}) obtained in the first step acts as a reference for the conditions when no diffuse surface is available. This reference must always be used while computing illuminance from luminance.

Table **6-34** and Table **6-35** show the illuminance and luminance values under different lighting conditions, estimated illuminance values applying the L_{DIFF}/L_{DESK} ratio, and the error in the estimation when compared to the measured illuminance values.

Table **6-34**: Illuminance (lx) and Luminance (cd/m^2) Values at TP-8

Luminaire	%dimming	Measured E	L w/ flour (L_{DIFF})	L w/o flour (L_{DESK})	Ratio R (L_{DIFF}/L_{DESK})	Projected E	% Error
L-2	100	45.5	11.3	4.31	2.622	47.53	-4.5
L-3	100	237.3	50.6	20.5	2.468	212.82	10.3
L-3+L-2	100	285	63.6	25	2.544	267.5	6.1
DL	-	96.7	23.2	9.04	2.566	97.58	-0.9

Table **6-35**: Illuminance (lx) and Luminance (cd/m^2) Values at TP-10

Luminaire	%dimming	Measured E	L w/ flour (L_{DIFF})	L w/o flour (L_{DESK})	Ratio R (L_{DIFF}/L_{DESK})	Projected E	% Error
L-2	100	160.6	34.8	13.4	2.597	146.37	8.9
L-3	100	101.5	24.2	8.91	2.716	101.79	-0.3
L-3+L-2	100	263.6	59.6	22.4	2.661	250.68	4.9
DL	-	141.6	32.8	12.2	2.689	137.96	2.6

For this experiment, the target illuminance values at TP-8 and TP-2 were assumed to be 90% of the corresponding electric light levels due to both the luminaires at full output. Table **6-36** lists the target illuminance values.

Table 6-36: Target Illuminance Levels (lx) at TP-8 and TP-10

Point	% electric for target	Target
TP-8	90	241
TP-10	90	226

Because of the presence of additional luminaires (DL), illuminance at both the test points will be more than the target light levels, necessitating the dimming of L-2 and L-3. the dimming algorithm discussed in the following sections determine the required light output from L-2 and L-3, so that the combined light output due to L-2, L-3 and the additional luminaires is close to the target illuminance at both test points.

In this experiment, L-1 dimmed to 70%, L-4 dimmed to 30% and L-5 and L-6 at full output were used as DL.

6.10.1 Determination of the Required Dimming Levels

Let us assume that x% of L-2 and y% of L-3 help meet the target illuminance values at both the test points. Values of x and y are to be determined. To find x and y, we must use the projected illuminance values at TP-8 and TP-10 due to L-2 and L-3 found previously.

Let ,

$E_{L2\text{-}8}$: illuminance at test point 8 due to L-2

$E_{L3\text{-}8}$: illuminance at test point 8 due to L-3

$E_{L2\text{-}10}$: illuminance at test point 10 due to L-2

$E_{L3\text{-}10}$: illuminance at test point 10 due to L-3

T_8: target light level at test point 8

T_{10}: target light level at test point 10

E_8: current illuminance at test point 8 due to all luminaires

E_{10}: current illuminance at test point 10 due to all luminaires

d_{L2}: present fractional light level of L-2 (value is 1 for full output)

d_{L3}: present fractional light level of L-3

Then, Eq. **14** and Eq. **15** can be formed:

$$x * E_{L2-8} + y * E_{L3-8} = T_8 - (E_8 - d_{L2} * E_{L2-8} - d_{L3} * E_{L3-8}) \quad (14)$$

$$x * E_{L2-10} + y * E_{L3-10} = T_{10} - (E_{10} - d_{L2} * E_{L2-10} - d_{L3} * E_{L3-10}) \quad (15)$$

Solving these two equations, we will get x and y. The values can be iteratively refined.

In the iterative steps, the differential light levels Δx and Δy, that is, the required change in the current light levels of d_{L2} and d_{L3} respectively, can be expressed by Eq. **16** and Eq. **17**:

$$\Delta x * d_{L2} * E_{L2-8} + \Delta y * d_{L3} * E_{L3-8} = T_8 - (E_8 - d_{L2} * E_{L2-8} - d_{L3} * E_{L3-8}) \quad (16)$$

$$\Delta x * d_{L2} * E_{L2-10} + \Delta y * d_{L3} * E_{L3-10} = T_{10} - (E_{10} - d_{L2} * E_{L2-10} - d_{L3} * E_{L3-10}) \quad (17)$$

Then, $(\Delta x * d_{L2})$ and $(\Delta y * d_{L3})$ will be the new dimming levels.

6.10.2 Iteration-1:

Table **6-37** lists the measured illuminance and luminance values before the iteration. The projected illuminance and the error in this estimation with respect to the measured value are also noted.

Table 6-37: Illuminance (lx) and Luminance (cd/m^2) Values Before Iteration-1

Point	Measured E	Measured L	Projected E	% Error
TP-8	386	34.3	362.77	6
TP-10	409	35.1	392.81	4

Here, the projected illuminance is the sum of estimated illuminance contributions due to L-2, L-3 and DL. The first two values were already computed. To determine the illuminance contribution due to DL at a test point, first the luminance due to DL alone is computed by subtracting the estimated individual luminance contributions on the desk (L_{DESK}) at that test point due to L-2 and L-3 (Table 6-34 and Table 6-35) from the measured luminance value listed in Table 6-37. Then this luminance value is multiplied by the ratio L_{DIFF}/L_{DESK} to obtain the estimated luminance with the diffuse surface. This, when multiplied by the Multiplication Factor (π / ρ = 4.206), gives the estimated illuminance due to DL. This is symbolically expressed in Eq. 18, where $E_{TP\text{-}X}$ and $L_{TP\text{-}X}$ are the present illuminance and luminance (before starting the iteration) at any test point.

$$E_{TP\text{-}X} = [L_{TP\text{-}X} - d_{L2} * (L_{DESK})_{L\text{-}2} - d_{L3} * (L_{DESK})_{L\text{-}3}] * (L_{DIFF}/L_{DESK})_{DL} * (\pi/\rho) + d_{L2} * E_{L\text{-}2} + d_{L3} * E_{L\text{-}3} \quad (18)$$

Here, d_{L2} and d_{L3} are unity for iteration-1.

For example, the current illuminance E at TP-8 is estimated from the computed luminance L as follows: E = (34.3 – 4.31 – 20.5) * 2.566 * 4.206 + 47.53 + 212.82 = 362.77 lx.

Now, Eq. 14 and Eq. 15 can be applied to determine the required fractional light levels x and y for L-2 and L-3 respectively. Eq. 19 and Eq. 20, for TP-8 and TP-10 respectively, have been formed using the data from Table 6-34, Table 6-35, Table 6-36 and Table 6-37.

$$x * 47.53 + y * 212.82 = 241 - (362.77 - 47.53 - 212.82) \quad (19)$$

$$x * 146.37 + y * 101.79 = 226 - (392.81 - 146.37 - 101.79) \quad (20)$$

Solving Eq. 19 and Eq. 20 by least square method, we get x = 0.1219 and y = 0.6239. So the required light outputs for L-2 and L-3 are 12% and 62% respectively. These correspond to 11% and 43% dimming levels respectively. Table 6-38 shows the error in reaching the target illuminance at the two test points.

Table 6-38: Target Illuminance and Achieved Illuminance After Iteration-1

Point	Target E	Measured E	% Error
TP-8	241	241.3	-0.1
TP-10	226	220.1	2.6

6.10.3 Iteration-2:

The purpose of the second and subsequent iterations is to refine the dimming levels so as to minimize the percent deviation from the target illuminance at both the points.

Table 6-39 shows the illuminance and luminance values before the second iteration is started. Projected illuminance is computed using Eq. 18 as before, only in this case d_{L2} and d_{L3} are 0.12 and 0.62 respectively.

Table 6-39: Illuminance (lx) and Luminance (cd/m^2) Values Before Iteration-2

Point	Measured E	Measured L	Projected E	% Error
TP-8	241.3	21.2	228.41	5.3
TP-10	220.1	18.6	207.26	5.8

Now, Eq. **16** and Eq. **17** can be used to find the corrective dimming levels Δx and Δy as shown in Eq. **21** and Eq. **22**.

$$\Delta x * 0.12 * 47.53 + \Delta y * 0.62 * 212.82 = 241 - (228.41 - 0.12 * 47.53 - 0.62 * 212.82) \quad (21)$$

$$\Delta x * 0.12 * 146.37 + \Delta y * 0.62 * 101.79 = 226 - (207.26 - 0.12 * 146.37 - 0.62 * 101.79) \quad (22)$$

Solving by least square method, Δx = 1.8283 and Δy = 1.0517. Thus, the new corrected light levels will be x = d_{L2} * Δx and y = d_{L3} * Δy. New light levels of L-2 and L-3 are 22% and 65% respectively. These correspond to 20% and 43% DALI dimming levels respectively. Table **6-40** shows the error in reaching the target illuminance at the two test points.

Table **6-40**: Target Illuminance and Achieved Illuminance After Iteration-2

Point	Target E	Measured E	% Error
TP-8	241	250	-3.7
TP-10	226	239.9	-6.2

6.10.4 Iteration-3:

Iteration-3 is a repetition of the same steps as followed in the previous iteration, with new values of d_{L2} and d_{L3}, namely, 0.22 and 0.65 respectively. Table **6-41** shows the values of E and L before the iteration.

Table **6-41**: Illuminance (lx) and Luminance (cd/m^2) Values Before Iteration-3

Point	Measured E	Measured L	Projected E	% Error
TP-8	250	22	236.25	5.5
TP-10	239.9	20.5	228.7	4.7

Solving Eq. 23 and Eq. 24, we get the corrective dimming levels Δx and Δy.

$$\Delta x * 0.22 * 47.53 + \Delta y * 0.65 * 212.82 = 241 - (236.25 - 0.22 * 47.53 - 0.65 * 212.82) \quad (23)$$

$$\Delta x * 0.22 * 146.37 + \Delta y * 0.65 * 101.79 = 226 - (228.7 - 0.22 * 146.37 - 0.65 * 101.79) \quad (24)$$

The least square solution to the above equations yields Δx = 0.8172 and Δy = 1.0482. Thus the new light levels for L-2 and L-3 are 18% and 68% respectively. These correspond to 11% and 51% dimming levels respectively. Table 6-42 shows that the measured illuminance is fairly close to the target illuminance.

Table 6-42: Target Illuminance and Achieved Illuminance After Iteration-3

Point	Target E	Measured E	% Error
TP-8	241	261.8	-8.6
TP-10	226	231.5	-2.4

There is not much variation in the results of iteration-2 and iteration-3, which shows that the solution is convergent and the dimming levels have stabilized after two iterations. The error in reaching the target light levels at both the points is the least in the case of 1st iteration. The error somewhat increases for subsequent iterations due to inaccurate estimation of available light at these two test points. The inaccurate estimation is partially caused by the error in the luminance and illuminance measurement, and also by the fact that bleached baking flour is not a perfectly Lambertian surface.

The larger the number of test points and luminaires, the greater is the possibility that a unique solution cannot be determined, simply because it might be impossible to reach the target illuminance level at all test points. At some points, the illuminance level may be higher than the target, and at other points it may be lower than the target. The deviation will really depend on

how practical the target light levels are, considering the daylight and electric light distributions and the test point locations in the space. **The key to this algorithm is to find an optimized combination of dimming levels that best achieves the set illuminance levels, thereby minimizing the overall percent deviation at all test points**. It will be shown in the final experiment that the algorithm works quite reliably even for six luminaires and twelve test points.

At times, it is likely that the dimming levels determined in subsequent iterations vary considerably, which might lead to a dramatic change in the lighting condition in the space. This problem can be circumvented in the present algorithm by not allowing drastic changes in the dimming levels. With dimming of the luminaires being a continuous process, slow adjustment in the dimming levels of different luminaires will be a desired feature of CamSensor. Using weighting factors for different luminaires is another alternative for setting a dimming preference, which will be appropriate and desired if the lighting quality in the space is a concern.

To conclude, this experiment proved that illuminance on any test point due to one or more luminaires can be estimated from the current luminance on the desk, provided the luminance contribution due to full output of individual luminaires at the test point, covered with a diffuse surface, is known. The method described in this section will be used in the final control algorithm, which is described in the next section.

Chapter 7

APPLYING CAMSENSOR TO DAYLIGHT CONTROL WITH DALI

Notations Used in This Chapter:

CF_{expX} **:** Calibration factor for converting the radiance values obtained from an image captured by CamSensor at exposure X, to the corresponding luminance values.

$E_{refsurf}$ **:** Average illuminance on the reference Lambertian surface (for example, a gray card if it is sufficiently matte), measured at the center.

$R_{refsurf\text{-}expX}$ **:** Radiance value at the center of the reference Lambertian surface, computed from an image captured by CamSensor at exposure X.

$\rho_{refsurf}$ **:** Average reflectance of the reference Lambertian surface (bleached baking flour with 75% reflectance used in the final experiment).

$L_{DIFF\text{-}LX\text{-}Y}$ **:** Luminance at test point Y due to luminaire X. The test points are covered with Lambertian surfaces[10].

E_Y **:** Present illuminance at test point Y due to daylight + electric light.

$E_{LX\text{-}Y}$ **:** Illuminance at test point Y due to luminaire X (irrespective of whether the illuminance is covered with Lambertian surfaces).

$L_{DIFF\text{-}L\text{-}ALL\text{-}Y}$ **:** Luminance at test point Y due to all luminaires. The test points are covered with Lambertian surfaces.

---

[10] Bleached flour powder pressed uniformly on diffuse bond papers, used throughout this chapter, unless otherwise specified

$E_{L\text{-}ALL\text{-}Y}$ **:** Illuminance at test point Y due to all luminaires operating at 100% output.

$L_{DIFF\text{-}DL\text{-}Y}$ **:** Luminance at test point Y due to daylight. The test points are covered with Lambertian surfaces.

$E_{DL\text{-}Y}$ **:** Illuminance at test point Y due to daylight (irrespective of whether the illuminance is covered with Lambertian surfaces).

$L_{DESK\text{-}LX\text{-}Y}$ **:** Luminance at test point Y on the workplane (desk) due to luminaire X.

$L_{DESK\text{-}L\text{-}ALL\text{-}Y}$ **:** Luminance at test point Y on the workplane (desk) due to all luminaires.

L_Y **:** Luminance at any test point Y due to daylight as well as electric light, obtained during operation (subscript *DIFF*/*DESK* is absent).

$L_{DL\text{-}Y}$ **:** Luminance at any test point Y due to daylight only, obtained during operation.

$L_{EL\text{-}Y}$ **:** Luminance at any test point Y due to electric light (DALI luminaires) only, obtained during operation.

T_Y **:** Target illuminance level at test point Y

x_{LX} **:** Required fractional dimming for luminaire X that best achieves the desired light levels at different test points on the work plane

d_{LX}**:** Present dimming level (ballast output) of the DALI luminaire X.

ρ_{DIFF}**:** Average reflectance of the Lambertian surface.

Based on all the experiments described in the previous chapter, we now formulate the steps to follow to ensure proper functioning of CamSensor. The application of CamSensor consists of two parts: calibration and operation. For the present prototype, the image capturing process is manual. Also, different components of the software are not integrated under a single environment, so they were run separately. However this process can easily be automated in a full-fledged system.

7.1 Calibration

The whole calibration procedure can be divided into two parts, factory calibration, which is done one time for a particular image sensor, and site calibration, which is done every time CamSensor is installed in a new location, or when the room configuration/characteristics change. In a full-fledged product, the former would be a part of the product development process and the latter would be part of the commissioning process.

7.1.1 Factory Calibration

1. Eight images of a high contrast scene (so that a part of the scene is very bright and another part is relatively dark) are captured with different exposure values (Figure 7-1). Digital exposure settings used in this step are: 2, 4, 8, 16, 32, 64, 128 and 255. These images are the input to the High Dynamic Range imaging algorithm.

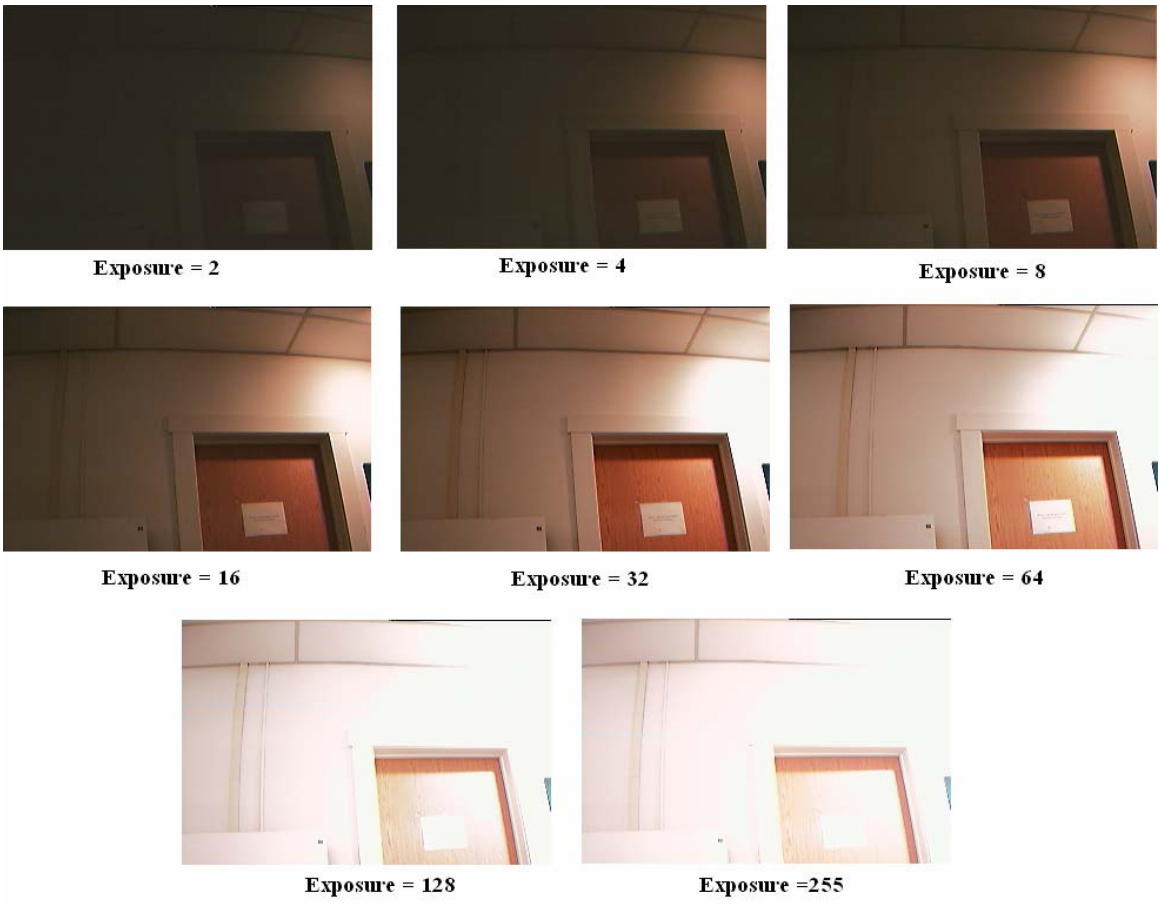

Figure 7-1: Images captured to determine the Image Response Function

2. Approximately 50 pixels are automatically selected from the image with exposure = 32 (5th in the series of 8). The selection criteria for these pixels are their even distribution throughout the image and a limited variation of their values from adjacent pixels. Here the value at a pixel refers to its relative radiance (or luminance, in photometric terms) given by the Y value in the CIE

XYZ chromaticity coordinates[11], obtained by converting the RGB values as described in Section **3.4**.

3. The High Dynamic Range imaging algorithm, discussed in Chapter 3, is used to determine the image response function based on the radiance values of the chosen pixels and also on the corresponding exposure settings. This response function is nothing but a table of 256 values corresponding to 256 pixel values that can be used to compute the radiance values at different pixels in an image, provided the exposure setting used in that image is known. The response function is stored in the master control computer for future reference.
4. Next, the calibration factors that convert the radiance values to corresponding absolute luminance are determined. Note that radiance values, obtained from an image taken with a given exposure setting and a given lighting condition, are proportional to the corresponding luminance values. The calibration factors are nothing but the proportionality factors. Thus, there is a calibration factor for every exposure setting. To determine these calibration factors, images of a scene are captured with all the exposure settings to be used later during site calibration and operation, namely, 4, 8, 16, 32, 64 and 128. A Lambertian surface with known reflectance should be present in the scene and illuminance level on it should also be known. The average radiance values ($R_{refsurf\text{-}expX}$) on this surface will be determined for each case. The CF at a particular exposure can be computed from Eq. **25**. Using this calibration factor, the luminance value can be obtained from the radiance value at any test point Y from an image captured with exposure setting X, as shown in Eq. **26**.

[11] An average value of eight pixels surrounding the test point plus the target pixel itself is used for computing the radiance value at the test point

$$CF_{expX} = E_{refsurf} / (R_{refsurf\text{-}expX} * \pi / \rho_{refsurf}) \quad (25)$$

$$L_Y = R_Y * CF_{expX} \quad (26)$$

It should be pointed out here that the camera response function is dependent not only on the exposure setting of the camera but also on the intensity and the Spectral Power Distribution (SPD) of the light source. To what extent these factors affect the response function is a topic that needs to be investigated in future research. In the present work, all luminaires were fitted with lamps with similar Correlated Color Temperature (CCT) and thus similar SPD.

7.1.2 Site Calibration

In this part of the calibration, our main objective is to determine illuminance contribution due to different luminaires at the different test points on the workplane. No electric light other than the DALI luminaires should be present at this stage. Once site calibration is complete, the location of CamSensor cannot be changed.

1. First, capture an image of the scene and identify the test points. These coordinates will be used during the calibration and operation of CamSensor. If the camera position changes for some reason, calibration must be redone.
2. Capture images of the workplane with the proper exposure setting and with the luminaires at full output, one at a time, with Lambertian surfaces placed on the test points. No daylight should be present. From these images, the luminance values at the different test points (denoted by $L_{DIFF\text{-}LX\text{-}Y}$, at any test point Y) due to the different luminaires can be obtained. Corresponding Illuminance level (denoted by $E_{LX\text{-}Y}$), is obtained from Eq. 27.

$$E_{LX\text{-}Y} = L_{DIFF\text{-}LX\text{-}Y} * \pi / \rho_p \quad (27)$$

3. Turn on all luminaires to full output and capture an image of the workplane with proper exposure setting (no daylight) with Lambertian surfaces placed on the test points. From this image, determine luminance values at different test points (denoted by $L_{DIFF\text{-}L\text{-}ALL\text{-}Y}$ at any test point Y) due to all luminaires at full output. Corresponding illuminance (denoted by $E_{DIFF\text{-}L\text{-}ALL\text{-}Y}$) can be obtained using Eq. **28**. This step is for verification purposes only and will not be used in a fully functional system.

$$E_{L\text{-}ALL\text{-}Y} = L_{DIFF\text{-}L\text{-}ALL\text{-}Y} * \pi / \rho_p \quad (28)$$

4. Capture an image of the workplane with proper exposure setting for a typical daylight condition, with Lambertian surfaces placed on the test points. No electric light should be present. Luminance value $L_{DIFF\text{-}L\text{-}ALL\text{-}Y}$ at any test point Y can be computed. Eq. **29** computes the illuminance at any test point Y due to daylight.

$$E_{DL\text{-}Y} = L_{DIFF\text{-}DL\text{-}Y} * \pi / \rho_p \quad (29)$$

5. Capture an image of the workplane with proper exposure setting for a typical daylight condition, without any electric light, with the Lambertian surfaces removed. Compute luminance values $L_{DESK\text{-}DL\text{-}Y}$ from this image. Daylight conditions should not change between Step 4 and 5. An extra test point with a Lambertian surface in both the steps can be used to verify that daylight has not changed.

6. Capture images of the workplane with proper exposure settings and with luminaires fully turned on, one at a time, with Lambertian surfaces removed**.** From these images, the luminance values at different test points (denoted by $L_{DESK\text{-}LX\text{-}Y}$, for any test point Y) due to different luminaires can be obtained.
7. $L_{DIFF\text{-}DL\text{-}Y}$ / $L_{DESK\text{-}DL\text{-}Y}$ is computed at the different points for a typical daylight condition and stored for future use.
8. Determine the target light levels in terms of % electric light at the different points. For example, at any test point Y, if the desired light level is 90% of the electric light on that point, it is computed as shown in Eq. **30**.

$$T_Y = 0.9 * (E_{L1\text{-}Y} + E_{L2\text{-}Y} + \ldots + E_{L6\text{-}Y}) \quad (30)$$

If there is any change in the configuration of the room causing a change in the test point locations, site calibration must be performed again.

The fact that daylight condition (both intensity and direction) is ever changing has a potential to affect CamSensor performance. Present calibration method considers a typical daylight condition to compute the luminance ratio L_{DIFF}/L_{DESK} (as discussed in the final experiment) in order to estimate illuminance contribution due to daylight during the operation. But more information on the daylight scenario may be required for proper calibration of CamSensor, particularly for spaces where daylight condition changes considerably at different times of the day and year. Again, this issue was not handled in this work in great detail, and will be an important topic for any future research.

7.2 Operation

1. Capture an image of the task area with proper exposure. The proper exposure will be the longest exposure that allows sufficient integration time, yet does not cause saturation near the test points in the image. If any of the test points is saturated (with a pixel value of 255), the exposure needs to be reduced. The correct exposure can be determined by trial and error. If no exposure meets the requirement, a High Dynamic Range imaging technique similar to the calibration method must be applied[12].
2. The present dimming levels of individual luminaires (d_X) are determined by sending query commands to individual ballasts.
3. The luminance value at any test point Y (L_Y) obtained from the image in the first step is the summation of the contribution due to daylight ($L_{DL\text{-}Y}$) and electric light ($L_{EL\text{-}Y}$) (Eq. **31**). Luminance due to electric light at any test point is the summation of individual contributions of the DALI luminaires at the same point, each operating at a different dimming (arc power) level. These individual contributions are obtained by multiplying the present fractional light output level (not the ballast output level) of each of the luminaires by its luminance contribution at the test point. When the total contribution due to all DALI luminaires is subtracted from L_Y, $L_{DL\text{-}Y}$ is obtained (Eq. **32**).

$$L_Y = L_{DL\text{-}Y} + L_{EL\text{-}Y} \quad (31)$$

[12] This could potentially occur when there is too much daylight entering the space, but seems unlikely under normal circumstances.

$$L_{DL-Y} = L_{Y} - (d_{L1} * L_{DESK-L1-Y} + d_{L2} * L_{DESK-L2-Y} + \ldots + d_{L6} * L_{DESK-L6-Y}) \quad (32)$$

4. The luminance at any test point Y due to daylight is now converted to the corresponding illuminance value (E_{DL-Y}) by multiplying the product of this luminance and the luminance ratio ($L_{DIFF-DL-Y} / L_{DESK-DL-Y}$) obtained in step 7 of calibration, by the constant π / ρ_p. Eq. **33** shows the mathematical relationship.

$$E_{DL-Y} = L_{DL-Y} * (L_{DIFF-DL-Y} / L_{DESK-DL-Y}) * \pi / \rho_p \quad (33)$$

5. Using Eq. **34**, Eq. **35** and Eq. **36**, the required change in each of the dimming levels of individual DALI luminaires is determined.

$$x_{L1} * E_{L1-1} + x_{L2} * E_{L2-1} + \ldots + x_{L6} * E_{L6-1} = T_1 - (E_1 - (d_{L1} * E_{L1-1} + d_{L2} * E_{L2-1} + \ldots + d_{L6} * E_{L6-1})) \quad (34)$$

$$x_{L1} * E_{L1-2} + x_{L2} * E_{L2-2} + \ldots + x_{L6} * E_{L6-2} = T_1 - (E_2 - (d_{L1} * E_{L1-2} + d_{L2} * E_{L2-2} + \ldots + d_{L6} * E_{L6-2})) \quad (35)$$

...

$$x_{L1} * E_{L1-12} + x_{L2} * E_{L2-12} + \ldots + x_{L6} * E_{L6-12} = T_1 - (E_{12} - (d_1 * E_{L1-12} + d_{L2} * E_{L2-12} + \ldots + d_{L6} * E_{L6-12})) \quad (36)$$

In matrix form,

$$\mathbf{[E_{LX-Y}].[x] = [T - D]}$$

Where, $[E_{LX-Y}]$ is the matrix for different luminaire contributions at different test points, [x] is the matrix for the dimming levels of the different luminaires, [T-D] is the matrix for the required electric light contributions at different test points (D signifies daylight contribution).

A least square solution for x is determined for the above system of equations.

6. New light output levels of different DALI luminaires are computed by multiplying the fractional numbers (corrective light output levels) obtained in the previous step by the present light output levels of individual luminaires (the product is multiplied by 100 to obtain the corresponding percent light output level). The dimming level of each DALI luminaire is then updated by sending appropriate DALI commands.
7. After a certain interval of time (set by the user of CamSensor), operational steps 1 through 6 are repeated.

7.3 Final Experiment

This experiment follows the calibration and operational steps described in the previous section. The method followed in this experiment is very similar to the one described in the last experiment in the previous chapter.

It was found in the earlier experiments (described in Chapter 6) that the conversion of radiance into luminance involves more error when the illuminance level is low. This is directly related to the signal-to-noise (S/N) ratio of the image sensor. In order to improve the S/N ratio and to estimate the illuminance at a given test point more accurately, a constant light level was maintained during the image capturing process and was subtracted out during the computation. This necessitated adjustment in the calibration and operational procedure, but it must be

emphasized that in a full-fledged system capable of detecting low illuminance variation, this adjustment will not be necessary.

Daylight penetration in the lighting laboratory where the research was carried out was limited, due to the time of the year (December – with mostly cloudy and partly cloudy skies) and also due to the location of the space. Only a small amount of diffuse daylight reached the workplane, and thus was not sufficient to require the electric lights to be dimmed. In order to get around this limitation of the test facility, four 2 X 4 lensed troffers were chosen to simulate diffuse daylight. Although this generated sufficient "daylight" for proper CamSensor operation, it did not generate the gradient of light typical of sidelighting, but was more of a toplighting situation (i.e. skylights). The simulated daylight level was not varied, but the operational procedure in case of that variation will remain the same, and the performance can be expected to be the same.

The following luminaires were used in this experiment:

Dimmable DALI luminaires (EL) – six DALI luminaires, all recessed, with L-1 and L-2 being direct VDT fixtures (2 lamps T8 32W), while L-3, L-4, L-5 and L-6 were recessed louvered fixtures (2 lamps T5 54W).

Luminaires for simulating daylight (DL) – four recessed 2 X 4 troffers (4 lamps T8 32W)

Luminaires for constant light level (ND) – four CFL downlights (CFL 42W) each dimmed to 30%.

Bleached flour pressed evenly on a diffuse white bond paper was used as a Lambertian surface in this experiment. The size of these surfaces was 11"x17" for test point 1, 2 and 8.5"x11" for the rest. A larger area was necessary for the remote test points because of the low resolution of the camera.

7.3.1 Factory Calibration

Table 7-1 shows the calibration factors for the different exposure settings. The values are obtained by comparing the luminance meter readings and radiance values computed at an arbitrarily chosen test point.

Table 7-1: Calibration Factors Based on the Exposure Settings

Exposure	CF (exposure)
4	8.103
8	8.229
16	8.638
32	9.394
64	10.436
128	11.004

7.3.2 Site Calibration

At first, an image of the workplane was captured and the coordinates of all test points in that image were identified, as shown in Table 7-2.

Table 7-2: Target Pixel Coordinates

Target Point	X	Y
TP-1	37	71
TP-2	37	166
TP-3	63	69
TP-4	59	169
TP-5	61	241
TP-6	62	286
TP-7	100	87
TP-8	103	173
TP-9	94	236
TP-10	89	285
TP-11	193	170
TP-12	182	283

Table 7-3 shows the computed luminance values (L_{DIFF}) at different test points covered with Lambertian surfaces, with each of the luminaires fully turned on, one at a time (L-1 through L-6); and also all dimmable luminaires fully turned on simultaneously (L-All). In addition, a typical daylight condition was used to estimate the luminance value due to daylight[13]. In all cases, a constant illuminance level was maintained using additional luminaires (ND). An image was captured with only these luminaires on and luminance values at the different test points were computed. These values are listed in the table and will be needed later in the calibration. The ND contribution was subtracted from the combined contribution to obtain individual luminaire contributions. A value of 0 signifies that the luminance contribution was too small to be detected by CamSensor.

[13] Here the daylight condition is simulated and does not change, but in the real-life situation this condition will be representative of the majority of the daylight conditions in the space.

Table 7-3: Computed Luminance Values (cd/m^2) on the Test points Covered with Lambertian Surface (L_{DIFF})

Luminaire	TP1	TP2	TP3	TP4	TP5	TP6
ND	8.82	11.24	35.61	34.25	33.66	12.77
Typical DL	9.6	11.33	23.6	24.84	30.26	28.28
L-All	36.57	66.74	67.78	118.25	106.27	83.77
L-1	27.62	31.89	53.66	58.56	36.14	6.59
L-2	4.6	34.04	3.63	50.08	63.41	64.8
L-3	0.38	0.3	6.25	8.26	5.37	1.49
L-4	0	0.25	0.11	6.02	9.66	9.85
L-5	0.25	0.51	0.98	1.53	1.1	0.78
L-6	0.28	0.38	0.72	1.42	1.29	1.14

Luminaire	TP7	TP8	TP9	TP10	TP11	TP12
ND	35.36	35.72	37.32	32.2	40.6	30.36
Typical DL	43.41	43.94	46.09	50.59	29.18	36.6
L-All	78.19	122.19	144.5	123.84	94.08	134.27
L-1	40.02	36.89	42.93	29.27	7.88	4.18
L-2	2.07	14.77	45.53	41.39	0.22	2.42
L-3	31.82	58.14	42.83	23.55	69.19	81.58
L-4	4.05	18.55	35.3	40.9	9.28	27.95
L-5	2.17	3.58	2.75	1.88	17.77	23.14
L-6	1.31	2.6	2.64	2.6	4.58	11.57

Table 7-4: Computed Luminance Values (cd/m^2) on the Test points (L_{DESK}) on the Desk

Luminaire	TP1	TP2	TP3	TP4	TP5	TP6
Typical DL	2.38	3.58	10.12	10.28	14.37	11.42
L-All	12.25	25.29	28.79	51.65	50.33	33.88
L-1	9.39	11.1	22.02	24.51	14.71	2.32
L-2	1.2	10.38	0	19.07	26.93	24.88
L-3	0.9	0.8	0.26	1.04	0.31	0.77
L-4	1.22	1.24	0	1.32	2.87	3.46
L-5	0	0.14	0.03	0.25	0.42	0.18
L-6	0	0	0	0	0	0

Luminaire	TP7	TP8	TP9	TP10	TP11	TP12
Typical DL	20.91	20.82	22.01	25.11	14.79	27.05
L-All	38.38	58.02	75.06	58.18	57.47	69.72
L-1	19.31	16.49	18.46	11.68	9.33	0.56
L-2	0	3.98	22.32	16.96	0	0.24
L-3	12.63	25.71	18.08	8.62	34.06	39.13
L-4	0.31	6.59	14.92	17.86	2.23	14.54
L-5	0.63	1.4	0.88	0.68	7.57	10.85
L-6	0	0.33	0.63	0.65	1.35	5.15

Table 7-4 shows the computed luminance values (L_{DESK}) at different test points with Lambertian surfaces removed, with each of the luminaires fully turned on, one at a time. Luminance values due to a typical daylight condition are also listed. ND contribution has not been listed in the table as it is not needed later, but was subtracted from the combined contribution as before to obtain the individual luminaire contribution.

Table 7-5 shows the measured luminance values at different test points.

Table 7-6 lists the ratio of computed luminance and measured luminance.

Table 7-5: Measured Luminance Values (cd/m^2) on the Test points on the Desk

Luminaire	TP1	TP2	TP3	TP4	TP5	TP6
ND	3.22	3.46	13.8	11.3	10.8	4.22
L-ALL	12.2	18.9	26.7	41.7	39.5	28.7
L-1	8.6	8.5	20.1	19.4	11.3	2.5
L-2	1.9	8.7	1.9	16	20.2	21
L-3	0.73	0.71	3.48	3.14	2.56	1.26
L-4	0.5	0.74	1.13	2.76	4.12	4.1
L-5	0.17	0.16	0.3	0.3	0.26	0.2
L-6	0.16	0.17	0.25	0.3	0.33	0.33

Luminaire	TP7	TP8	TP9	TP10	TP11	TP12
ND	13.6	11.7	12.3	11.1	13.9	12
L-ALL	32.9	45.5	61	49.8	48.4	64
L-1	16	12.7	13.4	10	7.5	2.2
L-2	1.25	5.2	17.2	13.6	1	1.86
L-3	12.7	20.4	17	9.51	30.4	34
L-4	2.15	6.45	13.6	16.8	3.86	15.1
L-5	0.69	0.95	0.81	0.63	5.71	8.22
L-6	0.44	0.7	0.9	0.87	1.5	4.1

Table 7-6: Ratio of Computed Luminance and Measured Luminance

Luminaire	TP1	TP2	TP3	TP4	TP5	TP6
ND	0.863	1.009	1.017	1.144	1.209	0.972
L-ALL	1.004	1.338	1.078	1.239	1.274	1.18
L-1	1.092	1.306	1.096	1.263	1.302	0.928
L-2	0.632	1.193	0	1.192	1.333	1.185
L-3	1.233	1.127	0.075	0.331	0.121	0.611
L-4	2.44	1.676	0	0.478	0.697	0.844
L-5	0	0.875	0.1	0.833	1.615	0.9
L-6	0	0	0	0	0	0

Luminaire	TP7	TP8	TP9	TP10	TP11	TP12
ND	1.14	1.264	1.258	1.123	1.253	1.085
L-ALL	1.167	1.275	1.23	1.168	1.187	1.089
L-1	1.207	1.298	1.378	1.168	1.244	0.255
L-2	0	0.765	1.298	1.247	0	0.129
L-3	0.994	1.26	1.064	0.906	1.12	1.151
L-4	0.144	1.022	1.097	1.063	0.578	0.963
L-5	0.913	1.474	1.086	1.079	1.326	1.32
L-6	0	0.471	0.7	0.747	0.9	1.256

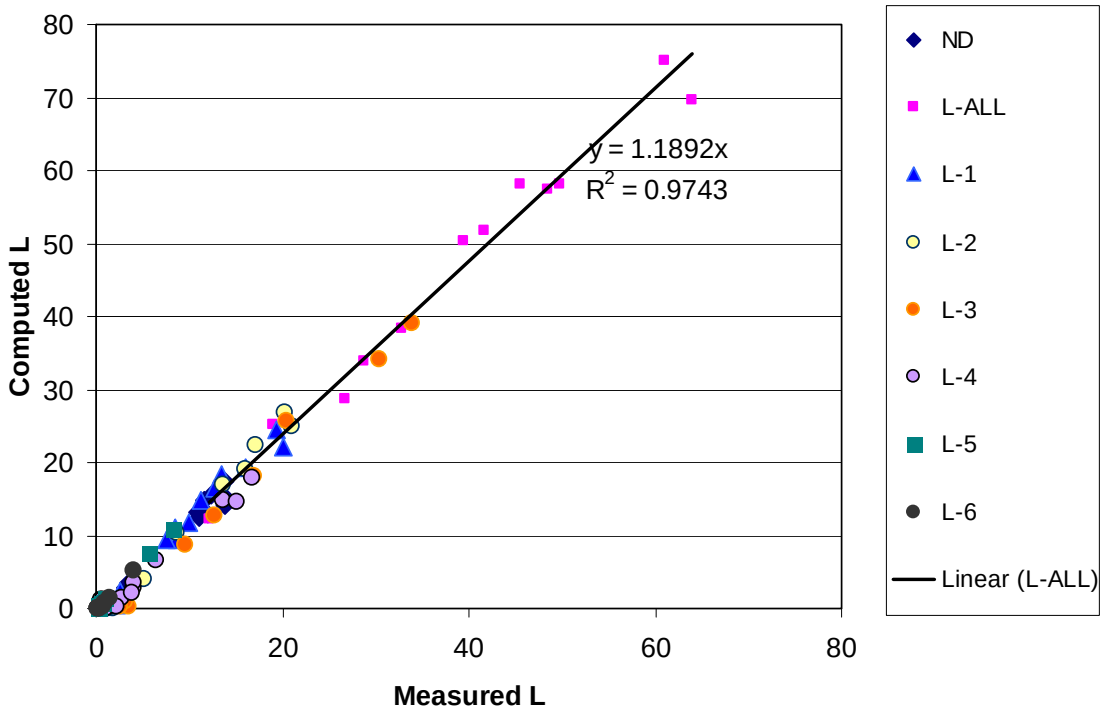

Figure 7-2: Measured vs. Computed Luminance Values (in cd/m^2) at Different Test points Due to Different Sources

Figure 7-2 plots computed luminance values against measured luminance values for different test points and different light sources.

Table 7-7: Computed Illuminance Contributions (lx) on Different Test points

Luminaire	TP1	TP2	TP3	TP4	TP5	TP6
ND	37.1	47.28	149.78	144.06	141.57	53.71
L-All	153.81	280.7	285.08	497.36	446.98	352.34
L-1	116.17	134.12	225.69	246.3	152.01	27.72
L-2	19.34	143.17	15.26	210.63	266.71	272.55
L-3	1.6	1.26	26.28	34.74	22.59	6.27
L-4	0	1.05	0.46	25.32	40.63	41.43
L-5	1.05	2.14	4.12	6.43	4.63	3.28
L-6	1.17	1.59	3.02	5.97	5.43	4.8

Luminaire	TP7	TP8	TP9	TP10	TP11	TP12
ND	148.72	150.24	156.97	135.43	170.76	127.69
L-All	328.87	513.93	607.76	520.87	395.7	564.74
L-1	168.33	155.16	180.56	123.11	33.15	17.59
L-2	8.71	62.12	191.5	174.09	0.93	10.18
L-3	133.84	244.54	180.14	99.05	291.02	343.13
L-4	17.04	78.02	148.47	172.03	39.04	117.56
L-5	9.13	15.06	11.56	7.91	74.74	97.33
L-6	5.51	10.93	11.1	10.94	19.27	48.67

The illuminance contributions due to different luminaires, ND and daylight (DL) shown in Table 7-7 are obtained by multiplying L_{DIFF} values with the Multiplication Factor (π / ρ) which is 4.206 and constant for the Lambertian surface used.

Table 7-8 shows the measured illuminance contributions at different test points.

Table 7-9 lists the percent errors at different test points for different sources. At lower illuminance levels, the error in estimating the illuminance is greater.

Table 7-8: Measured Illuminance Contributions (lx) on Different Test points

Luminaire	TP1	TP2	TP3	TP4	TP5	TP6
ND	42.7	48.6	162.4	138.7	136.8	48
L-All	165.3	276.6	323	519	492	357
L-1	123.9	126.1	250.6	252.8	142.4	24.52
L-2	23.54	130.5	21	199.9	274	273.5
L-3	9.1	8.9	35.3	38.1	26.5	13.2
L-4	6	9.2	11.93	31.6	45.8	44.9
L-5	1.93	1.85	3.03	3.28	2.7	2.13
L-6	1.8	2.1	2.7	3.5	3.85	3.74

Luminaire	TP7	TP8	TP9	TP10	TP11	TP12
ND	138	123.8	134.9	127.6	153.1	118.2
L-All	343	496	653	570	421	635
L-1	163.5	130.6	168.4	115.5	31	22.3
L-2	12.7	44.3	159.4	158.5	5.75	12.31
L-3	136.9	244.1	177	102.1	287	375
L-4	23.2	70.9	147.3	190.7	37.4	116.6
L-5	7	10.54	8.1	6.65	59.9	85.3
L-6	4.64	7.8	9	9.36	15.35	42.2

Table 7-9: Ratio of Computed Illuminance and Measured Illuminance

Luminaire	TP1	TP2	TP3	TP4	TP5	TP6
ND	0.869	0.973	0.922	1.039	1.035	1.119
L-All	0.93	1.015	0.883	0.958	0.908	0.987
L-1	0.938	1.064	0.901	0.974	1.067	1.131
L-2	0.822	1.097	0.727	1.054	0.973	0.997
L-3	0.176	0.142	0.744	0.912	0.852	0.475
L-4	0	0.114	0.039	0.801	0.887	0.923
L-5	0.544	1.157	1.36	1.96	1.715	1.54
L-6	0.65	0.757	1.119	1.706	1.41	1.283

Luminaire	TP7	TP8	TP9	TP10	TP11	TP12
ND	1.078	1.214	1.164	1.061	1.115	1.08
L-All	0.959	1.036	0.931	0.914	0.94	0.889
L-1	1.03	1.188	1.072	1.066	1.069	0.789
L-2	0.686	1.402	1.201	1.098	0.162	0.827
L-3	0.978	1.002	1.018	0.97	1.014	0.915
L-4	0.734	1.1	1.008	0.902	1.044	1.008
L-5	1.304	1.429	1.427	1.189	1.248	1.141
L-6	1.188	1.401	1.233	1.169	1.255	1.153

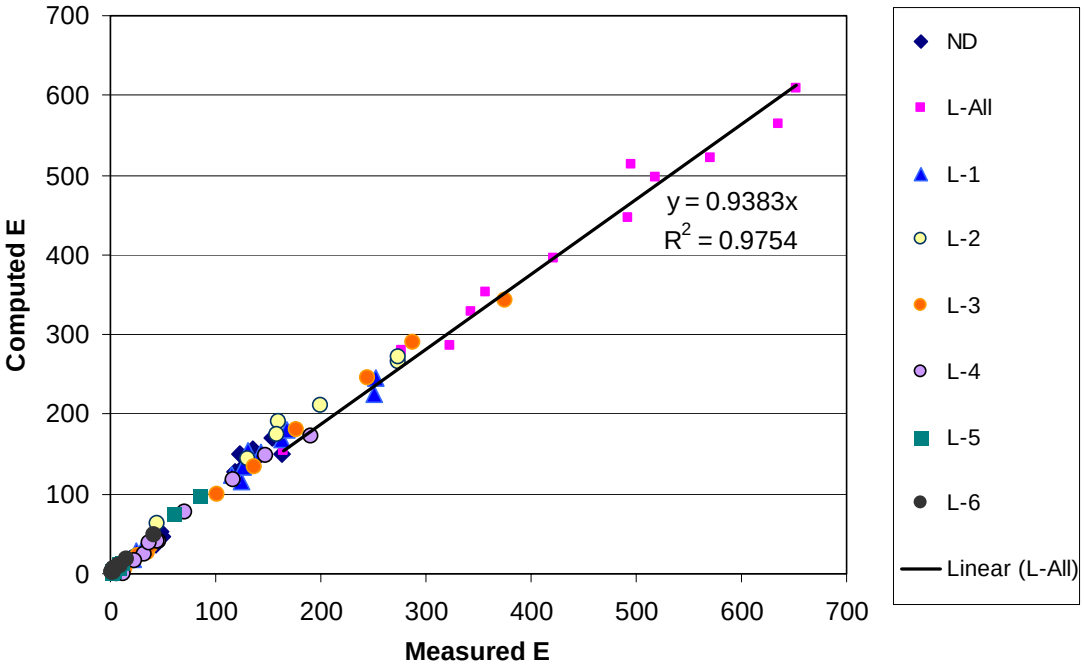

Figure 7-3: Measured vs. Computed Illuminance Values (in lux) at Different Test points Due to Different Sources

Figure 7-3 plots computed illuminance values against measured illuminance values for different test points and different light sources.

The ratio of luminance with and without the Lambertian surface for the typical daylighting condition (ND present as usual) is given in Table 7-10. These values will be used to estimate daylight level during operation.

Table 7-10: Ratio of (L_{DIFF} / L_{DESK}) for Typical Daylight (Constant Light Level Present)

Luminaire	TP1	TP2	TP3	TP4	TP5	TP6
ND + Typical DL	3.57	3.192	2.451	2.546	2.33	2.645

Luminaire	TP7	TP8	TP9	TP10	TP11	TP12
ND + Typical DL	2.163	2.237	2.225	2.203	2.167	1.671

Also, the target illuminance levels are established during the site calibration. In this test, the target illuminance level was set at 90% of the total contribution due to the dimmable DALI luminaires at any test point in question. Table 7-11 shows the target illuminance levels at different test points.

Table 7-11: Target Illuminance Levels at Different Test Points

% Electric	TP1	TP2	TP3	TP4	TP5	TP6
90	125.4	255	247.3	476.5	442.8	320.4

% Electric	TP7	TP8	TP9	TP10	TP11	TP12
90	308.3	509.2	651	528.4	412.3	571

7.3.3 Operation

The operation is a continuous process. An image of the workplane is captured and the illuminance levels at different test points are computed. Daylight level is estimated from the knowledge of the current dimming levels of the dimmable luminaires and, accordingly, the required dimming levels required to maintain target light levels are determined. The dimming levels are continually adjusted at a specified time interval. In order to evaluate the performance of CamSensor, three iterations were performed in this final test.

7.3.3.1 Iteration-1

In the beginning, all dimmable DALI luminaires are operating at full output.

An image with exposure setting 16 was captured and luminance values due to DALI dimmable luminaires (EL), daylight (DL) and ND for constant light level were computed. This is denoted as L (DL+EL+ND) in Table 7-12. Luminance values due to dimmable luminaires L (EL) at different test points are computed by summing the product of the current light level (which is 100%) of each luminaire by the corresponding luminance L_{DESK} given in Table 7-4 under full light output. For example, at TP-2, L (EL) = 11.1 + 10.38 + 0.8 + 1.24 + 0.14 + 0 = 23.66 cd/m^2. L (DL+ND) is obtained by subtracting L (EL) from L (DL+EL+ND). L (DL+ND) when multiplied by the ratio of (L_{DIFF} / L_{DESK}) for DL+ND and MF (π / ρ = 4.206), illuminance due to daylight and constant light level E (DL+ND) is obtained. From these values, illuminance due daylight (DL) can be obtained by subtracting the constant light level E (ND), listed in Table 7-7.

Table 7-12: Projected Values of Daylight and Dimmable Electric Lights Before Iteration-1

	TP1	TP2	TP3	TP4	TP5	TP6
L(DL+EL+ND)	17.11	33	51.92	72.71	75.48	48.21
L(DL+ND)	4.4	9.34	29.61	26.52	30.24	16.6
E(DL+ND)	66.07	125.39	305.25	283.99	296.35	184.67
E(DL)	28.97	78.11	155.47	139.93	154.78	130.96
E(EL)	139.33	283.33	274.83	529.39	492	356.05

	TP7	TP8	TP9	TP10	TP11	TP12
L(DL+EL+ND)	71.54	90.64	107.62	91.61	87.08	104.48
L(DL+ND)	38.66	36.14	32.33	35.16	32.54	34.01
E(DL+ND)	351.71	340.03	302.56	325.79	296.58	239.03
E(DL)	202.99	189.79	145.59	190.36	125.82	111.34
E(EL)	342.56	565.83	723.33	587.13	458.15	634.46

Table 7-13: Measured and Computed Illuminance and the Error in Estimation

	TP1	TP2	TP3	TP4	TP5	TP6
Measured E (EL+DL)	235.2	372	496	733	716	544
Projected E (EL+DL)	168.3	361.44	430.3	669.32	646.78	487.01
% Error (EL+DL)	28.4	2.8	13.2	8.7	9.7	10.5
Measured E (DL)	39.7	42.7	115.5	107.2	138	118.7
Projected E (DL)	28.97	78.11	155.47	139.93	154.78	130.96
% Error (DL)	27	-82.9	-34.6	-30.5	-12.2	-10.3

	TP7	TP8	TP9	TP10	TP11	TP12
Measured E (EL+DL)	624	764	982	932	626	895
Projected E (EL+DL)	545.55	755.62	868.92	777.49	583.97	745.8
% Error (EL+DL)	12.6	1.1	11.5	16.6	6.7	16.7
Measured E (DL)	224	190.6	211.9	264.3	137.2	169.1
Projected E (DL)	202.99	189.79	145.59	190.36	125.82	111.34
% Error (DL)	9.4	0.4	31.3	28	8.3	34.2

The error in estimating the illuminance due to daylight as well as daylight and electric light is shown in Table 7-13. E (EL+DL) is computed by adding E (DL) and E (EL) from Table 7-12.

Using the data given in Table 7-12 and the algorithm discussed in Section 7.2, required percent light levels are computed, as shown in Table 7-14.

Table 7-14: Required Percent Light Levels Determined in Iteration-1

Luminaire	% light levels
L-1	44
L-2	63
L-3	41
L-4	87
L-5	100
L-6	100

Table 7-15 shows the result after dimming to the required levels.

Table 7-15: Percent Deviation from Target Levels After Iteration-1

	TP1	TP2	TP3	TP4	TP5	TP6
Computed E (EL+DL)	95.15	232.48	282.7	429.67	444.36	361.56
Target E (From Computation)	125.4	255	247.3	476.5	442.8	320.4
% Error	24.1	8.8	-14.3	9.8	-0.4	-12.8
Measured E (EL+DL)	123	196.7	272.6	391	430	353
Target E (From Measurement)	148.77	248.94	290.7	467.1	442.8	321.3
% Error	-21	-26.6	-6.6	-19.5	-3	9

	TP7	TP8	TP9	TP10	TP11	TP12
Computed E (EL+DL)	366.88	491.32	571.37	563.33	388.28	514.45
Target E (From Computation)	308.3	509.2	651	528.4	412.3	571
% Error	-19	3.5	12.2	-6.6	5.8	9.9
Measured E (EL+DL)	390	451	605	640	375	564
Target E (From Measurement)	308.7	446.4	587.7	513	378.9	571.5
% Error	20.8	1	2.9	19.8	-1	-1.3

It was impossible to reach the target levels at all test points simultaneously, since some of the points were directly underneath the luminaires simulating daylight, for example, TP-7. Thus,

some points are bound to be under the target levels, while some others are likely to get more light than desired. The dimming algorithm tries to optimize the dimming levels.

Note that the percent Error from Computation is the percent deviation of the estimated illuminance after dimming from the estimated target illuminance. The percent error from Measurement gives the percent deviation of the current illuminance from target illuminance as measured.

7.3.3.2 Iteration-2

Using the dimming levels determined in the previous iteration and data in Table 7-4, present luminance contributions due to EL, DL and ND are determined as described under iteration-1. Individual contributions due to DL and EL are also computed and shown in Table 7-16.

Table 7-16: Projected Values of Daylight and Dimmable Electric Lights Before Iteration-2

	TP1	TP2	TP3	TP4	TP5	TP6
L(DL+EL+ND)	9.32	19.11	34.24	45.68	51.25	33.57
L(DL+ND)	3.0	6.14	24.41	21.06	24.77	13.37
E(DL+ND)	45.08	82.43	251.69	225.49	242.72	148.73
E(DL)	7.98	35.15	101.91	81.43	101.15	95.02
E(EL)	66.18	154.37	127.23	289.74	289.58	230.6

	TP7	TP8	TP9	TP10	TP11	TP12
L(DL+EL+ND)	50.23	60.28	70.41	65.77	57.33	73.02
L(DL+ND)	35.66	32.51	26.32	29.54	28.4	27.93
E(DL+ND)	324.38	305.91	246.34	273.75	258.85	196.29
E(DL)	175.66	155.67	89.37	138.32	88.09	68.6
E(EL)	163.89	301.53	425.78	372.97	262.46	403.11

Table 7-17: Measured and Computed Illuminance and the Error in Estimation

	TP1	TP2	TP3	TP4	TP5	TP6
Measured E (EL+DL)	123	196.7	272.6	391	430	353
Projected E (EL+DL)	74.2	189.5	229.1	371.2	390.7	325.6
% Error	39.7	3.7	16	5.1	9.1	7.8
Target E (from Measurement)	148.77	248.94	290.7	467.1	442.8	321.3
% Error	17.3	21	6.2	16.3	2.9	-9.9

	TP7	TP8	TP9	TP10	TP11	TP12
Measured E (EL+DL)	390	451	605	640	375	564
Projected E (EL+DL)	339.6	457.2	515.2	511.3	350.6	471.7
% Error	12.9	-1.4	14.8	20.1	6.5	16.4
Target E (from Measurement)	308.7	446.4	587.7	513	378.9	571.5
% Error	-26.3	-1	-2.9	-24.8	1	1.3

The error in estimating the illuminance due to daylight as well as daylight and electric light is shown in Table 7-17.

Using the data given in Table 7-16 and the algorithm discussed in Section 7.2, required light levels are computed, as shown in Table 7-18.

Table 7-18: Required Percent Light Levels Determined in Iteration-2

Luminaire	% light levels
L-1	63
L-2	71
L-3	33
L-4	99
L-5	100
L-6	100

Table 7-19 shows the result after dimming to the required levels.

Table 7-19: Percent Deviation from Target Levels After Iteration-2

	TP1	TP2	TP3	TP4	TP5	TP6
Computed E (EL+DL)	97.65	226.48	271.2	435.08	444.02	357.16
Target E (From Computation)	125.4	255	247.3	476.5	442.8	320.4
% Error	22.1	11.2	-9.7	8.7	-0.3	-11.5
Measured E (EL+DL)	148.2	234.1	321	459	485	385
Target E (from Measurement)	148.77	248.94	290.7	467.1	442.8	321.3
% Error	0.4	6	-10.4	1.7	-9.5	-19.8

	TP7	TP8	TP9	TP10	TP11	TP12
Computed E (EL+DL)	363.57	481.45	568.18	561.33	338.33	462.53
Target E (From Computation)	308.3	509.2	651	528.4	412.3	571
% Error	-17.9	5.4	12.7	-6.2	17.9	19
Measured E (EL+DL)	415	468	650	686	365	549
Target E (from Measurement)	308.7	446.4	587.7	513	378.9	571.5
% Error	-34.4	-4.8	-10.6	-33.7	3.7	3.9

Illuminance due to daylight and electric light has been computed by summing the individual luminaire contributions based on the current percent light levels and the contribution due to daylight.

Note that at several points the estimated error in achieving the target illuminance is considerably different from the actual error obtained from the measurement data, which is mainly due to the inaccurate estimation of daylight. This can be verified by considering total dimmable DALI contributions (EL) as shown in Table 7-20, which shows that the error in estimating the electric light contributions is much less at many of these points.

Table 7-20: Percent Error in Estimating Electric Light Levels (EL) at Different Test Points

	TP1	TP2	TP3	TP4	TP5	TP6
computed E (EL)	89.67	191.33	169.29	353.65	342.87	262.14
measured E (EL)	108.5	191.4	205.5	351.8	347	266.3
% Error	17.4	0	17.6	-0.5	1.2	1.6

	TP7	TP8	TP9	TP10	TP11	TP12
computed E (EL)	187.91	325.78	478.81	423.01	250.24	393.93
measured E (EL)	191	277.4	438.1	421.7	227.8	379.9
% Error	1.6	-17.4	-9.3	-0.3	-9.9	-3.7

7.3.3.3 Iteration-3

The dimming levels in the beginning of the iteration-3 are the same as determined the previous iteration.

As before, an image of the workplane was captured and luminance and illuminance values were estimated using the same procedure discussed before. The values are listed in Table 7-21.

Table 7-21: Projected Values of Daylight and Dimmable Electric Lights Before Iteration-3

	TP1	TP2	TP3	TP4	TP5	TP6
L(DL+EL+ND)	10.39	20.46	36.41	50.26	54.92	34.55
L(DL+ND)	2.12	4.47	22.42	19.38	23.17	11.56
E(DL+ND)	31.8	59.95	231.14	207.52	227.05	128.65
E(DL)	0	12.67	81.36	63.46	85.48	74.94
E(EL)	89.67	191.33	169.29	353.65	342.87	262.14

	TP7	TP8	TP9	TP10	TP11	TP12
L(DL+EL+ND)	51.62	61.44	76.97	69.76	56.35	73.49
L(DL+ND)	34.35	31.49	27.25	28.50	28.10	29.66
E(DL+ND)	312.5	296.26	254.98	264.11	256.16	208.45
E(DL)	163.78	146.02	98.01	128.68	85.4	80.76
E(EL)	187.91	325.78	478.81	423.01	250.24	393.93

The error in estimating the illuminance due to daylight as well as daylight and electric light is shown in Table 7-22.

Table 7-22: Projected Values of Daylight and Dimmable Electric Lights Before Iteration-3

	TP1	TP2	TP3	TP4	TP5	TP6
Measured E (EL+DL)	148.2	234.1	321	459	485	385
Projected E(EL+DL)	89.7	204	250.7	417.1	428.4	337.1
% Error	39.5	12.9	21.9	9.1	11.7	12.4
Target E (from Measurement)	148.77	248.94	290.7	467.1	442.8	321.3
% Error	0.4	6	-10.4	1.7	-9.5	-19.8

	TP7	TP8	TP9	TP10	TP11	TP12
Measured E (EL+DL)	415	468	650	686	365	549
Projected E(EL+DL)	351.7	471.8	576.8	551.7	335.6	474.7
% Error	15.3	-0.8	11.3	19.6	8.1	13.5
Target E (from Measurement)	308.7	446.4	587.7	513	378.9	571.5
% Error	-34.4	-4.8	-10.6	-33.7	3.7	3.9

Table 7-23: Required Percent Light Levels Determined in Iteration-3

Luminaire	% light levels
L-1	70
L-2	76
L-3	32
L-4	90
L-5	100
L-6	84

Using the data given in Table 7-16 and the algorithm discussed in Section 7.2, required percent light levels are computed, as shown in Table 7-23.

Table 7-24 shows the result after adjusting the dimming levels of the luminaires.

Table 7-24: Percent Deviation from Target Levels After Iteration-3

	TP1	TP2	TP3	TP4	TP5	TP6
Computed E (EL+DL)	98.56	220.19	266.42	441.3	447.57	348.09
Target E (From Computation)	125.4	255	247.3	476.5	442.8	320.4
% Error	21.4	13.7	-7.7	7.4	-1.1	-8.6
Measured E (EL+DL)	158.9	250	339	490	504	397
Target E (from Measurement)	148.77	248.94	290.7	467.1	442.8	321.3
% Error	-6.8	-0.4	-16.6	-4.9	-13.8	-23.6

	TP7	TP8	TP9	TP10	TP11	TP12
Computed E (EL+DL)	360.15	474.56	582.09	550.79	328.5	454.63
Target E (From Computation)	308.3	509.2	651	528.4	412.3	571
% Error	-16.8	6.8	10.6	-4.2	20.3	20.4
Measured E (EL+DL)	424	470	653	684	358	530
Target E (from Measurement)	308.7	446.4	587.7	513	378.9	571.5
% Error	-37.4	-5.3	-11.1	-33.3	5.5	7.3

As mentioned before, the estimated error in reaching the target light levels at several points is different than the actual error obtained from the measurement. This is evident from Table 7-25 as well.

Table 7-25: Percent Error in Estimating Electric Light Levels (EL) at Different Test Points

	TP1	TP2	TP3	TP4	TP5	TP6
computed E (EL)	98.56	207.52	185.06	377.84	362.09	273.15
measured E (EL)	119.2	207.3	223.5	382.8	366	278.3
% Error	17.3	-0.1	17.2	1.3	1.1	1.9

	TP7	TP8	TP9	TP10	TP11	TP12
computed E (EL)	196.37	328.54	484.09	422.11	243.10	373.87
measured E (EL)	200	279.4	441.1	419.7	220.8	360.9
% Error	1.8	-17.6	-9.7	-0.6	-10.1	-3.6

7.3.4 Performance Analysis

Table 7-26 compares the computed values of target and predicted illuminance due to daylight and electric light after each of the three iterations. Estimated errors in reaching the target light levels are also shown.

Table 7-26: Target and Predicted Illuminance Due to daylight and electric light (lx) As Computed After Each Iteration

Test Point	Target E (From Computation)	Iteration-1		Iteration-2		Iteration-3	
		Computed E (EL+DL)	% Error	Computed E (EL+DL)	% Error	Computed E (EL+DL)	% Error
TP1	125.4	95.15	24.1	97.65	22.1	97.65	22.1
TP2	255	232.48	8.8	226.48	11.2	226.48	11.2
TP3	247.3	282.7	-14.3	271.2	-9.7	271.2	-9.7
TP4	476.5	429.67	9.8	435.08	8.7	435.08	8.7
TP5	442.8	444.36	-0.4	444.02	-0.3	444.02	-0.3
TP6	320.4	361.56	-12.8	357.16	-11.5	357.16	-11.5
TP7	308.3	366.88	-19	363.57	-17.9	363.57	-17.9
TP8	509.2	491.32	3.5	481.45	5.4	481.45	5.4
TP9	651	571.37	12.2	568.18	12.7	568.18	12.7
TP10	528.4	563.33	-6.6	561.33	-6.2	561.33	-6.2
TP11	412.3	388.28	5.8	338.33	17.9	338.33	17.9
TP12	571	514.45	9.9	462.53	19	462.53	19

Table 7-27 compares the measured values of target and achieved illuminance due to daylight and electric light after each of the three iterations.

Table 7-27: Target and Achieved Illuminance Due to daylight and electric light (lx) As Measured After Each Iteration

Test Point	Target E (From Measurement)	Iteration-1		Iteration-2		Iteration-3	
		Measured E (EL+DL)	% Error	Measured E (EL+DL)	% Error	Measured E (EL+DL)	% Error
TP1	148.77	123	17.3	148.2	0.4	158.9	-6.8
TP2	248.94	196.7	21	234.1	6	250	-0.4
TP3	290.7	272.6	6.2	321	-10.4	339	-16.6
TP4	467.1	391	16.3	459	1.7	490	-4.9
TP5	442.8	430	2.9	485	-9.5	504	-13.8
TP6	321.3	353	-9.9	385	-19.8	397	-23.6
TP7	308.7	390	-26.3	415	-34.4	424	-37.4
TP8	446.4	451	-1	468	-4.8	470	-5.3
TP9	587.7	605	-2.9	650	-10.6	653	-11.1
TP10	513	640	-24.8	686	-33.7	684	-33.3
TP11	378.9	375	1	365	3.7	358	5.5
TP12	571.5	564	1.3	549	3.9	530	7.3

Note that in the course of the operation, the absolute deviation from the target illuminance level will reduce at some points, while it will increase at other points. For example, while at test points 5 and 6, the deviation increases during the iterations, at neighboring test point 4, the magnitude of the error first goes down from iteration 1 to 2, and then increases slightly during iteration 3. But at all three test points, the illuminance increases from one iteration to the next. It was impossible to reach the target level at test point 4 without overshooting at test points 5 and 6, since the contribution from L-2 was more at test points 5 and 6 than at test point 4. The dimming algorithm considers all the test points simultaneously and tries to optimize the light levels so that the overall error in reaching the target illuminance at all points can be minimized.

Table 7-28 shows the percent light levels determined by the dimming algorithm during the three iterations. Note that significant change in the percent light level occurs mainly for L-1 and L-6. If the current illuminance could be accurately estimated at all the test points, the required light levels (and the corresponding DALI dimming levels) could be precisely computed in the very first iteration. But the error in illuminance estimation at different test points led to an

adjustment in the light levels of different luminaires in successive iterations, based on the illuminance predicted by CamSensor.

Table 7-28: Percent Light Levels Determined by the Dimming Algorithm During the Three Iterations

Luminaire	Initial	Iteration-1	Iteration-2	Iteration-3
L-1	100	44	63	70
L-2	100	63	71	76
L-3	100	41	33	32
L-4	100	87	99	90
L-5	100	100	100	100
L-6	100	100	100	84

Figure 7-4 and Figure 7-5 further explain how the performance of CamSensor changes during the iterations.

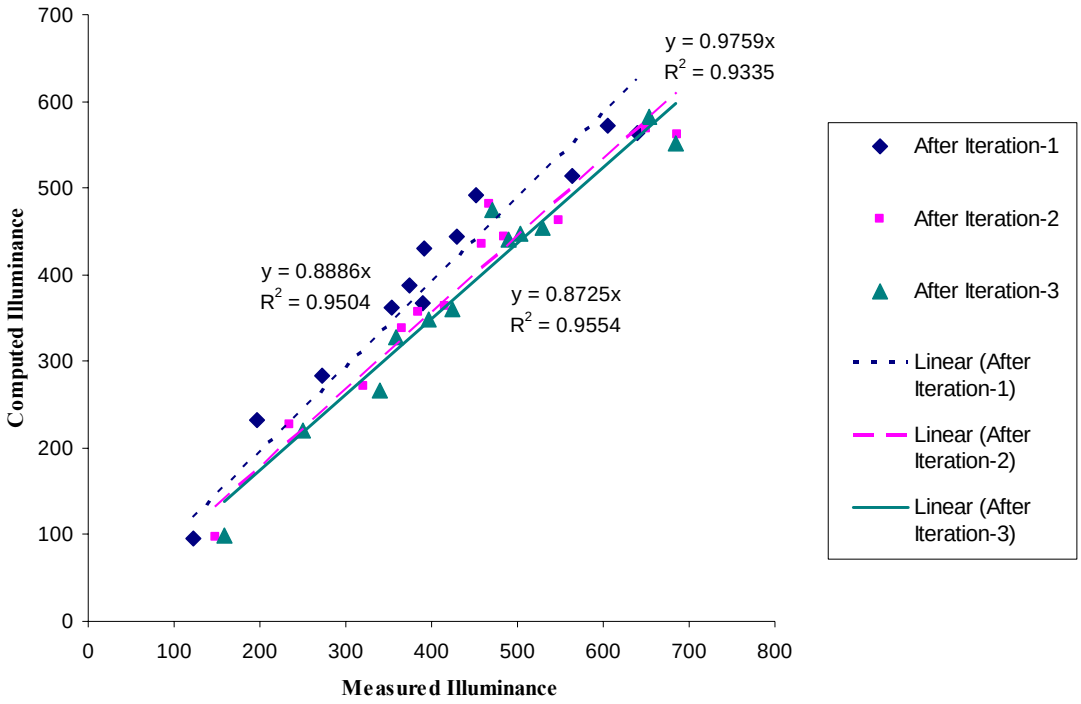

Figure 7-4: Comparison of the Plots of Measured and Computed Illuminance At Different Test Points After Different Iterations

Figure 7-4 compares the relationship between the measured and the computed illuminance levels after each of the iterations. Figure 7-5 does the same, but considers the measured illuminance and the target illuminance instead. The first figure helps analyze the performance of CamSensor as far as estimating the light levels are concerned and the second one helps analyze how successfully CamSensor achieved the target illuminance levels at different test points.

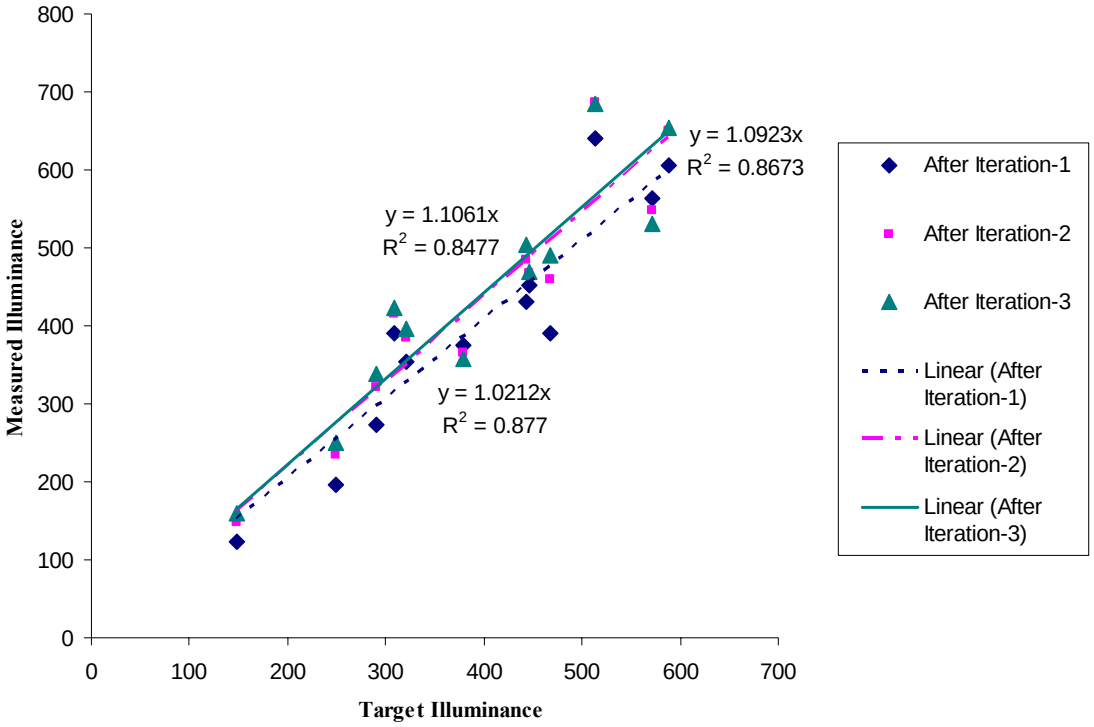

Figure 7-5: Comparison of the Plots of Measured and Target Illuminance (in lux) At Different Test Points After Different Iterations

The equation of the trend line is in the form y = m*x. Ideally, the value of m (slope) should be 1. An R^2 value (correlation coefficient) of 1 signifies perfect alignment of all the data points. Considering all these, it appears that iteration-1 produced a slightly better result than the other two.

To conclude, the final experiment clearly shows that the proposed solution works. The dimming algorithm also works, though its performance depends on the accuracy of its inputs, that is, the perceived daylight level in the space. This experiment also shows there are scopes of improvement as far as the imaging system is concerned, and once the imaging system is capable of estimating the illuminance levels more accurately, even at low light levels, CamSensor performance will improve.

Chapter 8

CONCLUSION

The objective of this research was to develop and evaluate a functional prototype based on an inexpensive image sensor acting as a light sensing device, and to use it as a photosensor. This is the first time a low end CMOS camera chip has been used in lighting research for the purpose of light level sensing and also for lighting control. From this consideration, CamSensor is a proof-of-concept for the application of CMOS sensor based digital imaging in the field of lighting control.

8.1 Objectives Fulfilled

The following objectives have been achieved in this work:

- The feasibility of the proposed solution was successfully demonstrated in this work.
- A suitable procedure for estimating illuminance values at different test points from the corresponding luminance values was suggested and the error associated with the method was estimated.
- A dimming algorithm that allows the system to achieve different target illuminance levels at different test points was proposed and successfully implemented.
- The possible effects of changing electric light conditions on the performance of the system were investigated.
- Guidelines for proper calibration and operation of CamSensor were established.

8.2 Limitations of the Prototype and Test Setup

Considering the possibilities, the present prototype is rather rudimentary from a functional point of view. The camera module could not be integrated with the CamSensor software because of hardware restrictions. Because of the requirement of interfacing the camera module with the computer, a placement constraint was imposed, which limited the workplane area considered in the research. A workplane area closer to the window could not be chosen for the same reason.

Based on the results of this study, the camera module was not perfectly suited for the application mainly due to low resolution and a large aperture setting. A fixed 6 mm, F1.6 optical lens was used with the image sensor. A smaller aperture setting would bring a larger workplane area into focus, and a little higher resolution might have been helpful in determining the scene radiance values more accurately. Better control over the exposure setting could have improved the performance of the camera module at low illuminance levels.

For several reasons, a CMOS sensor is preferred over a CCD sensor for this application. One major reason is the commercial prospect of such a solution. The results of this research justify the use of CMOS sensor for CamSensor. However, further research is needed in order to draw a final conclusion on the choice of the image sensor.

One major limitation of the test facility was limited daylight penetration. This necessitated the use of simulated daylight. Summertime would have been more appropriate for this research. However the timeframe of this project was not a matter of choice.

8.3 Limitations of the Proposed Solution

CamSensor is not a definite winner over conventional photosensor based systems. Like any other new technology, it has its own limitations. There is certain amount of approximation associated with estimating luminance from a scene image, and also with deriving illuminance from luminance. The calibration procedure will not be very straightforward or even automatic, since user intervention will be required in identifying the target points and also determining the luminance ratio with and without a Lambertian surface placed on those target points.

There will be a constraint regarding the location of such system, as it must be placed in a position where specular reflections from daylight do not occur. One such position would be to locate the camera on the same wall as the daylight delivery system, looking into the space. This location should also be such that most of the workplane area can be visible. An open office space with a low ceiling and cubicles is certainly not the ideal space for this application. A space with a high ceiling and considerable variation in daylight levels, requiring different target illuminance levels in different areas seems to be more appropriate for CamSensor. A possible solution to the problem of calibration and commissioning will be to use two cameras facing each other and use the lower of the two readings for all lighting conditions.

Another potential problem is the desk surface being covered with objects like books and papers, or occupants blocking the view from camera. One probable solution will be to automatically replace the affected target points by nearby points that are unaltered. Comparing images of the present scene with the one taken during the calibration can help detect the occurrence of this kind of situation.

It is important that the analysis points are located such that every luminaire has strong contribution at one or more test points. Luminaires outside the dimming zone can potentially be dimmed to an unacceptable level, unless the software algorithm for the least square solution takes

care of this scenario. Dimming levels of different luminaires can be controlled by introducing a weighting factor of every luminaire.

Further research may lead to an improved version of this proposed system that can circumvent many of the problems identified in this research.

8.4 Future Work

Given that this work is a proof-of-concept of a new application of a technology that has not been applied in the field of lighting control as yet, there is much need for further research on this application. A thorough investigation is required on the imaging system itself. The type of sensor, the resolution of the camera and the measurement of the sensor spectral response function are all important considerations for this application.

One major developmental research that needs to be undertaken is designing an embedded system that allows CamSensor to operate independent of a computer. Integration of the computer graphics algorithm with the dimming algorithm and CamSensor software in general will help the operation of the system to be fully automatic. Refinement and standardization of the calibration method will be another area where further research will be needed.

The strength of CamSensor lies in the fact that it can take advantage of the digital technology, including the digital imaging system and digitally controlled ballasts. This solution can be applied to the vertical surfaces as well, and can be used to evaluate other lighting quality issues. Blind control can also be integrated into CamSensor.

In the realm of analytical research, an energy analysis will be critical to understand how the system can save energy over time, and how it performs compared to the conventional system as far as energy saving is concerned. This can be a key to the market transformation that can usher the era of camera sensing technology in the field of lighting control.

Bibliography

1. Slater, A.I., *"Lighting and Energy in Buildings"*, presented at the 23rd Session of the CIE, New Delhi, vol. 1, 1995, Published by International Commission on Illumination, Vienna.

2. Rubinstein, F., Siminovitch, M. and Verderber, R., *"Fifty Percent Energy Savings with Automatic Lighting Control"*, IEEE Transactions on Industry Applications, vol. 29, no. 4, pp. 768-773, 1993.

3. New Buildings Institute, Inc., *"Advanced Lighting Guidelines"*, 2003.

4. California Energy Commission, 2001 Title 24 website, http://www.energy.ca.gov/2005_standards/rulemaking/documents/index.html

5. Technical Bulletin, The Watt Stopper, *"ASHRAE 90.1-1999: Lighting Provisions"*, http://www.wattstopper.com/pdf/TB156ASHRAE.pdf

6. Lighting Controls Association, white paper: *"Lighting Controls: current use, major trends and future direction"*, http://www.aboutlightingcontrols.com/education/papers/trends.shtml

7. IESNA, Rea, M. (Ed.), Lighting Handbook Reference & Application, Illuminating Engineering Society of North America, Ninth Edition (Chapter 27)

8. E Source Emerging Technology Series, Kinney, L., *"Practical Control Strategies for Harvesting Daylight Savings"*, ER-00-13, July 2000. http://www.esource.com/public/default.asp

9. National Lighting Product Information Program, *"Specifier Reports: Photosensors"*, vol. 6 no. 1, March 1998.

10. Rubinstein, F., Avery, D., Jennings, J. *"On the Calibration and Commissioning of Lighting Controls"*, presented at Right Light 4 Conference, Copenhagen, Denmark, 1997.

11. Kim, S. and Mistrick, R. *"Recommended Daylight Conditions for Photosensor System Calibration in a Small Office"*, Journal of the Illuminating Engineering Society, pp. 176-188, Summer 2001.

12. Mistrick, R.G. and Thongtipaya, J., *"Analysis of Daylight Photocell Placement and View in a Small Office"*, Journal of the Illuminating Engineering Society, pp. 150-160, Summer 1997.

13. Mistrick, R.G. and Sarkar, A., *"Daylight-Responsive Photosensor Control in Classrooms with Different Daylight Delivery Systems"*, presented at the IESNA Annual Conference in Tampa, Florida, July 2004.

14. Bierman, A. and Conway, K. M., *"Characterizing Daylight Photosensor System Performance to Help Overcome Market Barrier"*, Journal of the Illuminating Engineering Society, pp. 101-115, Winter 2000.

15. Theuwissen, A.J.P., *"Solid State Imaging with Charge-Coupled Devices"*, Dordrecht, The Netherlands: Kluwer, 1995.

16. Foveon, X3 Technology – Direct Image Sensors. http://www.foveon.com/X3_tech.html

17. Titus, H., *"Imaging Sensors That Capture Your Attention"*, KODAK Solid State Image Sensors: CMOS Publications. http://www.kodak.com/global/en/digital/ccd/products/cmos/cmosFamilyPublications.jhtml?id=0.1.10.10&lc=en

18. Eastman KODAK company, Microelectronics Technology Division, *"Application Note: Solid State Image Sensors Terminology"*, http://www.kodak.com/global/plugins/acrobat/en/digital/ccd/applicationNotes/terminology.pdf

19. Lo, Y., *"Solid State Image Sensor: Technologies and Applications"*, Input/Output and Imaging Technologies, Tsai, Y.T., Kung, T., Larsen, J., editors, Proc. SPIE Vol. 3422, pp. 70-80, July 1998.

20. Fossum, E. R., *"CMOS Active Pixel Image Sensors"*, Nuclear Instruments and Methods in Physics Research A, Vol. 395, pp. 291-297, 1997.

21. Fossum, E. R., *"CMOS Image Sensors: Electronic Camera-On-A-Chip"*, IEEE Transactions on Electron Devices, Vol. 44 (10), pp. 1689-1698 (Oct. 1997).

22. Imaging Resource, *"CMOS Versus CCD & What's It All Mean"*, http://www.imaging-resource.com/PRODS/D30/D30A4.HTM

23. Waeny, M., Tanner, S., Lauxtermann, S., Blanc, N., Willemin, M., Rechsteiner, M., Doering, E., Grupp, J., Seitz, P., Pellandini, F., Ansorge, M., *"High Sensitivity High Dynamic, Digital CMOS Imager"*, Sensors and Camera Systems for Scientific, Industrial, and Digital Photography Applications II, Blouke, M. M., Canosa, J., Sampat, N., editors, SPIE Proc. Vol. 4306, pp. 78-84, May 2001.

24. Biber, A., Seitz, P., Jackel H., *"Avalanche Photodiode Image Sensor in Standard Silicon BiCMOS Technology"*, Sensors and Actuators A, Vol. 90, pp. 82-88, 2001.

25. Ward, G., *"The Radiance Lighting Simulation and Rendering System"*, Computer Graphics (Proc. SIGGRAPH 94), ACM, 1994.

26. Ward, G., *"High Dynamic Range Imaging"*, Proceedings of the Ninth Color Imaging Conference, November 2001.

27. Ward, G., *"Real Pixels"*, Graphics Gems II, edited by Arvo, J., Academic Press, 1991.

28. Larson, G.W., *"The LogLUV Encoding for Full Gamut, High Dynamic Range Images"*, Journal of Graphic Tools, 3(1):15-31 1998.

29. G.M. Johnson and M.D. Fairchild, *"Rendering HDR images"* IS&T/SID 11th Color Imaging Conference, Scottsdale, 36-41 (2003).

30. Mann, S. and Picard, R.W., *"Being 'Undigital' with Digital Cameras: Extending Dynamic Range by Combining Differently Exposed Pictures"*, Proc. IS&T 46th Annual Conference, pp. 422-428, May 1995.

31. Rea, M.S. and Jeffrey, I.G., *"A New Luminance and Image Analysis System for Lighting and Vision I. Equipment and Calibration"*, Journal of the Illuminating Engineering Society, pp. 64-72, Winter 1990.

32. Glennie, W L, Thukral, I, Rea, M. S., *"Lighting Control: Feasibility Demonstration of a New Type of System"*, Lighting Research and Technology, Vol. 24 No. 4, pp. 235-242, 1992.

33. Berrutto, V. and Fontoynont, M., *"To What Extent Can Luminance Mapping Improve Lighting Quality Assessment?"*, Proc. 1st CIE Symposium on Lighting Quality (Ottawa, 9-10 May '98) ed. Veitch, J.A., CIE Central Bureau, Vienna, Austria, pp. 140-143, 1998.

34. IESNA, Rea, M. (Ed.), Lighting Handbook Reference & Application, Illuminating Engineering Society of North America, Ninth Edition (Chapter 2)

35. Debevec, P.E. and Malik, J. *"Recovering High Dynamic Range Radiance Maps from Photographs"*, ACM SIGGRAPH Proceedings of the 24th Annual Conference on Computer Graphics and Interactive Techniques, 1997.

36. Vora, P.L., Farrell, J.E., Tietz, J.D., Brainard, D.H., *"Digital Color Cameras – 1 – Response Models"*, Hewlett-Packard Technical Report, HPL-97-53, March 1997.

37. Vora, P.L., Farrell, J.E., Tietz, J.D., Brainard, D.H., *"Digital Color Cameras – 2 – Spectral Response"*, Hewlett-Packard Technical Report, HPL-97-54, March 1997.

38. Horn, B.K.P., *"Robot Vision"*, the MIT Press, Cambridge, Massachusetts, 1986, Chapter 10, pp. 206-209.

39. Inanici, M.N., *"Transformation of High Dynamic Images into Virtual Lighting Laboratories"*, Proceedings of Eighth IBPSA Conference, Eindhoven, Netherlands, Aug. 11-14, 2003

40. Inanici, M.N., *"Utilization of Image Technology in Virtual Lighting Laboratory"*, Proceedings of the CIE 2003 Conference, San Diego, June 26-28, 2003.

41. C3188A 1/3" Color Camera Module http://www.electronic-kits-and-projects.com/kit-files/cameras/d-c3188a.pdf

42. CEV38 Camera Evaluation board user manual for OV7620 sensor http://home.pacific.net.hk/~comedia/ or http://www.quasarelectronics.com/ev38.htm

43. OV7620 Single-Chip CMOS VGA Color Digital Camera Product Specification, Omnivision Technology, Sunnyvale, California.

44. Yeung, K.C., CoMedia Ltd, Hong Kong, *Personal Communication*, September 2004

45. Ward, G., *Personal Communication*, September 2004

46. Nourbakhsh, I., Carnegie Mellon University, *Personal Communication*, September 2004

47. Ronat, O., *"The digital addressable lighting interface (DALI): An emerging energy-conserving lighting solution"*, Technical Paper, TP4/9/2002, El Segundo, CA, International Rectifier.

48. Digital Addressable Lighting Interface Activity Group (DALI-AG), *"DALI Manual"*, Frankfurt, Germany, 2001.

49. White Paper – *"DALI- What's the Buzz About?"*, Lighting Controls Association, http://www.aboutlightingcontrols.com/education/papers/dalibuzz.shtml

50. Moeck, M., *"Proof-of-Concept: Digital Addressable Lighting System (DALI) for Intelligent Lighting Control"*, http://www.personal.psu.edu/faculty/m/u/mum13/pa2.pdf

51. Moeck, M., *"Developments in Digital Addressable Lighting Control"*, Journal of Light & Visual Environment, The Illuminating Engineering Institute of Japan, Vol. 28(2), 2004, pp. 104-106.

52. Moeck, M., *"Why DALI?"*, Professional Lighting Design 38, 2004, pp. 38-41.

53. Digital Addressable Lighting Interface Activity Group website: http://www.dali-ag.org/

54. Francois, Sillion X., Puech, Claude, *"Radiosity and Global Illumination"*, Morgan Kaufmann Publishers, San Francisco, CA, 1994, pp. 14-16.

Appendix A

FLOWCHARTS AND ALGORITHMS

Notations Used in This Chapter:

CF_{expX} **:** Calibration factor for converting the radiance values obtained from an image captured by CamSensor at exposure X, to the corresponding luminance values.

$\rho_{refsurf}$ **:** Average reflectance of the reference Lambertian surface (bleached baking flour with 75% reflectance used in the final experiment).

$L_{DIFF\text{-}LX\text{-}Y}$ **:** Luminance at test point Y due to luminaire X. The test points are covered with Lambertian surfaces[14].

E_{Y} **:** present light level at test point Y due to daylight + electric light.

$E_{LX\text{-}Y}$ **:** Illuminance at test point Y due to luminaire X (irrespective of whether the illuminance is covered with Lambertian surfaces).

$L_{DIFF\text{-}L\text{-}ALL\text{-}Y}$ **:** Luminance at test point Y due to all luminaires. The test points are covered with Lambertian surfaces.

$E_{L\text{-}ALL\text{-}Y}$ **:** Illuminance at test point Y due to all luminaires operating at 100% output (irrespective of whether the illuminance is covered with Lambertian surfaces).

$L_{DIFF\text{-}DL\text{-}Y}$ **:** Luminance at test point Y due to daylight. The test points are covered with Lambertian surfaces.

---

[14] bleached flour powder pressed uniformly on diffuse bond papers, used throughout this chapter, unless otherwise specified

$E_{DL\text{-}Y}$ **:** Illuminance at test point Y due to daylight (irrespective of whether the illuminance is covered with Lambertian surfaces).

$L_{DESK\text{-}LX\text{-}Y}$**:** Luminance at test point Y on the workplane (desk) due to luminaire X.

$L_{DESK\text{-}L\text{-}ALL\text{-}Y}$**:** Luminance at test point Y on the workplane (desk) due to all luminaires.

L_Y **:** Luminance at any test point Y due to daylight as well as electric light, obtained during operation (subscript *DIFF*/*DESK* is absent).

$L_{DL\text{-}Y}$**:** Luminance at any test point Y due to daylight only, obtained during operation.

$L_{EL\text{-}Y}$ **:** Luminance at any test point Y due to electric light (DALI luminaires) only, obtained during operation.

T_Y **:** target illuminance level at test point Y

x_{LX} **:** required fractional dimming for luminaire X that best achieves the desired light levels at different test points on the work plane

d_{LX}**:** Present dimming level of the DALI luminaire X.

ρ_{DIFF}**:** Average reflectance of the Lambertian surface.

A.1 Flowchart to Obtain Luminance from Radiance

At any particular exposure, the radiance computed from an image is proportional to the actual luminance. The proportionality factor (calibration factor) for any exposure setting can be obtained as follows:

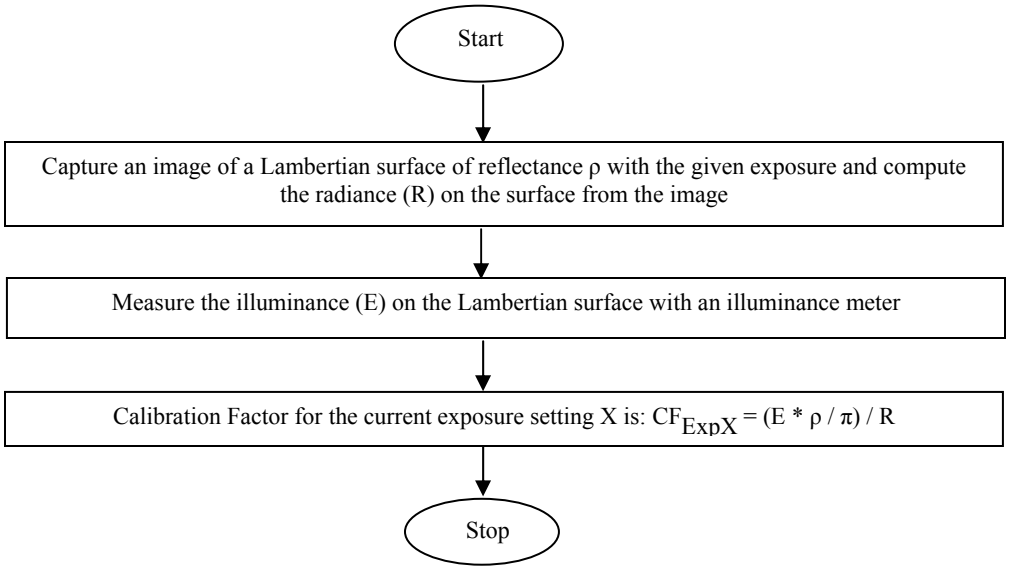

A.2 Flowchart to Illuminance from Luminance on the Desk Due to a Single Light Source

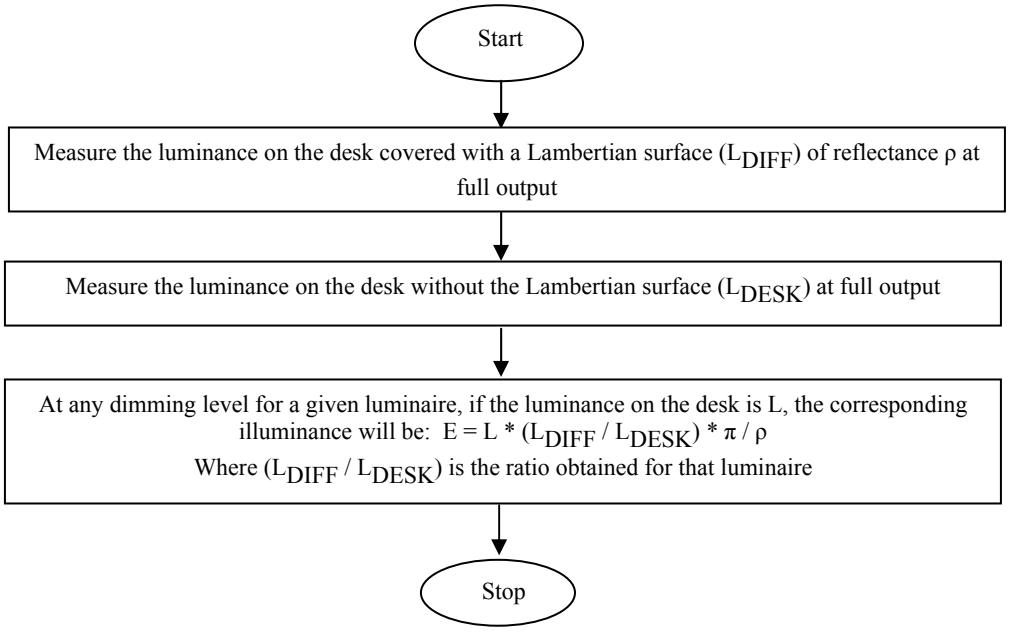

A.3 Flowchart for the Factory Calibration of CamSensor[15]

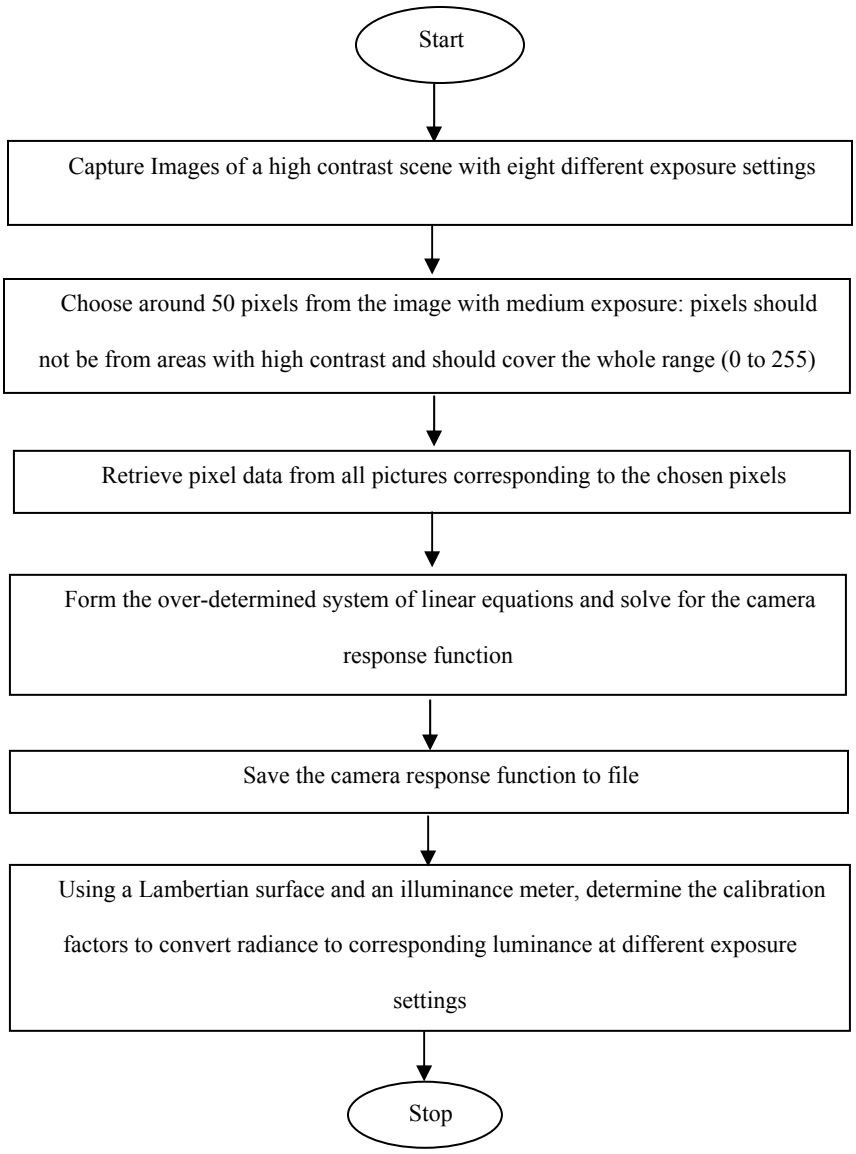

[15] Note: All steps except the image capture process are done through software and therefore automatic. The images are the input to the algorithm.

A.4 Flowchart for the Site Calibration of CamSensor

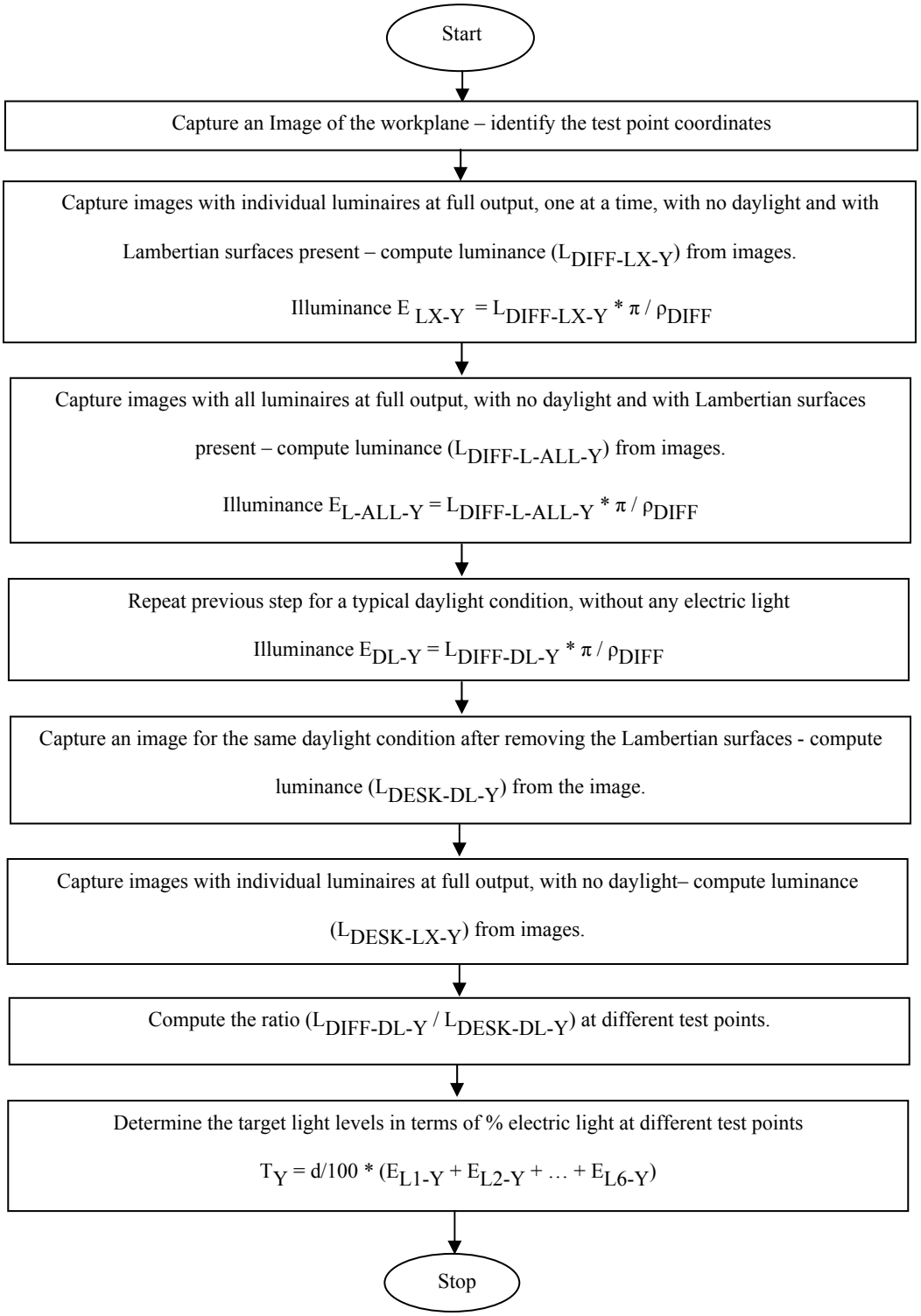

A.5 Flowchart for the Operation of CamSensor

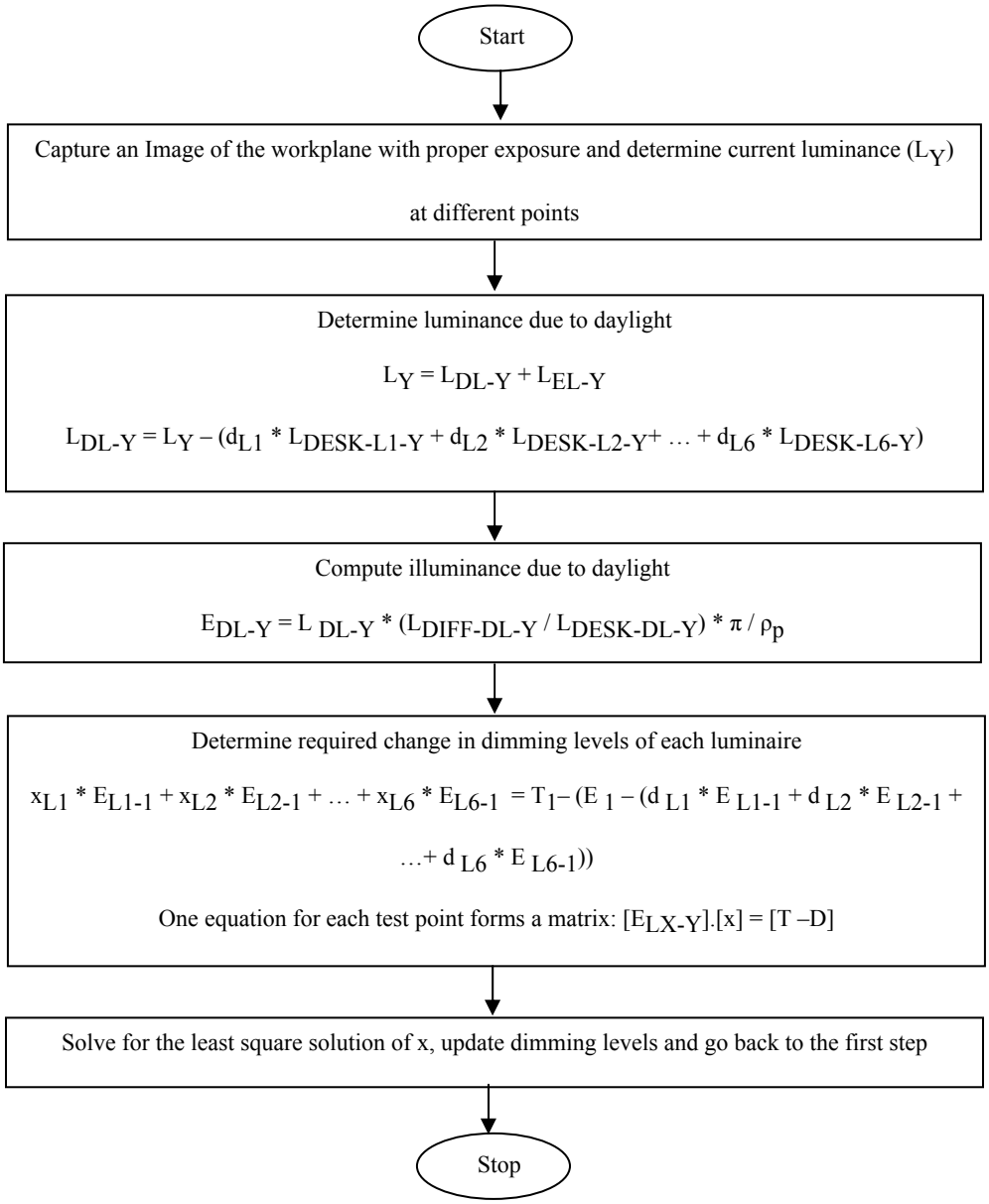

Appendix B

DESCRIPTION OF THE IMAGE SENSOR

This appendix contains technical details of OV7620 CMOS image sensor.

OV7620 is a single-chip color CMOS image sensor designed and manufactured by OmniVision Technologies, Sunnyvale, California. This sensor has high functionality in a single footprint package. It contains proprietary sensor technology that uses advanced algorithms to cancel Fixed Pattern Noise, eliminates smearing and reduces blooming [**43**]. The sensor is provided with camera functions like exposure control, gamma, gain, white balance, color matrix, color saturation, hue control, windowing etc, all programmable through the serial Software Configuration Control Board (SCCB) interface. Key specifications of the sensor are shown in Table **B-1**. The features include wide dynamic range, electronic exposure, gain and white balance control and line exposure option.

Table **B-1**: Key Specifications of OV7620

Array Size (VGA) (QVGA)	640x480 320x240
Pixel Size	7.6 µm x 7.6 µm
Image Area	4.86 mm x 3.64 mm
Max Frames/Sec (FPS)	Up to 60 FPS for QVGA
Electronics Exposure	Up to 648:1
Scan Mode	Progressive or Interlace
Gamma Correction	128 Curve Settings
Min. Illumination (3000K)	< 2.5 lux at f1.4
S/N Ratio	> 48 dB with Automatic Gain Control off and Gamma = 1
Fixed Pattern Noise (FPN)	< 0.03 % V_{pp}
Dark Current	< 1.94 nA/cm^2
Dynamic Range	> 72 dB
Power Supply	5V dc ± 5%
Power Requirements	< 120 mA Active <10 µA Standby (Power Down)
Package	48 pin LCC

This image sensor uses an electronic shutter. It is important to point out the difference between a mechanical shutter and an electronic shutter. A mechanical shutter controls the amount of light falling on the image sensor by opening and closing an orifice in front of the lens for a given amount of time. An electronic shutter does not have any mechanical component. Instead, it varies the effective integration time, during which the photosensitive pixels (charge collecting components) continue collecting the charge, which is caused by the light falling on the sensor. The amount of charge collected is proportional to the light intensity. The circuitry used to perform the shuttering operation drains all charge out of the pixels for a fraction of the total integration time [**18**]. This causes the accumulation of charge and thereby the sensing of light to vary, and that, in effect, controls the exposure.

It should be noted that aperture and shutter speeds are not separately controllable in case of electronic exposure, thus it is important that a proper aperture setting is chosen. The smaller the aperture, the better is the overall focusing ability of the camera. The camera module comes with an optional 6 mm lens (present in the module used in this research) with a fixed aperture of F1.6. A smaller aperture would have been more suitable for this application.

The image sensor spectral response is shown in Figure **B-1** [**43**]. As can be seen in the response curve, this sensor is very sensitive to infrared radiation. Thus an IR filter is necessary for our application. The sensor, as is the case with most of the image sensors, does not respond equally to different wavelengths. Thus, a spectral calibration of the image sensor is necessary if we want the camera response to be independent of the wavelength of the light source.

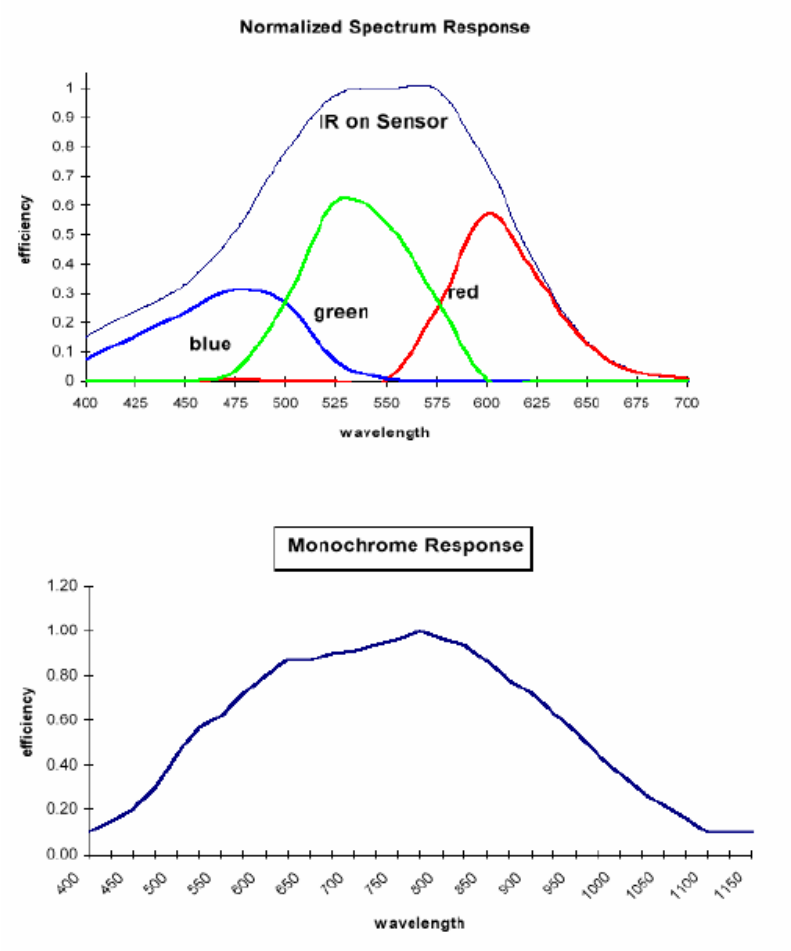

Figure **B-1**: OV7620 Spectral Response (Source: OmniVision Product Specification)